Eocene calcareous nannofossil biostratigraphy and community structure from Exmouth Plateau, Eastern Indian Ocean (ODP Site 762)

Jamie L. Shamrock[1*] and David K. Watkins[1]
[1]*Department of Geosciences, University of Nebraska, Lincoln, Nebraska 68588-0340*
Email: jamie.shamrock@huskers.unl.edu; dwatkins1@unl.edu

ABSTRACT: A relatively complete section of Eocene (~33.9-55.8 Ma) pelagic chalk from offshore northwestern Australia was used to analyze range and abundance data of ~250 Eocene species to test the efficacy of the existing CP (Okada and Bukry 1980) and NP (Martini 1971) biostratigraphic zonation schemes. Changes in nannofossil diversity, abundance, and community structure were monitored through several Eocene paleoenvironmental events, as identified by changes in $\delta^{13}C$ and $\delta^{18}O$ data, to examine variations in surface water conditions. Major changes in nannofossil assemblages, as indicated by dominance crossovers, correspond to paleoenvironmental shifts such as the PETM (Paleocene-Eocene thermal maximum) and the EECO (Early Eocene climatic optimum). This research also provides systematic paleontology and range data for one new genus (*Hexadelus*) and eight new species or variants (*Calcidiscus ellipticus, Cruciplacolithus nebulosus, Cruciplacolithus opacus, Cyclicargolithus parvus, Hexadelus archus, Hayella situliformis* var. *ovata*, *Markalius latus, Pedinocyclus annulus*) and addresses several taxonomic issues in other Eocene species.

INTRODUCTION

The Eocene Epoch is a critical transition period from the global greenhouse conditions of the Late Cretaceous and early Paleogene to the icehouse of the later Cenozoic. The lower boundary is marked by a distinct pulse of global warmth, the PETM, and the upper boundary by cooling associated with the onset of Antarctic glaciation, with a significant proportion of research focused on the conditions governing its lower and upper boundaries with the Paleocene and Oligocene, respectively.

Recent advances in our knowledge of calcareous nannofossils (Bown and Pearson 2009; Dunkley Jones et al. 2008; Agnini et al. 2006; Bown 2005; Raff, Backman and Pälike 2005; Tremolada and Bralower 2004, others) provide an opportunity to reevaluate the Eocene biostratigraphic succession and the nannofossil assemblage through significant paleoenvironmetnal changes. This research was conducted to fulfill a need for a continuous Eocene calcareous nannofossil reference section, containing range and abundance data for a vast number of Eocene species, relative to the preexisting CP and NP biostratigraphic zonation schemes. In addition we examine changes in nannofossil diversity, abundance, and community structure through several Eocene paleoenvironmetnal events. Ideally, this study would utilize a relatively complete succession of strata that could function as a reference section. Arguably, the best existing section for such a purpose was cored by Ocean Drilling Program Leg 122 off of northwest Australia in 1990. The thorough biostratigraphic characterization of Siesser & Bralower (1992) demonstrated a relatively complete and expanded Eocene succession with good nannofossil abundance and preservation. In addition, there is well-documented paleomagnetic (Galbrun 1992) and stable isotopic (Thomas Shackleton and Hall 1992) data for this site.

Several recent studies have been conducted on Eocene calcareous nannofossil biostratigraphy and/or paleoenvironmetnal assemblage trends, producing a wealth of new nannofossil data; however, many of these studies focus on high resolution analysis of a discrete event, such as the PETM (Bown and Pearson 2009; Raffi, Backman and Pälike 2005; Tremolada and Bralower 2004), MECO (middle Eocene climatic optimum) (Jovane et al 2007), and Oi-1 events (Dunkley Jones et al. 2008), or such research is restricted to only a portion of the epoch (Villa et al. 2008; Agnini et al. 2006). There are few studies where the nannofossil assemblage and range data has been quantitatively examined throughout the entire Eocene, particularly from one locality.

Recent research from the Southern Ocean (Persico and Villa 2008) and Tanzania (Bown Dunkley Jones and Young 2007; Bown and Dunkley Jones 2006; Bown 2005) has resulted in the identification of a significant number of new Eocene calcareous nannofossil species. This research confirms the presence of 41 of these species within the eastern Indian Ocean at Site 762, and expands the ranges of several of these taxa. In addition, we provide systematic paleontology and range data for eight additional new species and one new genus, and address taxonomic issues with several additional forms.

In addition to developments in nannofossil biostratigraphy, the construction of high-resolution $\delta^{13}C$ and $\delta^{18}O$ records (Galeotti et al. 2010; Bohaty et al. 2009; Nicolo et al. 2007; Lourens et al. 2005; Bohaty and Zachos 2003; Zachos et al. 2001) has allowed paleoenvironmental events such as the PETM, ETM2 (Eocene thermal maximum 2), ETM3, EECO, MECO and Oi-1 to be interpreted at Site 762. Lower resolution $\delta^{13}C$ and $\delta^{18}O$ records for Site 762 of Thomas Shackleton and Hall (1992) allows identification of many key excursions throughout the Eocene, which

*Corresponding author's present address: ExxonMobil Exploration Co Post Office Box 4778, Houston TX, 77210-4778; email: jamie.l.shamrock@exxonmobil.com

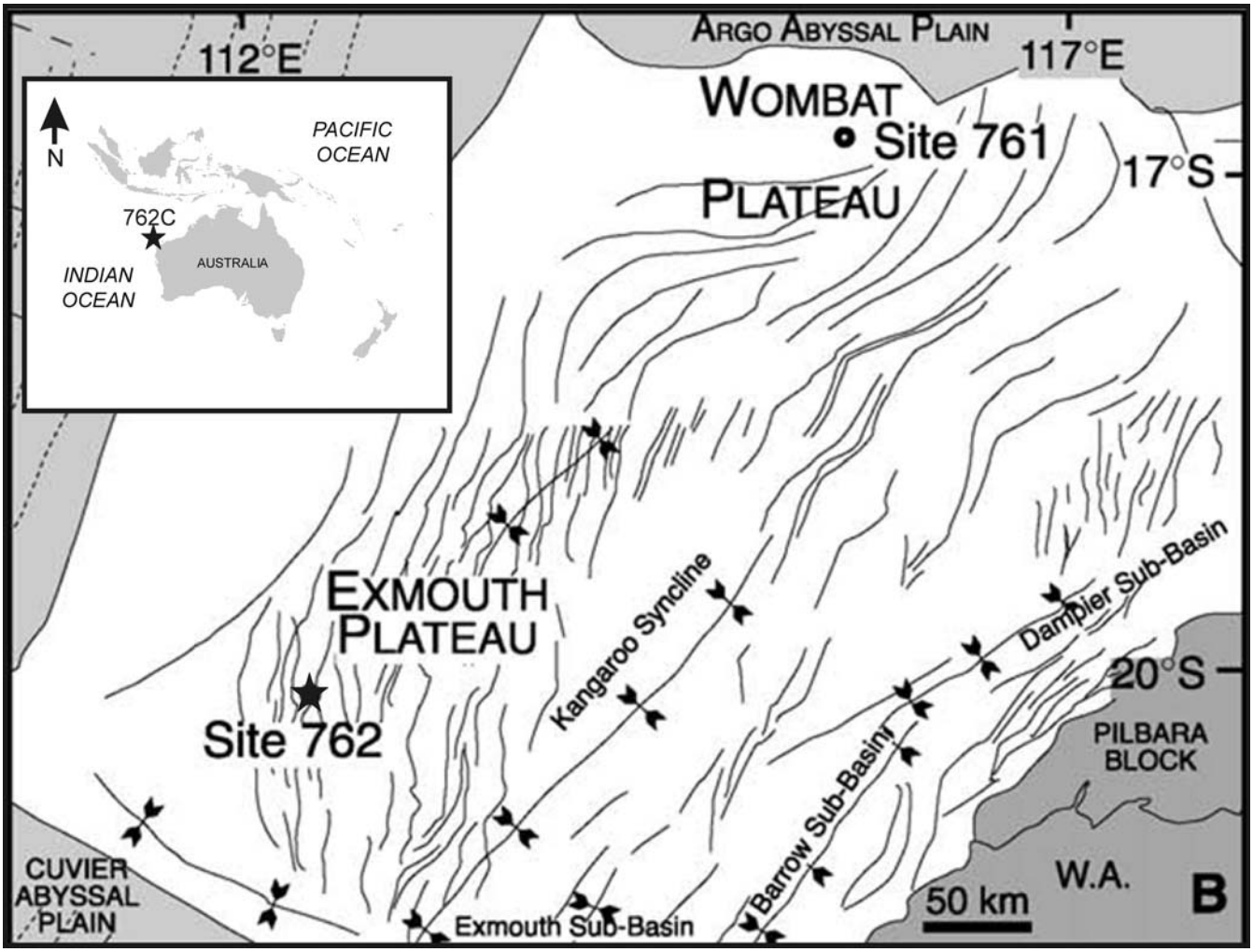

TEXT-FIGURE 1
Site map with inset showing location of ODP Leg 122 Site 762C (star) off the northwestern Australian shelf (19°53.23S, 112°15.24E). Detailed structural map modified from Campbell Howe and Rexilius (2004).

allows us to examine the dynamics of the nannofossil community with respect to such paleoenvironmental events. We identify significant assemblage turnovers in the middle Eocene and discuss the possible relationships of this data to both short term environmental perturbations and the long term climate transition from global greenhouse to icehouse.

MATERIALS AND METHODS

ODP (Ocean Drilling Program) Leg 122 Hole 762C was selected for this study based on the presence of a thick, expanded Eocene succession (~240m) as well as on data from Leg 122 *Initial Reports* (Haq et al. 1990) and *Scientific Results* (Rad et al. 1992) that indicate relatively continuous sedimentation. Site 762 (19°53.23S, 112°15.24E) is located on the central Exmouth Plateau (northern Carnavon Basin) and is separated from the Australian Northwest Shelf by the Kangaroo Syncline (Rad et al. 1992) (text-figure 1). Though stretched and rifted in its early history, the plateau has been relatively quiescent since the mid-Cretaceous, with fairly uniform thermal subsidence. Hole 762C was drilled in 1360m of water, with decompacted burial curves indicating little change in water depth since the time of original deposition (Haq et al. 1992).

Approximately 240m of Eocene sediments were penetrated in Cores 3-29 from ~184-422 msbf (meters below sea floor). Core recovery varies throughout this interval, ranging from 12.1 to = 100%, with an average recovery of ~67% (text-figure 2). Sedimentation rates are estimated at ~1-3cm/ky for the early Eocene and ~0.5-2cm/ky for the mid- and late Eocene (Shipboard Scientific Party 1990; Haq et al. 1992). Eocene pelagic sediments from this locality consist of white to green-grey, calcareous oozes, chalks, and marls, indicating an open-ocean setting (Rad et al. 1992). Clay content and bioturbation increased downward toward the lower Eocene. This interval is divided into three lithologic subunits as described in Haq et al. (1992) and is summarized in Table 1. Calcareous nannofossil data from Siesser & Bralower (1992) show a diverse and robust nannofossil assemblage, and biostratigraphy based on the NP zonation (Martini 1971) suggests a relatively complete Eocene succession. Calcareous nannofossils are extremely abundant and moderately to well preserved, with deposition well above the CCD (carbonate compensation depth).

A total of 187 samples were selected from the recovered core at approximately 0.75m intervals, as core availability would allow. Of these samples, 102 were used to collect detailed assemblage data, with the remaining samples used to increase precision of key biostratigraphic markers. Sample intervals and depths are provided in Table 2. All samples span a 1cm interval (downward), excluding 14-3-125 (2cm) and 13-2-71, 15-2-52, and 21-5-50.5 (1.5cm). Though some samples occur on half-centimeter intervals, depths have been rounded to two significant digits. Due to significant expansion of Core 26 (182% recovery), samples from this core required calibration of true depths (in mbsf) by taking the cored interval by the total thickness (4.5 m/7.8m recovered thickness) to get a ratio (0.616m true depth/ 1m recovered thickness). This ratio was applied to samples from Core 26 to generate the depths shown in Table 2. Sample midpoints in Table 3 represent the midpoint of the error between the observed event depth and the sample below (for the lowest occurrence (LOs)) or the sample above (for the highest occurrence (HOs)).

Core samples and smear slides, including holotype and paratype materials and photographs, are stored in the collections of the ODP Micropaleontological Reference Center at the University of Nebraska State Museum (UNSM). Smear slide preparation for Hole 762C followed standard techniques as described by Bown and Young (1998) and were mounted using Castolite AP Crystal Clear Polyester Resin. Smear slides were examined at 1000-1250x magnification with an Olympus BX51 and a Zeiss AxioImager A.2 under plane parallel light (PL), cross-polarized light (XPL), and with a one-quarter λ mica interference plate.

Assemblage data was collected by first identifying 500 specimens to species level, except members of Pontosphaeraceae and Syracosphaeraceae, which were rare and sporadic through the section (see Systematic Paleontology section). Additionally, two long traverses were examined to identify rare specimens, which were given a value of 1 and added to the total. This data was used to convert all species and genera to percent abundance for further analysis.

Counts of 300 specimens are considered statistically significant (Revets 2004; Dennison and Hay 1967; Phleger 1960) for identifying species that account for ~ 0.01% of the nannofossil assemblage with p = 0.05 (95% confidence interval); however, by generating counts > 456 specimens for percent abundance data, at the 95% confidence interval, the maximum second standard deviation will be = 5% of the actual proportion (Chang 1967). Diversity and univariate statistical analysis was conducted on the data using PAST (Paleontological Statistics) (Hammer et al. 2001).

RESULTS

Approximately 260 taxa were identified through this Eocene section, including 41 recently named and 8 new species, with nearly all CP and NP zones and subzones identified at Site 762. Calcareous nannofossils were abundant, with >10 – 100 specimens per FOV (field of view). Nannofossil specimens were moderately to well-preserved, with little or some etching, recrystallization, and alteration of primary morphology. Reworked Cretaceous and Paleogene specimens were very rare. Ranges are provided for all species as well as notable abundance trends and taxonomic issues (see Systematic Paleontology section). Raw nannofossil abundance data are archived online at the World Data Center for

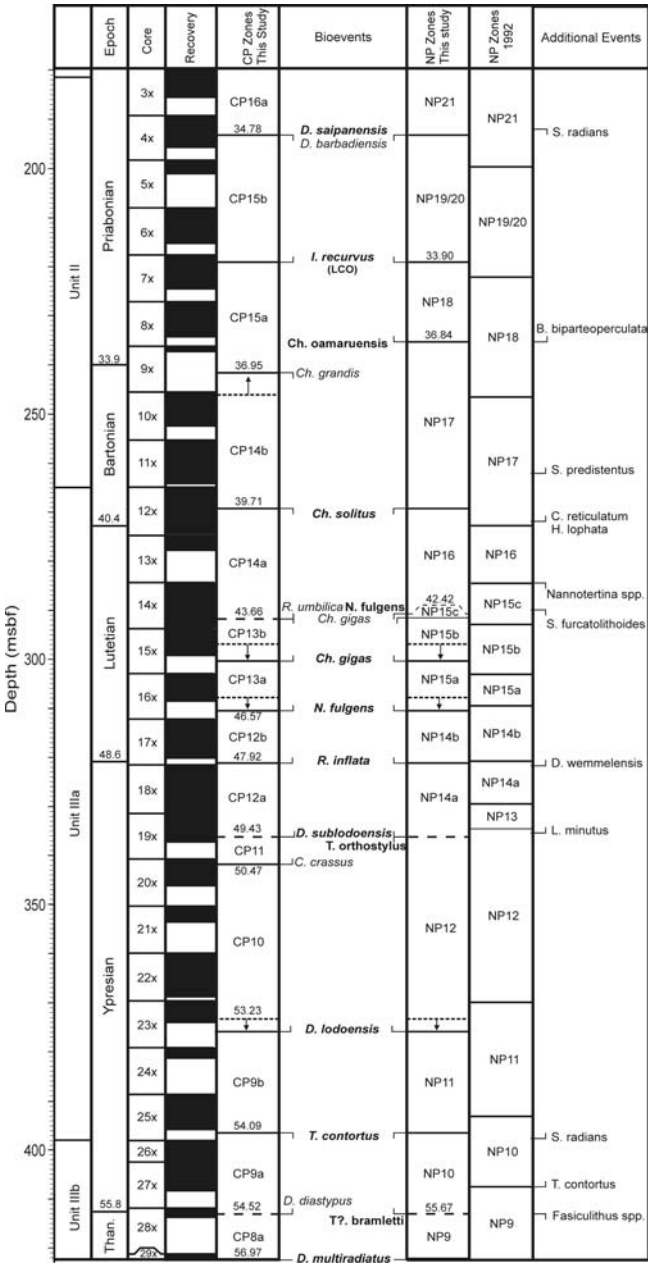

TEXT-FIGURE 2
Calcareous nannofossil biostratigraphy for Site 762C. Depth (msbf), lithologic subunit, epoch, core, and core recovery shown from left. Biomarkers from the CP zonation (Okada and Bukry 1980) are shown in bold. NP zonal markers from Martini (1971) with select subzones of Aubry (1991) shown in italic. Joint markers for CP and NP zones are shown in bold and italic. Original interpretation of Siesser and Bralower (1992) shown at right, with alternate biomarkers of that study at far right. Ages (Ma) are given for epoch boundaries and CP/NP zonal boundaries (Ogg Ogg and Gradstein 2008). Locations of zonal boundaries reflect the midpoint between the observed event and the sample above (for HOs) or the sample below (for LOs). These values are provided in Table 3. Actual sample depths are given as dotted lines where coring gaps create > 2 m offset between the observed event depth and the extrapolated event midpoint. Biostratigraphic hiatuses are shown as dashed lines.

TABLE 1
Summary of lithologic subunits through the sampled interval at Site 762C, derived from Haq et al. (1990, table 2, p. 221).

LITHOLOGIC SUMMARY			
Unit	Core Interval	Depth (mbsf)	Lithology
II	3-3-0cm – 12-1-0cm	181.5-265.0	White nannofossil chalk
IIIA	12-1-0cm – 26-10-0cm	265.0-398.0	Light green-grey and white nannofossil chalk with foraminifera
IIIB	26-10-0cm – 29-1-50cm	398.0-554.8	Light green nannofossil chalk

Paleoclimatology http://www.ncdc.noaa.gov/paleo/data.html (Shamrock and Watkins 2012).

Several families have been attributed to neritic/shelf environments due to their general paucity in open-ocean settings, such as Syracosphaeraceae (Siesser 1998; Roth and Berger 1975), Rhabdosphaeraceae (Perch-Nielsen 1985; Roth and Thierstein 1972), Pontosphaeraceae (Perch-Nielsen 1985), Braarudosphaeraceae (Bybell and Gartner 1972; Sullivan 1965), and many holococcoliths, although these may be transported into deeper water by turbidity currents (Perch-Nielsen 1985). The nannofossil assemblage at Hole 762C is consistent with an open ocean setting, as all such taxa were rare, sporadic, and/or absent from this locality. Despite the relative absence of some families, the nannofossil assemblage shows high species richness (S) throughout the Eocene (μ (mean) = 53.4, max. = 66, min. = 41). Additional data and results are incorporated into the biostratigraphy and paleoenvironmental discussions.

Calcareous nannofossil biostratigraphy

Two well known and widely employed biozonation schemes are generally utilized in Paleogene calcareous nannofossil biostratigraphy: the low-latitude Okada-Bukry (1980) CP Zonation and the cosmopolitan to high-latitude Martini (1971) NP Zonation. Calcareous nannofossil biostratigraphy for ODP Leg 122 Site 762C was originally examined by Siesser and Bralower (1992) using a modified version of the NP zonation, that incorporated CP markers and other alternative markers, where the range and abundance of NP markers were in question. This locality has been reexamined using both the standard CP and NP zonations, with select NP subzones of Aubry (1991), as a means of comparing the consistency of these two zonation schemes to one another, as well as the secondary and alternative markers frequently employed. Strict application of some zones was not possible, due the rarity or absence of some marker taxa at Hole 762C (*R. gladius, D. bifax, N. alata*). Subzones in the NP zonation scheme were not originally identified in Siesser and Bralower (1992) but have been extrapolated based on data from that study. Sample intervals and depths of key marker taxa are provided in Table 3. text-figure 2 illustrates the CP and NP nannofossil biostratigraphy at Hole 762C from the current study, as well as from Siesser and Bralower (1992). Placement of boundaries between the Eocene stages is tentative, as no nannofossil bioevents directly mark these horizons (Ogg Ogg and Gradstein 2008). Stage boundaries were approximated using nannofossil events in conjunction with dated isotopic excursions, identified from original ODP Leg 122 $\delta^{13}C$ and $\delta^{18}O$ data of Thomas, Shackleton and Hall (1992) (See "Nannofossil Abundance Trends", below). A partial range chart of zonal markers, as well as select additional taxa, as observed in Hole 762C is provided in text-figure 3.

The original interpretation of Siesser and Bralower (1992) identified all NP zones with no apparent hiatuses; however, this study identifies zones and subzones that are absent from both the NP and CP zonation schemes. The NP zonal boundaries are essentially congruent between Siesser and Bralower (1992) and this study for NP9, NP11, NP12, NP13, NP15, NP19/20, and NP21. Minor differences are due to core recovery issues, sample spacing between studies, or perhaps time spent examining each sample: Many key taxa were very rare at Site 762, and significant time was spent searching for rare marker taxa, subsequently shifting the zonal boundaries. Significant differences do exist at the NP10, NP14, NP16, NP17, and NP18 boundaries, related either to use of CP and/or alternative markers or from a stratigraphic hiatus, and are discussed in greater detail below. Nannofossil zones are discussed with respect to the basal biomarker, with the top defined by the base of the following zone.

The variations in the NP and CP interpretations, both within our data and in comparison to earlier work, show some issues that can arise with identification of rare, diachronous, and/or secondary taxa. When possible it may be best practice to employ both zonation schemes, as comparison of the two interpretations may shed light on hiatuses and/or marker taxa that occur too high or too low in the section. An increase in latitudinal temperature gradients, as seen in the late Eocene, tends to increase both the degree of taxonomic provinciality and the severity of diachronism for many paleontological proxies. This decreases the resolution of the biostratigraphic record during dynamic transitions when it is most needed, and gives further support to the application of a robust and diverse set of biomarkers whose stratigraphic relationships to one another are well understood.

Zones CP8a/NP9

The basal sample in this study (29-1-50cm, 422.00 msbf) contains *Discoaster multiradiatus* Bramlette and Riedel 1954, the marker taxa for the base of CP8/NP9. Siesser and Bralower (1992) sampled significantly deeper through the section and their midpoint for the LO of *D. multiradiatus* also occurs at 422.00 msbf, so our section begins near the base of this zone.

Subzone CP8b is absent from Hole 762C. Both the primary marker (LO *Campylosphaera eodela* Bukry and Percival 1971) and the secondary marker (LO *Rhomboaster* spp.) at Hole 762C are concurrent with the LO of *Discoaster diastypus* Bramlette and Sullivan 1961, which marks the base of subzone CP9a (28-1-59cm, 412.59 mbsf). This convergence is most noticeable using CP subzonal markers, and may not be identified with the NP scheme (text-figure 2). This hiatus occurs in association with the PETM (412.65 msbf), and corresponds to a notable change in the nannofossil assemblage, treated more thoroughly in the PETM discussion below.

TABLE 2
Core intervals and depths (mbsf) for the 187 nannofossil samples used in this study. *Samples used for detailed assemblage study marked with an asterisk (*).

Samp. No.	Core Interval	Depth (mbsf)	Samp. No.	Core Interval	Depth (mbsf)	Samp. No.	Core Interval	Depth (mbsf)	Samp. No.	Core Interval	Depth (mbsf)
1*	3-4-49	184.49	48	10-4-120	251.70	95	16-2-52	303.52	142	22-2-12 5	362.75
2*	3-4-101	185.01	49*	11-1-50	256.00	96*	16-2-125	304.25	143*	22-3-52	363.52
3*	4-1-46.5	189.47	50	11-1-125	256.75	97*	16-3-52	306.52	144	22-3-12 5	364.25
4*	4-1-123.5	190.24	51*	11-2-50	257.50	98	16-3-125	307.25	145*	22-4-47 5	364.98
5*	4-2-50	191.00	52	11-2-125	258.25	99*	16-4-45	307.95	146	22-4-12 5	365.75
6*	4-2-126.5	191.77	53	11-3-51..5	159.02	100*	17-1-51	313.01	147*	22-5-46	366.46
7*	4-3-50	192.50	54*	11-3-125	259.75	101	17-1-145	313.95	148	22-5-12 5	367.25
8*	4-3-100	193.00	55*	11-4-50	260.50	102*	17-2-52	314.52	149*	22-6-53	368.03
9*	4-4-50	194.00	56	11-4-125	261.25	103	17-2-125	315.25	150	22-6-11 0	368.60
10	4-4-147	194.97	57*	11-5-50	262.00	104	17-3-52	316.02	151*	23-1-49 5	370.00
11*	5-1-50	199.00	58	11-5-125	262.75	105*	17-3-125	316.75	152*	23-1-12 5	370.75
12	5-1-125	199.75	59*	11-6-50	263.50	106*	17-4-52	317.52	153*	23-2-49	371.49
13	5-2-53	200.53	60	11-6-140	262.40	107	17-4-116..5	318.17	154	23-2-11 3	372.13
14*	6-1-48	208.48	61*	12-1-51	265.51	108*	17-5-49.5	319.00	155*	23-3-51	373.01
15	6-1-125	209.25	62	12-1-125	266.25	109	17-5-148	319.98	156*	24-1-54	379.54
16*	6-2-46	209.96	63*	12-2-51	267.01	110*	18-1-50	322.50	157	24-1-14 2	378.42
17	6-2-125	210.75	64	12-2-125	267.75	111	18-1-124.5	323.25	158*	25-1-50 5	389.01
18*	6-3-50	211.50	65*	12-3-50	268.50	112*	18-2-50	324.00	159	25-1-12 5	389.75
19	6-3-125	212.25	66	12-3-125	269.25	113	18-2-125	324.75	160*	25-2-47 5	390.48
20*	6-4-50	213.00	67*	12-4-50	270.00	114	18-3-50.5	325.51	161	25-2-11 5	391.15
21	6-4-125	213.75	68	12-4-125	270.75	115*	18-3-125	326.25	162*	25-3-52	392.02
22*	6-5-40	214.40	69*	12-5-50	271.50	116*	18-4-53	327.03	163	25-3-12 5	392.75
23*	7-1-50	218.00	70	12-5-125	272.25	117	18-4-125	327.75	164	25-4-54	393.54
24	7-1-125	218.75	71	12-6-50	273.00	118*	18-5-50	328.50	165*	25-4-12 5	394.25
25	7-2-54	219.54	72*	12-6-147	273.97	119	18-5-125	329.25	166	25-5-43	394.93
26*	7-2-125	220.25	73*	13-1-50	275.00	120*	18-6-52	330.02	167*	26-1-49	398.30
27	7-3-50	221.00	74	13-1-125	275.75	121	18-6-148.5	330.99	168	26-1-12 5	398.77
28*	7-3-119	221.69	75*	13-2-71	276.71	122	19-1-52	331.52	169*	26-2-49	399.17
29	7-4-50	222.5	76*	14-1-5	284.05	123*	19-1-125	332.75	170	26-2-12 5	399.69
30*	7-4-146	223.46	77	14-1-72.5	284.73	124*	19-2-52	333.52	171*	26-3-51	400.16
31	8-1-50	227.50	78*	14-2-50	286.00	125	19-2-125	334.25	172	26-3-12 5	400.62
32*	8-1-125	228.25	79	14-2-125	286.75	126*	19-3-53	335.03	173*	26-4-47	401.06
33*	8-2-53	229.03	80	14-3-52.5	287.53	127	19-3-125	335.75	174	26-4-11 3.5	401.47
34	8-2-126	229.76	81*	14-3-126	288.26	128*	19-4-52	336.52	175*	26-5-50	402.01
35	8-3-52	230.52	82*	14-4-55	289.05	129*	20-1-50	341.50	176	26-5-14 8.5	402.61
36*	8-3-125	231.25	83	14-4-125	289.75	130	20-1-125	342.25	177*	27-1-50	403.00
37*	8-4-50	232.00	84*	14-5-50	290.50	131*	20-2-50	343.00	178	27-1-12 5	403.75
38	8-4-125	232.75	85	14-5-115	291.15	132	20-2-115	343.65	179*	27-2-50	404.50
39*	8-5-50	233.50	86*	14-6-50	292.00	133*	20-3-52	344.52	180	27-2-12 5	405.25
40*	9-1-46	236.96	87	14-6-147	292.97	134	20-3-125	345.25	181*	27-3-50	406.00
41*	10-1-50	246.50	88*	15-1-48	293.98	135*	20-4-47.5	345.98	182	27-3-12 5	406.75
42	10-1-125	247.25	89	15-1-125	294.75	136*	21-1-50	351.00	183*	27-4-50	407.5
43*	10-2-49.5	248.00	90	15-2-52	295.52	137	21-1-129	351.79	184	27-4-13 8	408.38
44	10-2-125	248.75	91*	15-2-124	296.24	138*	21-2-50	352.20	185*	28-1-59	412.59
45*	10-3-50	249.50	92*	15-3-48	296.98	139*	22-1-50	360.50	186*	28-1-12 5	413.25
46	10-3-115	250.15	93*	16-1-48	303.48	140	22-1-125	361.25	187*	29-1-50	422.00
47*	10-4-50	251.00	94	16-1-125	304.25	141*	22-2-46	361.96			

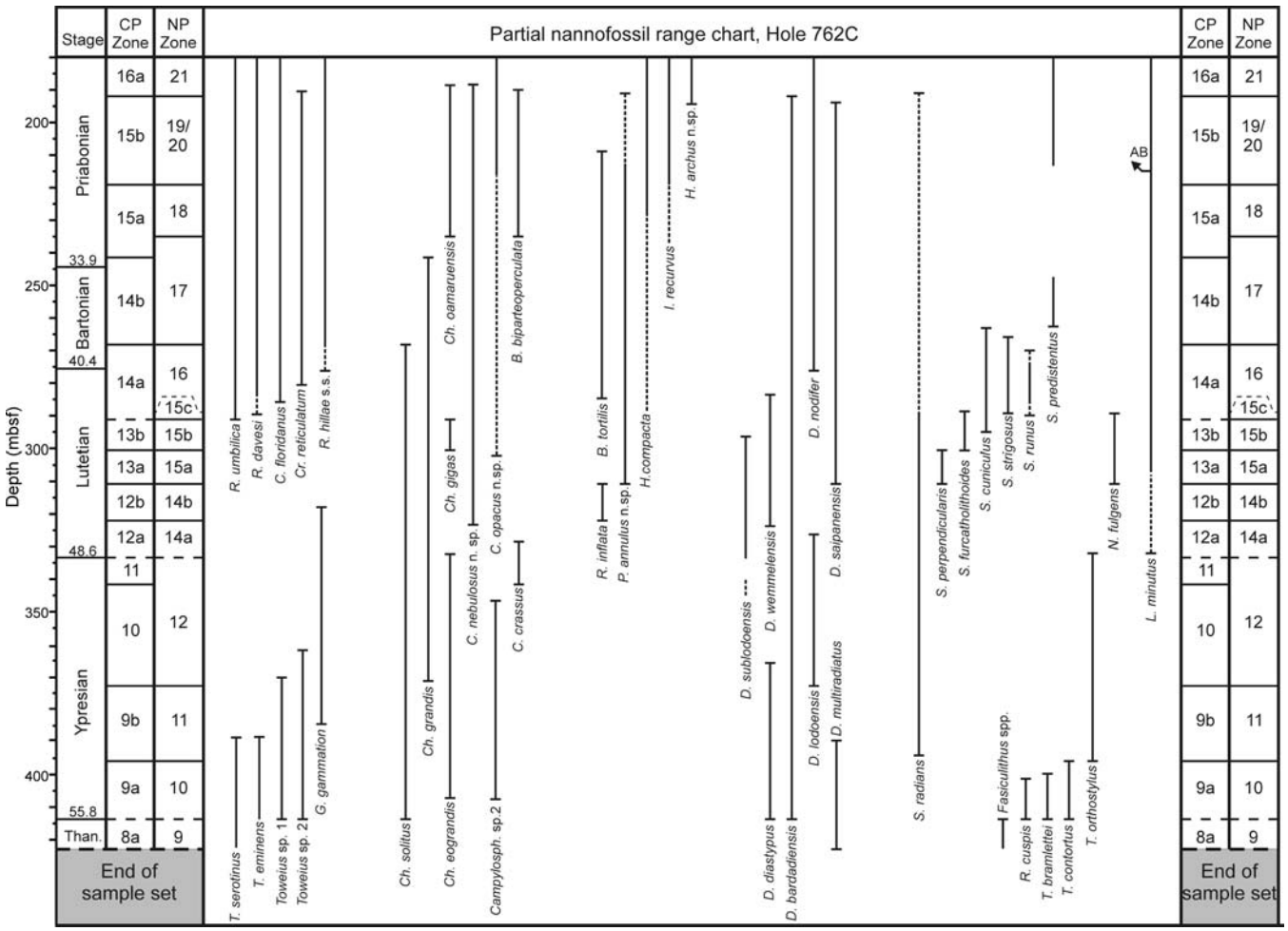

TEXT-FIGURE 3
Partial range zone of CP and NP marker taxa with select additional taxa, as observed in Hole 762C. Some new or recently named species are included for comparison. Core depth (msbf), epoch, CP zones and NP zones from left. Solid vertical lines show consistent occurrence. Dashed vertical lines indicate inconsistent or patchy occurrence. Solid horizontal lines indicate base or top of stratigraphic range.

Zones CP9a/NP10

The base of CP9a is based on the Los of both *Tribrachiatus contortus* and *Discoaster diastypus* at Hole 762C, and may be slightly younger than the base of NP10 (LO *Tribrachiatus (Rhomboaster) bramlettei* (Brönnimann and Stradner 1960) Bybell and Self-Trail 1995) (Ogg Ogg and Gradstein 2008). These bioevents were observed in the same sample (28-1-59cm, 412.59 mbsf) in Hole 762C, suggesting a hiatus is present. The LO of *D. diastypus* may serve as a proxy for the NP marker in sections where members of Rhomboasteraceae are rare. The secondary marker of Perch-Nielsen (1985), the HO of *Fasciculithus* spp., was also observed in this sample. Though these three bioevents are in good agreement at Hole 762C, this convergence may be due to the underlying hiatus and truncation of the true event depths.

The base of NP10 in Siesser and Bralower (1992) was marked by the LO of *Tribrachiatus contortus* (Stradner 1958) Bukry 1972 (27-3-99cm, 406.49 mbsf), as it was observed before the primary marker (LO *T. bramlettei*) (27-1-99cm, 403.49 mbsf) in that study. We observed the LO of *T. bramlettei* significantly below this depth (28-1-59, 412.59 mbsf). This discrepancy is likely a reflection of the general rarity of these forms at Site 762 and that relationship to probability of identification (see above). Raffi, Backman and Pälike (2005) also note that rarity and identification issues with intermediate forms may hinder use of the *Tribrachiatus* lineage. Agnini et al. (2007a) also questions the reliability of *T. bramlettei* as a primary marker taxa, suggesting that observed diachroniety may be a true environmental signal, or may be a preservational issue, related to dissolution of basal Eocene deposits in conjunction with the PETM.

Zones CP9b/NP11

The bases of both CP9b and NP11 are marked by HO of *Tribrachiatus contortus* (26-1-49cm, 398.30 mbsf). The secondary marker of Perch-Nielsen (1985), the LO of *Tribrachiatus orthostylus* (Bramlette and Riedel 1954) Shamrai 1963, is not concurrent in Hole 762C, but occurs immediately above (25-5-43cm, 394.93 mbsf). This secondary marker taxa

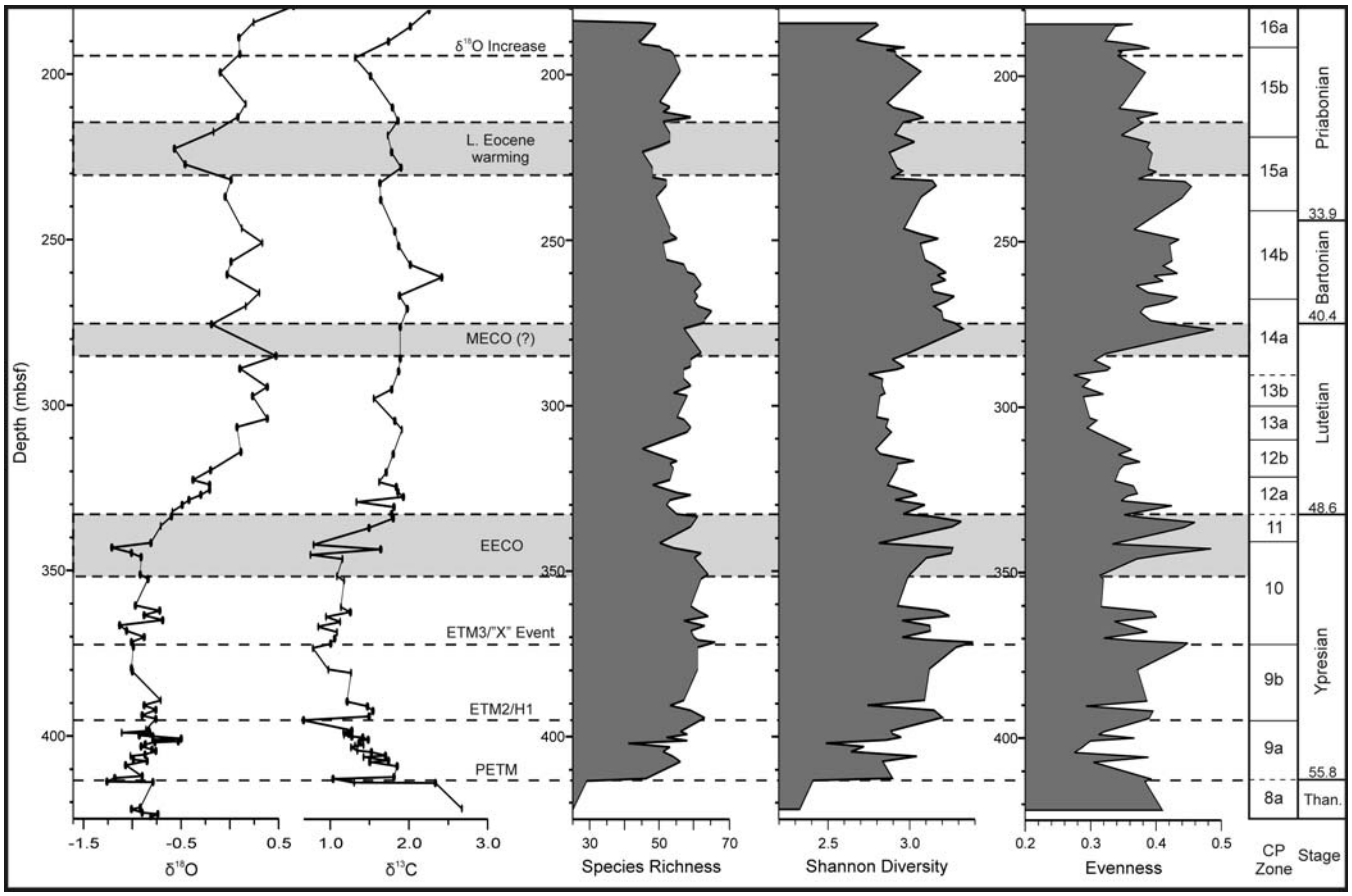

TEXT-FIGURE 4
δO and δC isotopic data from Site 762C (Thomas, Shakleton and Hall, 1992), with interpretation of isotopic events shown as dashed lines or shaded boxes. Species richness (S), Shannon diversity (H), and evenness are correlated to depth (msbf, left), nannofossil CP zones (right), and geologic epoch with boundary ages (Ma) (far right) (Ogg Ogg and Gradstein 2008).

may be more readily applied, as *T. orthostylus* is often more abundant than *T. contortus*.

Agnini et al. (2007a) have proposed the LO of *Sphenolithus radians* Deflandre in Grasse 1952 as an alternate biomarker for the base of NP11/CP9b. The LO of *S. radians* was observed in the same sample as the LO of *T. orthostylus* at Site 762 (Indian Ocean), and agrees with data from the southeast Atlantic (Agnini et al. 2007a), equatorial Pacific (Raffi, Backman and Pälike 2005) and western Tethys (Agnini et al. 2006).

Zones CP10/NP12

The LO of *Discoaster lodoensis* Bramlette and Riedel 1954 (23-3-51cm, 373.01 mbsf) marks the base of both CP10 and NP12. One of the secondary bioevents of Perch Nielsen (1985) for CP10, the LO of *Discoaster kuepperi* Stradner 1959, was concurrent with the LO of *D. lodoensis* and significantly more abundant at the base of its range that the primary marker, suggesting high potential as a proxy event. The second alternate marker of Perch-Nielsen (1985) (LO *Rhabdosphaera truncata* Bramlette and Sullivan 1961) was observed below *D. lodoensis* (24-1-54cm, 379.54 mbsf) and was relatively rare and sporadic through its range.

Zones CP11/NP13

These zones mark the first real taxonomic divergence of the two biozonation schemes, resulting in quite different interpretations of Hole 762C depending upon which scheme is employed. The base of CP11 is marked by the LO of *Coccolithus crassus* Bramlette and Sullivan 1961 (20-1-50cm, 341.50 mbsf) and the base of NP13 is marked by the HO of *T. orthostylus* (also the secondary marker for CP11 (Perch-Nielsen, 1985)*;* however, there is no apparent separation between this event and the base of NP14a (LO *Discoaster sublodoensis* Bramlette and Sullivan 1961). In fact, use of sample midpoints show that *D. sublodoensis* and *T. orthostylus* overlap at Hole 762C (Table 3).

Co-occurrence of *T. orthostylus* and *D. sublodoensis* (19-2-52cm, 333.52 mbsf) makes it impossible to identify NP13 as a discrete zone at Site 762. Identification of CP11 without concurrent identification of NP13 is possible in several ways: First, the HO of *T. orthostylus* may occur too high in the section (the HO of *T. orthostylus* is noted as unreliable by Wei and Wise (1989b), occurring between 51-54.8 Ma in the south Atlantic and Pacific Oceans). Second, *Discoaster sublodoensis* may show an early first occurrence at Site 762C, reducing the thickness of CP11 and compressing or eliminating NP13 (See be-

TABLE 3
Summary of Eocene nannofossil biostratigraphy at Site 762C. Standard CP Zonation of Okada and Bukry (1980) shown above. NP zonation of Martini (1971) with select subzones of Aubry (1991) below, with comparison of the current study (center) and original ODP results of Siesser and Bralower (1992) (right). Bioevents were observed in the italicized sample intervals. Event midpoints were extrapolated using the sample below (for LOs) or sample above (for HOs).

CP Zonation				This study			
Zone/Subzone		Event	Marker Taxa	Sample Interval	Base	Top	Midpoint
16	a	LO	*D. saipanensis ; D. barbadiensis*	4-3-100/4-3-50	193.00	192.50	192.75
	b	FO	*I. recurvus*	7-1-50/7-2-125	220.25	218.00	219.13
15	a	LO	*Ch. grandis*	10-1-50/9-1-46	246.50	236.96	241.73
	b	LO	*C. solitus*	12-3-125/12-3-50	269.25	268.50	268.88
14	a	FO	*R. umbilica*	13-2-71/14-1-5	284.05	276.71	280.38
	c	LO	*Ch. gigas*	14-6-50/14-5-115	292.00	291.15	291.58
	b	FO	*Ch. gigas*	15-3-48/16-1-48	303.48	296.98	300.23
13	a	FO	*N. fulgens*	16-4-45/17-1-51	313.01	307.95	310.48
	b	FO	*R. inflata*	17-5-148/18-1-50	322.50	319.98	321.24
12	a	FO	*D. sublodoensis*	19-2-52/19-2-125	334.25	333.52	333.89
11		FO	*C. crassus*	20-1-50/20-1-125	342.25	341.50	341.88
10		FO	*D. lodoensis*	24-1-54/23-3-51	379.54	373.01	376.28
	b	LO	*T. contortus*	26-1-49/25-5-43	398.30	394.93	396.62
9	a	FO	*D.diastypus*	28-1-59/28-1-125	413.25	412.59	412.92
	b	FO	*C. eodela; Rhomboaster spp.*	28-1-59/28-1-126	413.25	412.59	412.92
8	a	FO	*D. multiradiatus*	29-1-50	422.00		422.00

NP Zonation				This Study				Seisser & Bralower			
Zone/Subzone		Event	Marker Taxa	Sample Interval	Base	Top	Midpoint	Sample Interval	Base	Top	Midpoint
21		LO	*D. saipanensis* [5]	4-3-100/4-3-50	193.00	192.50	192.75	5-1-54/5-2-36	200.36	199.04	199.70
19/20		FO	*I. recurvus*	7-1-50/7-2-125	220.25	218.00	219.13	7-3-100-/7-4-100	223.00	221.50	222.25
18		FO	*Ch. oamaruensis* [4]	8-5-50/9-1-46	236.96	233.50	235.23	9x, CC/10-1-105	247.05	246.00	246.53
17		LO	*Ch. Solitus* [3]	12-3-125/12-3-50	269.25	268.50	268.88	12-5-100/12-6-100	273.50	272.00	272.75
16		LO	*B. gladius; N. fulgens* [2]	14-5-115/14-5-50	291.15	290.50	290.83	13x, CC/14-1-100	285.00	284.00	284.50
	c	LO	*Ch. gigas*	14-6-50/14-5-115	292.00	291.15	291.58	14-5-100/14-6-100	293.00	291.50	292.25
	b	FO	*Ch. gigas*	15-3-48/16-1-48	303.48	296.98	300.23	15x, CC/16-1-99	303.99	303.00	303.50
15	a	FO	*N. fulgens*	16-4-45/17-1-51	313.01	307.95	310.48	16-3-99/16x, CC	312.50	306.99	309.75
	b	FO	*R. inflata*	17-5-148/18-1-50	322.50	319.98	321.24	17-5-99/17x, CC	322.00	319.49	320.75
14	a	FO	*D. sublodoensis*	19-2-52/19-2-125	334.25	333.52	333.89	18-5-100/18-6-100	330.50	329.00	329.75
13		LO	*T. orthostylus*	19-2-52/19-1-125	333.52	332.75	333.14	19-2-100/19-3-100	335.50	334.00	334.75
12		FO	*D. lododensis*	24-1-54/23-3-51	379.54	373.01	376.28	22x, CC/23-1-100	370.50	369.50	370.00
11		LO	*T. contortus*	26-1-49/25-5-43	398.30	394.93	396.62	25-3-100/25-4-100	394.00	392.50	393.25
10		FO	*T?. bramlettii* [1]	28-1-59/28-1-126	413.25	412.59	412.92	27-3-100/27-4-99	408.00	406.49	407.25
9		FO	*D. multiradiatus*	29-1-50	422.00	NA	422.00	28x, CC/29-1-100	422.50	421.50	422.00

low). Third, there may be a hiatus that removed NP13 and the upper portion of CP11, leaving only the basal portion of CP11 in the biostratigraphic record. This issue may not have been recognized if only the CP zonation scheme was applied, but is quite obvious in the NP scheme, or when the two are used in conjunction.

Zones CP12a/NP14(a)

Both CP and NP zones are marked by the LO of *Discoaster sublodoensis*. As mentioned above, *D. sublodoensis* may occur too low in the section, and we observe the LO of *D. sublodoensis* even deeper (from CP10, 20-3-52, 344.52 msbf) than the LCO (19-1-125, 332.75m) used here to mark the base of these zones. A similar distribution is also observed by Agnini et al. (2006), Mita (2001), Wei and Wise (1990a), and Monechi and Thierstein (1985) in CP10 and CP11, prior to the LCO and base of CP12a. Only specimens with five straight, pointed rays were identified as *D. sublodoensis,* so it is unlikely that these early forms are misidentified specimens of *D. lodoensis* (Plate 8-13), though calcite overgrowth is potentially an issue for this species. Siesser and Bralower (1992) identified this bioevent slightly higher in the section (330.50 msbf) resulting in a modest NP13 in the original interpretation. It is possible that *D. sublodoensis* shows an early LO at Exmouth Plateau, reducing the thickness of both CP11 and NP13.

Zones CP12b/NP14(b)

The LO of *Rhabdosphaera inflata* Bramlette and Sullivan 1961 (17-5-148cm, 319.98 mbsf) marks the base of both CP12b and NP14b. Though relatively rare, this species is consistently present through its range.

Zones CP13(a-b)/NP15(a-c?)

The base of CP13(a) and NP15 is marked by the LO *Nannotetrina fulgens* (Stradner in Martini and Stradner 1960) Achuthan and Stradner 1969 (16-4-45cm, 307.95 mbsf). The secondary marker of Perch-Nielsen (1985) for the base of CP13a, the HO of *R. inflata* (17-1-51cm, 313.01 mbsf) occurs in the sample immediately below the LO of *N. fulgens*, and extrap-

TABLE 4
Summary of key Eocene nannofossil bioevents at Site 762C. Samples provided represent the interval and depth in which the event was observed. Mid-points may be extrapolated using sample list in Table 2. LO = lowest occurrence; LCO = lowest consistent occurrence; HO = highest occurrence; HCO = consistent common occurrence; AB= acme begin; AE = acme end; INC = increase; CO = cross-over.

Event	Species	Sample	Depth (msbf)
AB	*Clausicoccus spp.*	3-4-101	185.01
HO	*C. reticulatum*	4-1-123.5	190.24
LO	*H. archus*	4-4-50	194.00
HO	*D. saipanensis*		
HCO	*C. reticulatum*	5-1-50	199.00
LO	*R. oamaruensis*	6-4-50	213.00
INC	*L. minutus*	6-5-40	214.40
LCO	*I. recurvus*	7-1-50	218.00
HO	*H. lophota*		
LO	*Ch. oamaruensis*	8-5-50	233.50
LO	*I. recurvus*	9-1-46	236.96
LO	*H. reticulata*		
HO	*Ch. titus*		
HO	*D. strictus*		
HO	*Ch. grandis*	10-1-50	246.50
HO	*Cl. vanheckiae*		
LO	*Ch. eoaltus*	10-3-50	249.50
HO	*C. dela*		
HO	*P. inversus*		
HO	*N. minutus*	11-2-50	257.50
HO	*S. spiniger*		
	C. dela	11-3-125	259.75
LO	*D. stavensis*	11-5-50	262.00
LCO	*R. lockeri*	11-6-50	263.50
HO	*S. cuniculus*		
LCO	*D. bisectus*	12-1-51	265.51
HO	*S. strigosus*	12-2-51	267.01
HO	*C. prionion*	12-3-50	268.50
HO	*Ch. solitus*	12-3-125	269.25
LCO	*R. hillae*	12-4-50	270.00
LO	*S. pseudoradians*	13-1-50	275.00
HCO	*Ch. expansus*		
LO	*H. situliformis*	13-2-71	276.71
LO	*C. reticulatum*		
LCO	*R. umbilica*		
HO	*D. wemmelensis*	14-1-5	284.05
LO	*C. floridanus*	14-2-50	286.00
LO	*H. compacta*	14-3-126	288.26
LO	*S. strigosus*	14-4-55	289.05
HO	*S. furcatolithoides*		
HO	*N. fulgens*	14-5-115	291.15
HO	*Ch. gigas*	14-6-50	292.00
LO	*B. serraculoides*	15-1-48	293.98
LO	*S. cuniculus*		
LO	*Ch. gigas*	15-3-48	296.98
LO	*S. furcatolithoides*		
HO	*D. sublodoensis*		
LO	*Cr. opacus*	16-1-48	303.48
HO	*S. perpendicularis*		
LO	*Ch. titus*	16-4-45	307.95
LO	*D. saipanensis*		
LO	*N. fulgens*		
LO	*S. perpendicularis*		
HO	*R. inflata*	17-1-51	313.01
HO	*T. callosus*	17-4-52	317.52
HO	*T. magnicrassus*		
LO	*Nannotetrina spp.*	17-5-49.5	319.00
HO	*D. kuepperi*		
HO	*G. gammation*		
LO	*R. inflata*	17-5-148	319.98
LO	*Cl. vanheckiae*	18-1-50	322.50
LCO	*D. wemmelensis*	18-2-50	324.05
LO	*D. strictus*		
HO	*D. lodoensis*	18-3-125	326.25
LO	*C. protoannulus*	18-4-53	327.03
LO	*C. eopelagicus*	18-5-50	328.50
HO	*C. crassus*		

Event	Species	Sample	Depth (msbf)
INC	*D. scrippsae*	18-6-52	330.02
LO	*N. minutus*		
LO	*P. inversus*		
LO	*S. spiniger*		
LO	*L. minutus*	19-1-125	332.75
AE	*Discoaster spp*		
HO	*Ch. eograndis*		
HO	*T. pertusus*		
LCO	*D. sublodoensis*	19-2-52	333.52
HO	*T. orthostylus*		
HO	*D. binodosus*		
HO	*Ch. californicus*		
LO	*D. praebifax*	19-3-53	335.03
LO	*Cl. subdistichus*	19-4-52	336.52
LO	*D. scrippsae*		
HO	*L. nascens*		
LO	*C. crassus*		
HO	*H. lophota*	20-1-50	341.50
HO	*D. salisburgensis*		
HCO	*T. pertusus*		
HO	*L. reniformis*	20-2-50	343.00
AB	*Discoaster spp*	20-4-47.5	345.98
HO	*Chiphragmalithus spp.*		
LO	*R. dictyoda*	21-1-50	351.00
LO	*C. prionion*	21-2-50	352.20
HO	*N. rosenkrantzii*	22-5-46	366.46
HO	*D. diastypus*		
LO	*Ch. expansus*	22-6-53	368.03
HO	*Ch. bidens*	23-1-49.5	370.00
LO	*C. grandis*	23-2-49	371.49
LO	*P. larvalis*		
LO	*N. dubius*	23-3-51	373.01
LO	*D. kuepperi*		
LO	*D. lodoensis*		
LO	*Chiphragmalithus spp.*		
LO	*G. gammation*	24-1-54	379.54
LO	*L. reniformis*		
HO	*C. eodela*		
HO	*T. eminens*	25-1-50.5	389.01
HO	*D. multiradiatus*	25-2-47.5	390.48
HO	*D. lenticularis*		
HO	*T. serotinus*		
LO	*D. deflandrei*	25-3-52	392.02
LO	*T. magnicrassus*		
LO	*S. radians*	25-4-125	394.25
HCO	*T. eminens*		
LO	*T. orthostylus*	25-5-43	394.93
HO	*T. contortus*	26-1-49	398.30
LO	*U. jordanii*		
LO	*S. editus*	26-2-49	399.17
HO	*Rhomboaster spp.*	26-4-47	401.06
LO	*C. dela*	27-1-50	403.00
LO	*Ch. eograndis*	27-3-50	406.00
LO	*D. elegans*		
LO	*Cl. fenestratus*	28-1-59	412.57
LO	*C. eodela*		
LO	*E. formosa*		
HO	*Fasciculithus spp.*		
LO	*D. barbadiensis*		
LO	*D. diastypus*		
LO	*L. nascens*		
LO	*T. bramlettei*		
LO	*T. contortus*		
LO	*S. moriformis*	28-1-125	413.25
HO	*P. bisulcus*		
HO	*E. robusta*	29-1-50	422.00
LO	*D. multiradiatus*		

TABLE 5
Sample midpoints of isotopic excursion events identified at Site 762C from δC and δO data of Thomas Shackleton and Hall (1992). Dates originally given in the CK95 or BKSA95 timescales were also converted to the GPTS of Ogg Ogg and Gradstein (2008). Primary references used to identify and date isotopic events given at far right.

Isotopic Event	Midpoint (msbf)	Age 2008 GPTS, Ogg et al	Age CK95/BKSA95	Reference
Oi-1, Step 1	187.00	33.93	33.75	Pearson et al. 2008
End Late Eocene warming/ "Vonhof" cooling event	213.30	35.50	35.50	Vonhof et al. 2000 Zachos et al. 2001
MECO?	277.00	39.87	40.00	Bohaty et al. 2009 Jovane et al. 2007
End EECO	331.22	49.78	49.00	Bohaty & Zachos 2003
ETM3/"X" event/Event "K"	372.35	52.88		Galeotti et al. 2010
ETM2/H1/ELMO	394.85	53.91	53.44	Lourens et al. 2005
PETM	412.65	55.74	54.98	Cramer et al. 2003

olation of midpoints makes these events nearly isochronous. CP13 is subdivided into CP13b and CP13c by the LO and HO of *Chiasmolithus gigas* (Bramlette and Sullivan 1961) Radomski 1968, respectively, and these subzonal markers are often similarly applied to NP15. The HO of *Ch. gigas* and the LO of *Reticulofenestra umbilica* (Levin 1965) Martini and Ritzkowski 1968 were observed in the same sample (292.00 msbf), suggesting a hiatus through this subzone. A very thin interval can be attributed to NP15c (Table 3), as the NP and CP schemes use different taxa for the boundaries above; however, this thin (~0.75m) interval may be an artifact of sample spacing or rarity of marker taxa.

Zones CP14a/NP16

The base of CP14a is marked by the LO of *R. umbilica*, while the base of NP16 is marked by the HO(s) of *B. gladius* and/or *N. fulgens*. The primary zonal marker, *Blackites gladius* (Locker 1967) Varol 1989, was not observed in this section, so this zone has been identified by the HO *N. fulgens*, though the genus as a whole is notably rare at this locality. The LO of *R. umbilica* (14-6-50; 292.00 mbsf), the HO of *N. fulgens* (14-5-115cm, 291.15 mbsf) and the HO of *Ch. gigas* (14-6-50cm, 292.00 mbsf) show very little stratigraphic separation in Hole 762C, indicating a hiatus comprising all of CP13c and at least a significant portion of NP15c.

There appears to be a significant difference in the location of the NP16 boundary between this study and Siesser and Bralower (1992) (Table 3), which uses the HO of *Nannotetrina* spp. to identify the base of NP16. The HO of *N. fulgens* and the HO of *Nannotetrina* spp. are nearly congruent between studies (2.35 and 0.95m separation, respectively), and strict application of the NP zonation scheme resolves this apparent offset. The HO of *Nannotetrina* spp. may be observed higher in the section than the HO of *N. fulgens*, which highlights the biostratigraphic issues that occur with rare taxa, where nannofossil workers are often required to use alternative markers that may or may not be well correlated to primary events.

Zones CP14b/NP17

The HO *Chiasmolithus solitus* (Bramlette and Sullivan 1961) Locker 1968 (12-3-125cm, 269.25 mbsf) marks the base of both CP14b and NP17. This species was rare at Site 762 and was often not identified until > 3 traverses. Siesser and Bralower (1992) identify the HO of *Ch. solitus* significantly lower in the section (13CC, 284.00 mbsf), and do not use the HO of this species to mark the NP17 boundary, due to its rarity. Differences in the apparent range are likely related to the number of FOVs and probability of finding rare taxa. This results in low confidence when picking the CP14b/NP17 boundary, particularly at mid- to low-latitude sites where *Chiasmolithus* spp. may be rare (Agnini et al. 2011; Villa et al. 2008, Tremolada and Bralower 2004). Siesser and Bralower (1992) instead use two events as a proxy for the NP17 boundary: the LOs of *Cribrocentrum (Reticulofenestra) reticulatum* (Gartner and Smith 1967) Perch-Nielsen 1971 and *Helicosphaera compacta* Bramlette and Wilcoxon 1967, which they identify at 12-6-100cm (273.50 mbsf) and 12-5-100cm (272.00 mbsf), respectively. The authors' events are reasonably near our observed HO of *Ch. solitus* (269.25 msbf); however, these bioevents are placed in CP14a in this study.

Tremolada and Bralower (2004) suggest that the HO of *Ch. solitus* is time transgressive over varying paleolatitudes: com-

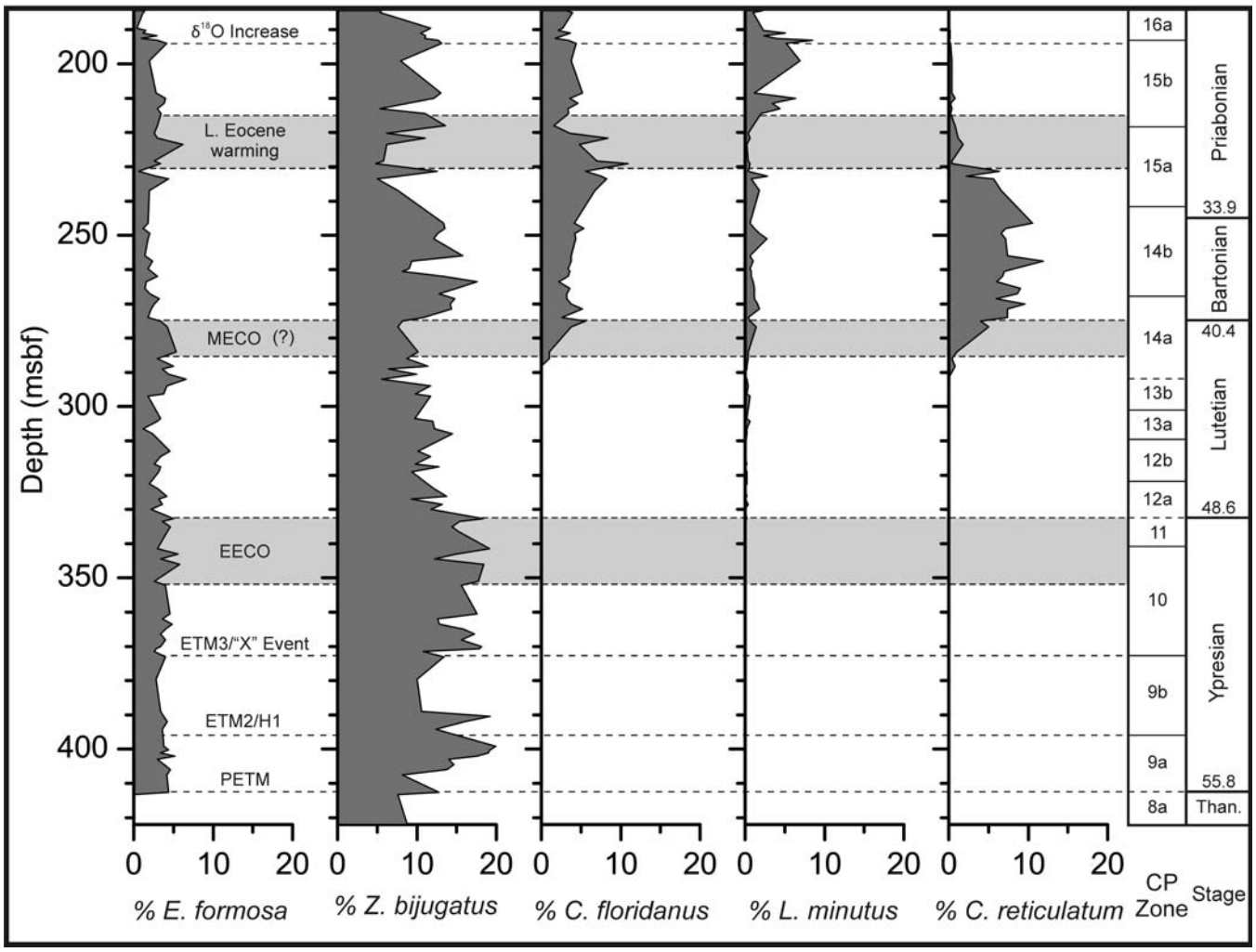

TEXT-FIGURE 5
Abundance patterns of select nannofossil species correlated to depth (msbf, left), nannofossil CP zones (right), and geologic epoch with boundary ages (Ma) (far right) (Ogg Ogg and Gradstein 2008). Isotopic events identified in text-figure 3 are shown as dashed lines or shaded boxes. Data is expressed as percentage of 500 specimens.

mon at high latitudes until extinction, but rare and sporadic at lower latitudes prior to the HO, so that the event becomes older as latitude decreases. The predominantly mid- to low-latitude assemblage identified at Site 762 suggests that such rarity and/or diachroniety may affect the HO of this biostratigraphic marker.

These issues highlight the need for a reliable alternative bioevent. The HO of *Discoaster bifax* Bukry, 1971 has also been used to mark the base of CP14b, but *D. bifax* can be extremely rare, and few specimens were identified in Hole 762C. In addition, Wei and Wise (1989a) suggest that the morphological transition between *Discoaster praebifax* Wei and Wise 1989 and *D. bifax* may hinder its use. Alternatively, the FCO of *Reticulofenestra hillae* Bukry and Percival 1971 and the LO of *Dictyococcites (Reticulofenestra) bisectus* (Hay et al. 1966), Bukry and Percival 1971 (< 10µm) were both observed in sample 12-4-50cm (270.0 mbsf), and closely approximate the HO of *Ch. solitus* (12-3-125, 269.25m). Bown (2005) and Marino and Flores (2002) also identify the LO of *D. bisectus* just above the HO of *Ch. solitus*, suggesting potential for this species as an alternate marker for CP14b/NP17.

Zones CP15a/NP18

The base of CP15a is marked by the HO *Chiasmolithus grandis* Perch-Nielsen 1971 (10-1-50cm, 246.5 mbsf), while the base of NP18 is marked by the LO *Chiasmolithus oamaruensis* (Deflandre 1954) Hay et al. 1966 (8-5-50cm, 233.5 mbsf). These events are shown as nearly contemporaneous in the 2008 Time Scale (Ogg Ogg and Gradstein 2008). The stratigraphic separation between these bioevents in Hole 762C may be artificially expanded by poor recovery of Core 9x (text-figure 2). In addition, *Ch. grandis* and *Ch. oamaruensis* are quite rare near their HO and LO, respectively, and were often only identified after >3 traverses across a slide. Use of sample mid-points greatly reduces this separation, but still results in stratigraphic offset and uncertainty in placement of zonal boundaries (text-figure 2). Though some specimens of *Ch. oamaruensis* are readily identified, the narrow angle between cross-bars that defines this species can be difficult to distinguish from similar taxa

TABLE 6
Summary of key nannofossil abundance trends through the PETM interval, along with species richness and Shannon diversity. Columns A and B give absolute and relative (%) abundance of taxa, respectively. Maximum δC excursion occurs at 412.65 msbf, with shaded row highlighting nannofossil sample that most closely approximates this interval (412.59 msbf), with the nannofossil assemblage showing significant increases in species richness and

Sample Interval	Depth (mbsf)	Species Richness (S)	Diversity (H)	*Z. bijugatus*		*Fasciculithus* spp.		*Discoaster* spp.		*Chiasmolithus* spp.		*Sphenolithus* spp.		*Toweius* spp.		*Ericsonia* spp.		*Ericsonia formosa*	
				A	B	A	B	A	B	A	B	A	B	A	B	A	B	A	B
27-2-50	404.5	51	2.64	73	14.6	0	0	21	4.2	8	1.6	11	2.2	112	22.4	55	11	19	3.8
27-3-50	406	54	3.04	69	13.8	0	0	39	7.8	18	3.6	12	2.4	133	26.6	61	12.2	23	4.6
27-4-50	407.5	56	2.84	41	8.2	0	0	18	3.6	13	2.6	10	2	113	22.6	76	15.2	21	4.2
28-1-59	412.59	46	2.90	64	12.8	1	0.2	57	11.4	12	2.4	17	3.4	105	21	54	10.8	22	4.4
28-1-125	413.25	29	2.41	38	7.6	170	33.9	25	5	4	0.8	2	0.4	119	23.8	15	3	0	0
29-1-50	422	25	2.33	44	8.8	160	31.9	9	1.8	2	0.4	0	0	140	27.9	20	4	0	0

such as *Ch. altus* Bukry and Percival 1971 and *Ch. eoaltus* Persico and Villa 2008, which have a larger angle between cross-bars. This uncertainty, combined with rarity, can create difficulties when applying this marker. Issues concerning the biostratigraphic application of *Ch. solitus, Ch. grandis* and *Ch. oamaruensis,* as well as potential resolutions, are discussed in detail in Fornaciari et al. (2010).

Zones CP15b/NP19/20

The LO of *Isthmolithus* Deflandre in Deflandre and Fert 1954 marks the base of both CP15b and NP19/20. The LCO is used to mark the base of the (sub)zone at Site 762 (7-1-50cm, 218.0 mbsf), as isolated specimens were observed deeper in the section (236.96 and 223.46 msbf). Agnini et al (2011), Fornaciari et al. (2010) and Villa et al. (2008) identify rare occurrences of *I. recurvus* in CP15a, and also use the LCO to mark the base of the subzone.

The secondary CP marker of Perch-Nielsen (1985), the HO of *Cr. reticulatum* (4-1-123.5cm, 190.24 mbsf), was observed significantly above the LCO of *I. recurvus*. This stratigraphic relationship is also shown by Fornaciari et al. (2010), Cascella and Dinarés-Turell (2009), Villa et al. (2008), Marino and Flores (2002a, b), Berggren et al. (1995), and Wei and Wise (1989b). Calibration of the HO of *Cr. reticulatum* by Berggren et al (1995) dates the HO of this species approximately 1 mya earlier at high latitudes than at low latitudes.

Zones CP16a/NP21

The CP16a and NP21 boundaries are marked by the HO of *Discoaster saipanensis* Bramlette and Riedel 1954 (and/or the HO *Discoaster barbadiensis* (Tan 1927) emend. Bramlette and Riedel 1954). The HO of *D. saipanensis* (and *D. barbadiensis*) has been problematic at Site 762. Very rare and sporadic specimens of both species were observed quite high in the section, through the highest sample in this study (3-1-49cm; 184.49 mbsf) and through sample 2-2-100cm (172.5 mbsf) in the original interpretation. This difficulty in boundary placement due to rarity has also been noted by Dunkley Jones et al. (2008) and Siesser and Bralower (1992), and may be affected by reworking at Site 762. Rare but consistent specimens of *D. saipanensis* and *D. barbadiensis* were observed through 4-3-100cm (193.0 mbsf), marking the HCO of both species, and the base of CP16a in this study. The upper two samples in this study are located within CP16a, as both contain *Reticulofenestra oamaruensis* (Deflandre in Deflandre and Fert 1954) Stradner in Haq 1968 and show a considerable increase in *Clausicoccus* spp., marking the base of this acme event.

Synthesis

Application of both the Okada and Bukry (1980) CP zonation and the Martini (1971) NP zonation facilitated the identification of three stratigraphic hiatuses. Hiatus A was identified with the CP zonation, by the concurrent LOs of *C. eodela, Rhomboaster* spp., and *D. diastypus* (412. 59 msbf) and indicates the absence of subzone CP8b. Hiatus B was identified with the NP zonation, based on the convergence of the HO of *T. orthostylus* and the LO of *D. sublodoensis* (333.52 msbf), and indicates the absence of NP13. Hiatus C was identified using both the CP and NP zonation, as both the LO of *R. umbilica* and *N. fulgens* converge with the HO of *Ch. gigas*, including the absence of subzone CP13c/NP15c. While hiatus C can be identified with either zonation scheme, both the NP and CP zonation are insufficient to readily identify all three hiatuses. These schemes become more robust when used in conjunction, due to the greater number of nannofossil markers. This allows both greater biostratigraphic resolution when events are offset (LO *R. umbilica*/CP14a and *N. fulgens*/NP16), and greater confidence when two bioevents are nearly isochronous (HO *Ch. gigas*/CP15a and LO *Ch. oamaruensis*/NP18).

The standard CP and NP nannofossil zonation schemes provided a series of bioevents that are extremely useful in biostratigraphy, most of which are consistent, reliable, and well-calibrated; however, some of these taxa are shown to be inconsistent in this research and in several other studies, such as *D. sublodoensis*, *Ch. oamaruensis*, and *T. bramlettei.* This is well illustrated when comparing the Site 762 nannofossil biostratigraphy of Siesser and Bralower (1992) to this reexamination, as all significant divergence in interpretations are linked to these problem taxa.

The placement of some zonal boundaries is compromised simply by the rarity of the biomarker that defines it. Such rarity is often linked to paleoecological preference, such as temperature (Villa et al. 2008, Tremolada and Bralower 2004; Perch-Nielsen 1985). The CP and NP biozonation schemes each utilize three species of *Chiasmolithus* (*Ch. gigas*, *Ch. grandis*, *Ch. oamaruensis*, and/or *Ch. solitus)*. While most morphological characteristics are extremely diagnostic, the cool-water preference of this genus makes these taxa quite rare at mid- to low-latitude sites, particularly during the warm Eocene where latitudinal climate zones were expanded poleward. We compensated for the rarity of such taxa by increasing the number of traverses across a slide; however, additional time is not always available for analysis, and more readily identifiable proxy events will greatly improve biostratigraphic confidence. Paleoecological restriction

TABLE 7
Summary of taxa groupings applied in this study. Taxa with questionable or disputed affinity have not been included (see Villa et al. 2008), but abundance patterns are compared to taxa with more confident paleoecological affinities. Eocene-Oligocene transitional group from Dunkley Jones et al. (2008, fig. 6). *Pemma papillatum* and *Varolia maceleodii* are not included as they are absent at Site 762C.

Reticulofenestra Group	Warm Taxa	Cool Taxa	Holococcoliths	E-O transitional (Group 1)
Reticulofenestra spp. *Dictyococcites* spp. (*D. bisecta, D. stavensis, D. scrippsae)*	*Discoaster* spp. *Sphenolithus* spp. *E. formosa*	*Chiasmolithus* spp. *I. recurvus* *R. daviesii*	*Z. bijugatus* *Lanternlithus* spp.	*C. protoannulus* *R. dictyoda* *L. minutus* *Z. bijugatus*

is also seen in this open-ocean site with respect to the shelf/neritic) preference of Rhabdosphaeraceae. While marker taxa such as *B. gladius* and *R. truncata* may be quite useful in some sections (such as Tanzania [Bown and Dunkley Jones 2006; Bown 2005]), both were extremely rare and sporadic at Site 762. While rarity can be mitigated with increased FOVs, the sporadic nature of these taxa greatly reduced the confidence of these bioevents, and neither could be used in the biostratigraphic scheme at Site 762. Some markers appear rare despite their ecological preference: The warm-water, oligotrophic, open-ocean setting of this site suggests *D. bifax* should be relatively common; however, this species was essentially absent from Hole 762C and rarity prohibited use of this bioevent in the CP zonation scheme.

In addition to rarity, diachroniety may affect other markers in the standard zonations. The relative stratigraphic relationship of individual species of the *Tribrachiatus* lineage may be consistent, but the potential diachroniety of *T. bramlettei* (Agnini et al. 2007a), and the rarity of this group in many sections, warrants calibration of alternate bioevents. Fornaciari et al (2010), Villa et al (2008), Tremolada and Bralower (2004) and others also identify potential diachroniety in *Ch. solitus*, with HO in low latitudes prior to high-latitude sites. Though issues with diachroniety (Berggren et al. 1995) prohibits use of the HO of *Cr. reticulatum* as a proxy for the LO of *I. recurvus*, the relative overlap in range may have potential for use as a qualitative paleotemperature proxy, with the greatest overlap at lower latitudes.

Well-calibrated secondary markers are needed to act as substitutes for rare and/or diachronous bioevents. This would allow for robust age comparison in different paleoceanographic environments or for marker taxa that are rare near their LO or HO. Both the LO of *T. orthostylus* and the LO of *S. radians* appear to be good alternate bioevents for the HO of *T. contortus,* as both closely approximate this event and are frequently more abundant and consistent than *T. contortus*. *Discoaster lodoensis* can be rare near it's LO, and the potentially more abundant secondary event, the LO of *D. kuepperi*, can help identify this zonal boundary. Both the LO of *Cr. reticulatum* and the LO of *D. bisectus* have potential to approximate the HO of *Ch. solitus* when that primary marker is rare, but each will need to be assessed from several sites to ensure consistency and to calibrate the age offset from *Ch. solitus*, particularly at varying latitudes.

Discoaster sublodoensis appears to be the most inconsistent bioevent in both zonation schemes and should be applied tentatively: This species marks the base of CP12a/NP14a, but has been identified as low as CP10/NP12 at Site 762 and in several sections globally, at both high- and low-latitudes, even with a strict taxonomic definition. Potential proxies from Site 762 include the HO of *C. crassus* and the LO of *S. spiniger*, but both events require additional calibration.

Additional potential proxies may be present in well known species, but a large body of recently named Eocene taxa (>70 species) (Fornaciari et al. 2010; Shamrock 2010; Persico and Villa 2008; Bown Dunkley Jones and Young 2007; Bown and Dunkley Jones 2006; Bown 2005, and this work) may also contain potential alternative bioevents. Currently, the CP and NP schemes each give a stratigraphic resolution of > 1 My through the Eocene (15-16 events in >20 My). In addition to identifying taxa that may serve as proxies for existing biomarkers, we should also strive to calibrate and integrate additional events, in hopes of increasing current the biostratigraphic resolution to < 0.5 My. The best hope for such improvement may be in the development of the high-resolution, high-precision orbitally –tuned biochronology (Galeotti et al. 2010; Pälike et al. 2006; Raffi et al. 2006), which will greatly increase our understanding of the placement of bioevents in the biostratigraphic record.

Nannofossil abundance trends

Paleoceanographic events and environmental response

The Eocene Epoch is a critical transition period from the global greenhouse conditions of the Late Cretaceous and early Paleogene to the icehouse of the later Cenozoic. The lower boundary is marked by a hyperthermal event, the PETM, and the upper boundary by cooling associated with the onset of Antarctic glaciation. As concern with anthropogenic CO_2 emissions rises, interest in Eocene and mid-Pliocene climate has increased as the most recent greenhouse analogue; however, a large proportion of research has focused on the conditions governing its lower and upper boundaries with the Paleocene and Oligocene, respectively.

Between these climatic extremes, the Eocene has been viewed as a time of relatively uniform decline in global temperatures and CO_2, setting the stage for the icehouse transition. It is now understood that the Eocene was not a period of monotonous climatic decline, but rather consisted of several distinct periods of warming and cooling (Galeotti et al. 2010; Bohaty et al. 2009; Nicolo et al. 2007; Lourens et al. 2005; Bohaty and Zachos 2003; Zachos et al. 2001; and others). Calcareous nannofossil assemblages also show fluctuations in diversity and dominance through the Eocene (Bown and Pearson 2009; Jiang and Wise 2009; Agnini et al. 2006; Tremolada and Bralower 2004; and

others) and many fluctuations observed in Hole 762C correlate closely with known isotopic excursions (discussed below), and are likely in response to environmental variability. These events include the PETM, the ETM2 (H1) and ETM3 ("X") hyperthermal events, the EECO, the MECO, and a period of warming within an overall cooling trend within the Priabonian. The depths of these events as identified in Hole 762C, as well as the event data and primary references, are given in Table 5. Changes in nannofossil diversity through the Eocene broadly mirror changes in temperature, as reflected in $\delta^{18}O$ values, with diversity increasing during warming events and decreasing during cool periods, particularly within the Lutetian (text-figure 4). Isotopic data ($\delta^{18}O$ and $\delta^{13}C$) are taken from the original Scientific Results of Site 762 (Thomas, Shackleton and Hall 1992). Many planktic taxa show assemblage trends that fluctuate across latitudinal climate zones, and have been seen to contract and expand with changes in climate (Kahn and Aubry 2004; Lees 2002; Aubry 1992; Wei and Wise 1990b; Haq and Lohmann 1976); however, the direct relationship between diversity, temperature, and nutrient levels may be difficult to distinguish (Villa et al. 2008). These intervals and the calcareous nannofossil response will be discussed in greater detail below.

Paleocene-Eocene thermal maximum (PETM)

Interest in the PETM and the associated CIE (carbon isotope excursion) that mark the Paleocene-Eocene boundary has generated several recent studies on nannofossil assemblage changes through this event. Raffi, Backman and Pälike (2005) synthesized these assemblage changes from several studies across 18 sites in the northern Indian, Atlantic, Pacific, and Mediterranean. Additional research has confirmed these shifts, adding further evidence to several distinct, seemingly global, assemblage changes across the PETM (Bown and Pearson 2009; Jiang and Wise 2009; Agnini et al. 2007a, 2007b; Agnini et al. 2006; Gibbs et al. 2006a, 2006b; Raffi, Backman and Pälike 2005; Tremolada and Bralower 2004). To date, the eastern Indian Ocean has been excluded from such studies.

Many PETM specific studies were conducted at centimeter-scale sample spacing in order to capture the rapid sequence of bioevents across this isotopic excursion, resulting in a robust set of nannofossil events, including identification of short ranging 'excursion' taxa and assemblage turnovers. Poor recovery of Cores 28 and 29 (22.1% and 48.4%, respectively) (text-figure 2) makes the Exmouth Plateau less than ideal for studying the PETM interval, and sample spacing for biostratigraphy and isotope data is much greater than usually seen in PETM-specific studies; however, nannofossil studies covering longer time intervals are often conducted at lower resolution, and it is important to understand which bioevents can be identified across the PETM at a greater sample spacing. Despite poor core recovery, a notable $\delta^{13}C$ excursion (-1.3 ‰, 412.65 msbf) is accompanied by an $\delta^{18}O$ shift of -0.39‰ (Thomas, Shackleton and Hall 1992), indicating that this event may be partially captured at this locality (text-figure 4). The overall magnitude of the CIE at Site 762 is low relative to several other sites (Ex: Site 690 = ~2.4‰, Site 1263 = ~2.5‰), and may be truncated by Hiatus A, between 413.25-412.59 msbf (text-figure 2, Table 3). This hiatus includes all of CP8b, but may also include a portion of CP8a and/or CP9a (See biostratigraphy section).

Several authors noted a barren interval associated with the CIE at other localities (Jiang and Wise 2009; Monechi and Angori 2006; Kahn and Aubry 2004), as well as the selective dissolution of more fragile taxa across and above the PETM boundary (Agnini et al. 2007b, Agnini et al. 2006; Tremolada and Bralower 2004). This includes low species richness and dominance of dissolution resistant taxa such as *Fasciculithus, Discoaster* and *Sphenolithus* spp. (Bown and Pearson 2009; Jiang and Wise 2009; Monechi and Angori 2006; Kahn and Aubry 2004). Raffi and De Bernardi (2008, fig 5) attribute these observations to truncation of the basal PETM sequence from acidification and dissolution, and this is likely responsible for at least a portion of Hiatus A.

A notably reduced and poorly preserved nannofossil assemblage is also observed in Hole 762C just below and at the CIE, with the lowest species richness (25 and 29) and Shannon H diversity (2.33 and 2.41) of the entire Eocene section (Table 6, text-figure 4). In general, the assemblage is quite similar to that described from Site 1263 (Raffi and De Bernardi 2008), composed primarily of etched *Discoaster*, *Coccolithus*, and *Toweius* spp., with anomalously high abundance of *Fasciculithus* spp. (Table 6). At Site 762, *Fasciculithus* spp., *Toweius eminens* (Bramlette and Sullivan 1961) Perch-Nielsen 1971, *D. multiradiatus*, and *Prinsius bisulcus* (Stradner 1963) Hay and Mohler 1967 account for 53.0% and 48.5% of the assemblage immediately below and during the CIE, respectively. Enrichment in *Fasciculithus* spp. (Table 6) is also noted by Tremolada and Bralower (2004) and Bralower (2002). *Toweius* spp. are also notably abundant, particularly large specimens (8-14 μm) of *T. eminens* (Table 6). Both species richness and diversity increase immediately above the PETM interval (46 and 2.90, respectively).

One of the most consistently noted changes in the nannofossil assemblage at various sites is the 'crossover' between *Fasciculithus* spp. and *Zygrhablithus bijugatus* (Deflandre Deflandre and Fert 1954) Deflandre 1959 across the PETM. Many authors note the HO of *Fasciculithus* spp. near the top of the CIE, and a sharp increase in *Z. bijugatus* in the upper portion of, or immediately above, the CIE (Bown and Pearson 2009; Jiang and Wise 2009; Raffi and De Bernardi 2008; Agnini et al. 2007a, b; Agnini et al. 2006; Monechi and Angori 2006; Raffi, Backman and Pälike 2005; Tremolada and Bralower 2004; Bralower 2002; Monechi, Angori and von Salis 2000). This change is also observed at Site 762, though the crossover is more apparent for the sharp decrease and abrupt extinction in *Fasciculithus* spp., from nearly 34% during the excursion to <0.01% above the recovery. The increase in *Z. bijugatus* may be less pronounced due to its moderate abundance at the base of the section (8.8%, Table 6), though the relative abundance does increase up to 20% within CP9a and into CP 9b (NP11) (text-figure 5).

Sphenolithus spp. are rare but rebound during the CIE recovery, also showing an inverse relationship to *Fasciculithus* spp., though of lesser magnitude than *Z. bijugatus* (text-figure 6). *Sphenolithus* spp. are absent below the CIE and < 0.4% at the base of the excursion, but recover to 3.4% just above the event (Table 6). Similar changes were noted by Bown and Pearson (2009), Jiang and Wise (2009), Agnini et al. (2007a, 2007b), Gibbs et al. (2006a), Tremolada and Bralower (2004), and Bralower (2002). Agnini et al. (2007b) and Bralower (2002) suggest the increase in both *Sphenolithus* spp. and *Z. bijugatus* indicates a return to more oligotrophic conditions above the CIE

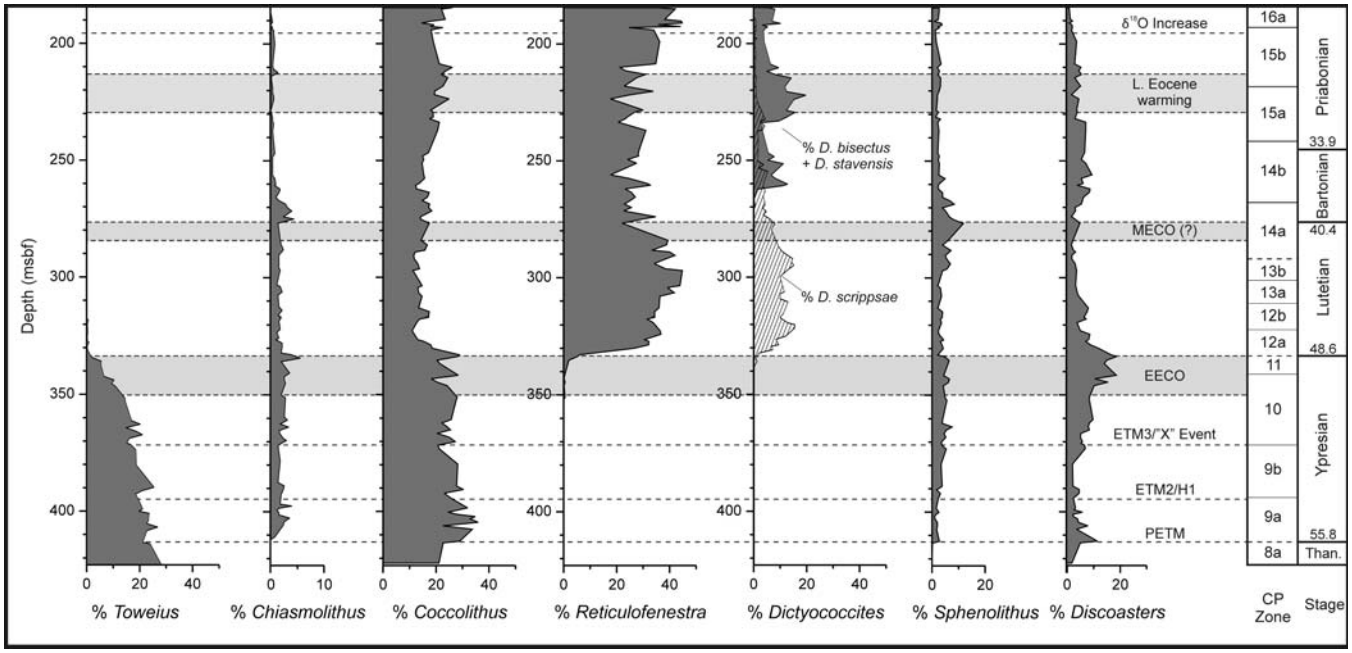

TEXT-FIGURE 6
Abundance patterns of select nannofossil genera correlated to depth (msbf, left), nannofossil CP zones (right), and geologic epoch with boundary ages (Ma) (far right) (Ogg Ogg and Gradstein 2008). Isotopic events identified in text-figure 3 are shown as dashed lines or shaded boxes. Data is expressed as percentage of 500 specimens

Other significant trends include an increase in *Chiasmolithus* spp. (Table 6) above the CIE, also noted in Jiang and Wise 2009. *Ericsonia* spp. increases from ~3% at the base of the CIE to > 10% directly above (Table 6), linked to both the LO of *Ericsonia formosa* (Bukry and Bramlette 1968) Romein 1979 and an increase in *Ericsonia cava* (Hay and Mohler 1967) Perch-Nielsen 1969, also noted by Agnini et al. (2007b), Tremolada and Bralower (2004), and Bralower (2002). These authors, as well as Bown and Pearson (2009) and Agnini et al. (2007a), also note a relative increase in *Discoaster* spp. At Site 762, peak abundance of *D. multiradiatus* (~3%) and *Discoaster* spp. (11.4%) both occur during peak $\delta^{13}C$ excursion (412.59 msbf) (Table 6, text-figure 6).

In summary, reduced preservation through this interval is indicated by enrichment in, and overgrowth on, dissolution resistant forms, such as *Fasciculithus, Discoaster* and *Chiasmolithus* spp. Minimum Shannon diversity and species richness for the entire Eocene section in Hole 762C occur just below the PETM. This is attributed to increased acidity associated with the hyperthermal event and subsequent dissolution of less resistant taxa in sediment near the sediment-water interface (Steinmetz 1994). Both rebound significantly at/just above peak CIE (Table 6, text-figure 4), linked to increases in *Coccolithus* spp., *Discoaster* spp., *Sphenolithus* spp., and *Z. bijugatus* (text-figures 4, 5). Several additional changes are observed during the PETM including key dominance crossovers between *Fasciculithus* spp. and *Z. bijugatus*/*Sphenolithus* spp., as well as a long-term decline in *Toweius* spp. during the PETM recovery. Poor core recovery and relatively coarse sample spacing does not permit resolution of the many short-lived species and events identified in other high-resolution, PETM-specific studies. It should be noted, however, that observations in Hole 762C indicate this event can be readily identified through even poorly recovered or coarsely-sampled intervals (Jiang and Wise 2009).

ETM2/H1

Though the PETM is the most intensely studied event of the latest Paleocene-early Eocene, it is now known that several less well-defined hyperthermal events occurred through the Ypresian (Bohaty et al. 2009; Sluijs et al. 2008; Nicolo et al. 2007; Lourens et al. 2005; Cramer et al. 2003). The most pronounced of these is the H1 event (Cramer et al. 2003), or ETM2 (Eocene thermal maximum 2) (Sluijs et al. 2008), and the associated clay-rich Elmo horizon (Lourens et al, 2005). This event has an associated $\delta^{13}C$ excursion ~= 1.0 ‰ (Nicolo et al. 2007; Lourens et al. 2005), and is dated to ~53.44 Ma (to Berggren et al 1995; Table 5), which closely correlates to the base of nannofossil zones CP9b/NP11 (53.6 Ma; Berggren et al. 1995). This hyperthermal event is expressed well at Site 762, by a negative $\delta^{13}C$ excursion and rebound of ~0.8‰ (text-figure 4) between 398.15-393.80 mbsf, and closely correlates to the base of CP9b (396.62 mbsf) (text-figure 2, Table 3). The nannofossil assemblage shows a rapid increase in species richness (63), evenness (0.40) and Shannon diversity (3.20), with peak values (at 394.25 mbsf) coinciding with peak negative shift in $\delta^{13}C$ (0.64‰, 394.85 mbsf) (text-figure 4).

Unlike the PETM, few prominent changes in the nannofossil assemblage are observed across the ETM2. A transient decrease is seen in *Coccolithus pelagicus* (Wallich 1877) Schiller 1930 and *Z. bijugatus* of = 4.0-6.0 % each (text-figure 5), as well as a permanent reduction in *Toweius serotinus* Bybell and Self-Trail 1995 (~1-2% to ~0.20 %) prior to extinction. Changes in species richness, evenness, and Shannon diversity in this interval are linked to minor increases (~1-2%) in *Sphenolithus* spp.,

Discoaster spp. (text-figure 6), *Umbilicosphaera bramlettei* (Hay and Towe 1962) Bown, Dunkley Jones and Young 2007, *Cruciplacolithus parvus* n. sp., *Neococcolithes protenus* (Bramlette and Sullivan 1961) Black 1967, and members of Pontosphaeraceae immediately above the isotope excursion, as well as by the LOs of *S. radians*, *T. orthostylus*, and *Discoaster robustus* Haq 1970.

ETM3/"X"-event/Event "K"

Warming is associated with another carbon excursion, the ETM3. Originally identified by Röhl et al. (2005) as the "X" event, this hyperthermal is correlated to foraminiferal zone P7 and nannofossil zone CP10. The ETM3 is placed in Chron C24n.1n (52.65-53.00 Ma) by Agnini et al. (2007) and by Galeotti et al. (2010). The date provided (Table 5) is based on the relative placement of this event in Chron C24n.1n within the Contessa Road Section, as well as the association by Galeotti et al. (2010) of the isotopic excursion with the LO of *D. lodoensis* (identified at 372.35 and 373.01 msbf in Hole 762C, respectively).

Species richness remains high throughout the ETM3, with 66 and 61 species identified in the nannofossil samples immediately above (371.49 msbf) and below (373.01 msbf) the isotopic excursion, respectively. This interval shows the highest Shannon diversity of the Ypresian (3.389, 371.49 msbf), and assemblage evenness is high (0.449, 371.49 msbf), approaching the maximum seen in the EECO (text-figure 4). A significant drop is observed in both Shannon diversity and evenness immediately above the $\delta^{13}C$ excursion, to 2.955 and 0.320, respectively. *Discoaster* spp. increase from ~2.0% below the ETM3 to 6.7% during the event, beginning a general rise in the genus through the remaining Ypresian that peaks at the end of the EECO (text-figure 6). A peak in warm-water taxa (8.6% to ~14.5%, text-figure 7) is also associated with this rise in *Discoaster* spp. Holococcolith abundance also increases just above the ETM3 (text-figure 7), from 10.8% (371.49 msbf) to ~18.0% (370.75, 370.00 msbf).

The most significant change in the nannofossil assemblage is the high species turnover near this event relative to background rates, particularly originations. Six species show LOs at 373.01 msbf (*Chiphragmolithus barbatus* Perch-Nielsen 1967, *Chiphragmolithus calathus* Bramlette and Sullivan 1961, *Discoaster gemmifer* Stradner 1961, *D. kuepperi*, *D. lodoensis*, *Neococcolithes dubius* (Deflandre in Deflandre and Fert 1954) Black 1967) while five have LOs at 371.49 msbf (*Ch. grandis*, *Discoaster germanicus* Stradner 1962, *Discoaster septemradiatus* (Klumpp 1953) Martini 1958, *Pedinocyclus larvalis* (Bukry and Bramlette 1969) Loeblich and Tappan, *Girgisia gammation* (Bramlette and Sullivan 1961) Varol 1989 (LCO)). This is in significant contrast to the rate of 0-2 species for several samples above and below this interval. This increased rate of speciation is of particular interest because, unlike the higher rates associated with the PETM and the EECO, this event has no stratigraphic hiatus associated with it at Site 762. While the increased turnover at the PETM and the EECO is likely dominated by the environmental component, it is difficult to definitively unravel the true turnover from the apparent turnover that occurs across a hiatus.

Early Eocene climatic optimum (EECO)

Temperatures continued to increase through the early Eocene, peaking in the late Ypresian with the EECO. Minimum $\delta^{18}O$ values occur between ~52-50 Ma (Zachos et al. 2001; Bohaty and Zachos 2003; Tripati et al. 2003), within nannofossil biozones CP10-11 (Ogg Ogg and Gradstein 2008). Following the initial rebound above the PETM, nannofossil diversity and species richness show a long-term, sustained increase through much of the early Eocene ($max_{diversity}$ = 3.39; $max_{richness}$ = 66; 371.49 mbsf) (text-figure 4).

Early Eocene peaks in nannofossil species richness (μ = ~60), evenness (0.485) and Shannon diversity (μ =3.13) occur within the EECO (~331.0-352.0 msbf) at Site 762 (text-figure 4). Maximum nannofossil diversity (3.32, 335.03 msbf) occurs near the end of this warm interval, followed by a rapid, and sustained, decline. There is significant turnover in the nannofossil assemblage associated with the end of the EECO as defined at Site 762: A significant drop in diversity (3.317 to 2.961, text-figure 4) is linked to 13 extinctions but only three LOs (333.52-332.75 mbsf); however, poor core recovery and erosion of sediments may have resulted in a stratigraphic hiatus (Hiatus B), as indicated by the thinness of CP11 and by the absence of NP13.

The most prominent event documented from the EECO is the dominance shift in the background assemblage, from *Toweius* spp. in the lower Eocene to *Reticulofenestra/Dictyococcites* spp. in the middle and upper Eocene. This crossover is closely associated with the EECO in Hole 762C, and is linked by a substantial acme in *Discoaster* spp. (text-figure 8). These transitions from *Toweius* to *Discoaster* to *Reticulofenestra*/ *Dictyococcites* spp. represent two assemblage turnovers that closely approximate the base and top of the EECO interval, respectively, as defined chemically and biostratigraphically at Site 762.

Toweius spp. show a steady decline through the Ypresian, from a peak abundance of 28.0% near the PETM (μ = 23.8%) to ~14.4% at the base of the EECO (text-figure 6). This decline becomes more rapid within the EECO, dropping to < 1.0% by the top of the interval, with extinction shortly above. This trend is concurrent with a notable shift in *Discoaster* spp. mean abundance from 8.6% below the basal EECO boundary to 15.1% through the event (max. = 18.6%). The EECO acme in *Discoaster* spp. is primarily linked to peaks in *D. kuepperi, D.lodoensis* and, to a lesser extent, *D. barbadiensis*.

The LO of the *Reticulofenestra*/*Dictyococcites* group is observed just above the base of the EECO, but remains extremely rare through much this interval (μ = 0.8%; max. = 1.9%) (text-figure 8). An abrupt, but sustained, increase occurs across the upper EECO boundary, from 7.8% to 33.6% just above, and is concurrent with an abrupt and sustained decline in *Discoaster* spp., from 16.6% at the upper EECO boundary to 8.8% above (text-figure 8). Abundance of *Reticulofenestra*/*Dictyococcites* continues to increase through much of the Lutetian (μ = 40.4%; max. = 56.4%). This *Discoaster* acme linking the *Toweius* and *Reticulofenestra/Dictyococcites* assemblages is also seen in the Possango (Italy) section from which Agnini et al. (2006) suggest that warm, oligotrophic conditions originally favor *Discoaster* spp., but a collapse in surface water stratification later favors the more mesotrophic to eutrophic *Reticulofenestra* group.

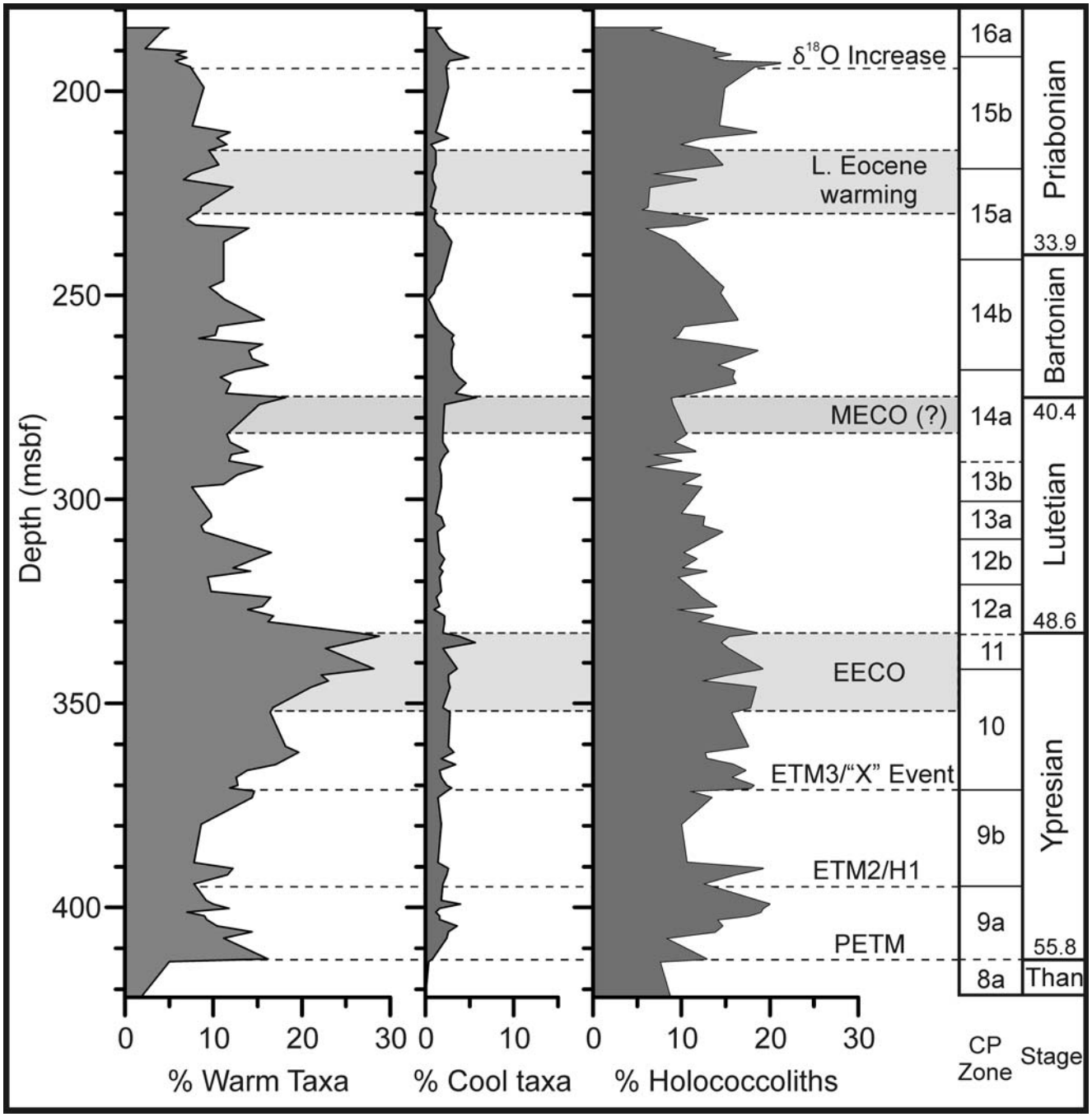

TEXT-FIGURE 7
Abundance patterns of warm taxa (*Discoaster* spp., *Sphenolithus* spp., *Ericsonia formosa*), cool taxa (*Reticulofenestra daviesii, R. hillae*, *Isthmolithus recurvus*, *Chiasmolithus* spp.), and holococcoliths (*Zygrhablithus bijugatus, Lanternithus minutus*) from Site 762C, correlated to depth (msbf, left), nannofossil CP zones (right), and geologic epoch with boundary ages (Ma) (far right) (Ogg Ogg and Gradstein, 2008). Isotopic events identified in text-figure 3 are shown as dashed lines or shaded boxes. Data is expressed as percentage of 500 specimens. Groups based on Perch-Nielsen (1985) and a well-researched summary by Villa et al. (2008, table 3).

In addition to the *Toweius-Discoaster-Reticulofenestra* cross-overs associated with the EECO, several changes are observed in other nannofossil taxa through the interval. *Sphenolithus* spp. decreases from μ = 5.5% (max. = 6.6%) through this interval to 2.2% at the end of the EECO (text-figure 6), linked to the Eocene peak (μ = 2.3%) and decline (μ = 0.8%) of *S. radians*. *Zygrhablithus bijugatus* increases with peak abundance through the EECO (μ = 16.2%; max. = 19.2%), but declines through much of the Lutetian (μ =10.7%) (text-figure 5). The LO of *C. crassus* occurs during the EECO and rapidly increases (μ = 6.3%; max. = 8.6%) within this interval. This species shows an abrupt decline just above the upper boundary (0.8%) before

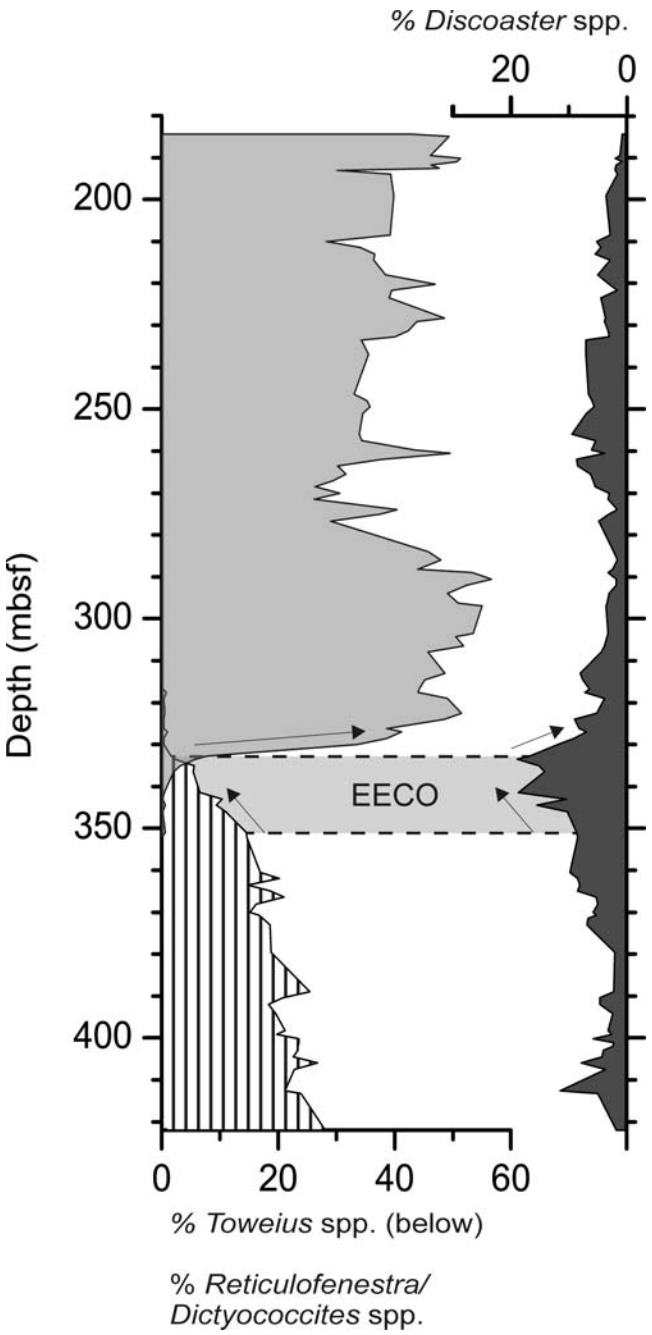

TEXT-FIGURE 8
Abundance patterns of key taxa from the lower-middle Ecoene dominance reversals correlated to depth (msbf). *Toweius* spp. plotted on lower left, with *Reticulofenestra* spp. (including *Dictyococcites bisecta, D. stavensis, D. scrippsae*) on upper left. *Discoaster* spp. is plotted on right. Major abundance shifts are highlighted with arrows showing the relationship to the isotopic shift to the end of the EECO.

rapid extinction, suggesting an affinity for warm temperatures or oligotrophic conditions.

The nannofossil assemblage shows a sustained increase in warm water taxa (Table 7) from the ETM2/H1 through the Ypresian, with peak abundance for the Eocene within the upper EECO (μ = 24.4%; max. = 28.8%) (text-figure 7). Abundance of warm water taxa drops rapidly above the EECO to 16.1%, and continues to decline in the Lutetian. Cool water taxa (Table 7) show a short pulse at near the top of the event (text-figure 7), linked to an increase in *Chiasmolithus* spp., particularly large species such as *Ch. grandis* and *Chiasmolithus californicus* (Sullivan 1964) Hay and Mohler 1967, but do not show a significant increase through the Lutetian.

Campylosphaera dela (Bramlette and Sullivan 1961) Hay and Mohler 1967*, Calcidiscus pacificanus* (Bukry 1971) Varol 1989 and *G. gammation* also increase to μ = 2-3% through the EECO but drop to μ = = 1.0% at or just above the upper boundary. These taxa may have affinity to either warm water or oligotrophic nutrient conditions; however, this suggestion would require further study in sections where these taxa show greater abundance.

Middle Eocene cooling

The end of the EECO marks the beginning of long term cooling through much of the Lutetian, with trends in the nannofossil assemblages mirroring the general rise in $\delta^{18}O$ of ~1.2‰ through this time period (text-figure 4). A significant, step-wise decline is seen in both Shannon H diversity (3.265 to 2.749) and evenness (0.460 to 0.274) in CP12a-CP13b, which reach a minimum (2.75 and 0.274, respectively) just above the CP14a boundary. Species richness also decreases above the EECO, but appears to rebound more rapidly, due to the diversification of the *Reticulofenestra*/*Dictyococcites* group, which dominates the assemblage through the Lutetian (μ = 46.2%; max. = 56.6%; text-figures 5, 6). Warm water taxa, which peak in the Ypresian, decline above the EECO through the Lutetian (μ = 12.5%; min.: 8.5%; text-figures 5, 6).

Middle Eocene climatic optimum (MECO)

The Middle Eocene Climatic Optimum (MECO) was a transient warming event in the late middle Eocene (~40.0 Ma), superimposed on a long-term middle and late Eocene cooling trend (Bohaty et al. 2009; Jovane et al. 2007; Bohaty and Zachos 2003). Recent work by Bohaty et al. (2009) correlated the MECO to two nannofossil events: 1) the LO of *Dictyococcites scrippsae* Bukry and Percival 1971 at low latitudes and 2) the LO of *Cr. reticulatum* at southern high-latitude sites. The LO of *D. scrippsae* cannot be used as a proxy for the MECO at Site 762 due to differing taxonomic concepts, and the known latitudinal diachroniety of *Cr. reticulatum* (discussed above) at this mid- to low-latitude site also prohibits use as a proxy for this event. Despite these restrictions, the general isotopic pattern can be identified from Hole 762C: A long term increase in $\delta^{18}O$ in the middle Eocene, followed by a rapid decrease of ~1.0‰ (text-figure 4). The long Lutetian cooling shows evidence of reversal at Site 762 with a -0.66 ‰ shift in $\delta^{18}O$ within CP14a.

The decrease in $\delta^{18}O$ coincides with a rapid increase in Shannon diversity (2.89 to 3.33) and evenness (0.306 to 0.489) (text-figure 4). This transition initiated the second sustained period of high diversity in the Eocene, which gradually deteriorated through the Bartonian and Priabonian. Warm taxa increased through the event (*Discoaster, Sphenolithus* spp.: text-figure 6; *Ericsonia formosa*: text-figure 5) with peak abundance at the end of the MECO (18.2%, text-figure 7), but underwent a slow decline through the remaining interval (text-figure 7). Similar to

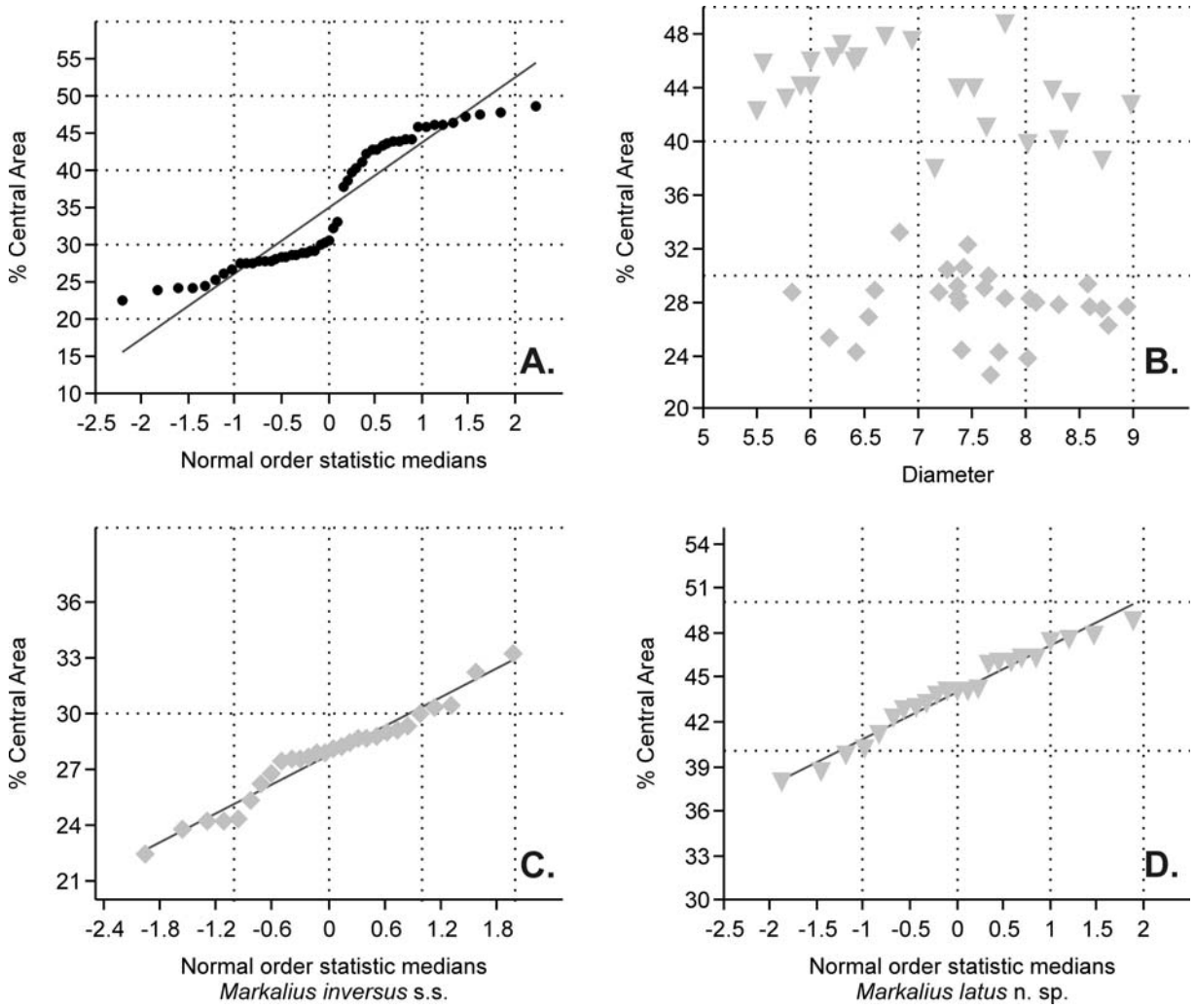

TEXT-FIGURE 9
Univariate statistical analysis of the genus *Markalius*: A) Non-normal distribution of *Markalius* specimens with respect to size of the CA (central area). B) Distribution of *Markalius* specimens showing clear separation between forms with relatively small CA (< 35%; *Markalius inversus* s.s.) and those with a larger CA (>35%; *Markalius latus* **n.sp.**) (see Systematic Paleontology section). C, D) Near normal distributions of *Markalius* specimens when separated by the relative size of the CA into two distinct populations.

the EECO, cool taxa exhibited a short pulse at near the top of the event, linked to the LO of *Reticulofenestra daviesii* (Haq 1968) Perch-Nielsen 1971 (text-figure 7). Specimens of *Helicosphaera* spp. show a slight increase near the end of the MECO, similar to the trend shown in Toffanin et al. (2010, fig.3). *Reticulofenestra* spp. and *D. scrippsae* both declined near the MECO (text-figure 6). Abundance trends of *D. scrippsae* near the EECO and MECO suggests a cool affinity for this species. The LO of *Cribrocentrum reticulatum* is observed slightly below the MECO but does not show a notable increase in abundance until the post-MECO recovery (text-figure 5).

Late Eocene cooling

In general, the Bartonian and Priabonian are marked by global cooling. The peaks in diversity, evenness, and species richness that occur near the MECO turn to a long-term decline through CP14a-16a (text-figure 4) and correlate to a long term global shift in $\delta^{13}C$ and $\delta^{18}O$ (Salamy and Zachos 1999; Zachos et al. 2001). At least two distinct phases of warming are superimposed on this long term trend. Jovane et al. (2007, fig 10) show shifts in $\delta^{18}O$ (~ -1.0‰) and $\delta^{13}C$ (~ 0.7‰) at the Contessa Highway Section (Italy) between ~37-36.5 Ma, with the main warming occurring over ~2.0 My. Bohaty and Zachos (2003, fig.2) show similar $\delta^{18}O$ and $\delta^{13}C$ trends in the Southern Ocean, with an initial rise beginning ~37 Ma and ending ~1.5 My later. These dates correlate to upper CP15a-lower CP15b, which coincides with a conspicuous peak in $\delta^{18}O$ (-0.1 ‰ to -0.6‰) at Site 762 (~232.0-213.0 mbsf; text-figure 4).

This isotopic shift actually corresponds to a slight drop in diversity, evenness and species richness at Site 762 (text-figure 4). Smaller scale warming events such as these may have acted to temporarily suspend or reverse the middle to late Eocene trend; however, the late Eocene (Priabonian) warming does not appear to reverse the long term decrease in the nannofossil assemblage seen through the late Eocene (text-figure 4).

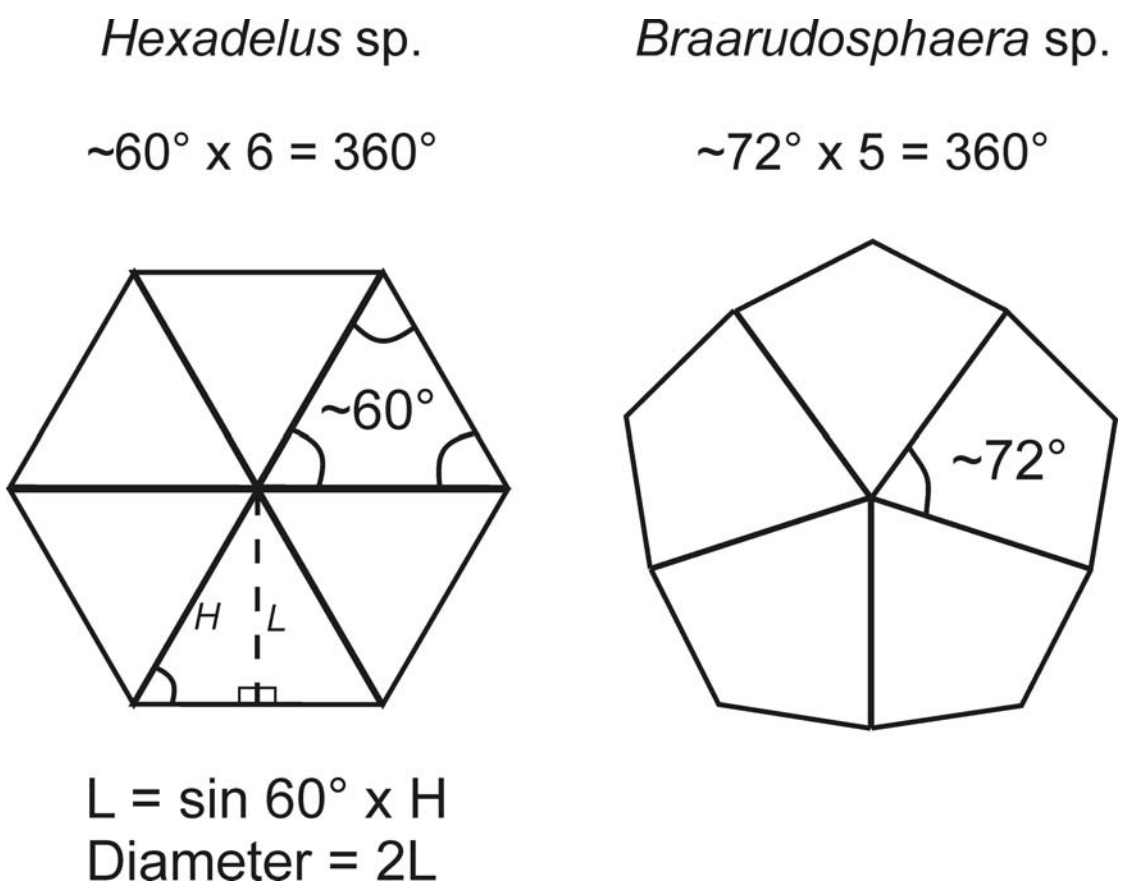

TEXT-FIGURE 10
Stylized figure showing the morphological relationship between disarticulated plates of the pentalith family Braarudosphaeraceae and those of the newly described genus *Hexadelus*. Geometrically, the interior angle of a pentalith must average ~72°, while plates that are 60° require six segments in order to complete a cycle.

The abundance of *Sphenolithus* spp. declined through the Bartonian cooling particularly in CP14b-early CP15a (μ = 2.7%; min. = 1.4%), but showed only a modest increase in association with the late Eocene warming (text-figure 6). *Ericsonia formosa* declined above the MECO through the Bartonian (μ = 2.0%), but showed a notable peak through the late Eocene warming (μ = 3.7%; max. = 6.2%) (text-figure 5). *Dictyococcites bisectus* and *Dictyococcites stavensis* (Levin and Joerger 1967) Varol 1989 appeared in the Bartonian, with peak abundance through the late Eocene warming (μ = 14.3%; max. = 19.4%) but declined significantly above the event (μ = 5.0%, min. = 3.1%). Peak abundance near the middle-late Eocene boundary is seen by Villa et al. (2008), and Wei and Wise (1990b, fig. 12) also show that *D. bisectus* is significantly more abundant below 40° latitude. These patterns of abundance, with respect to late Eocene warming and other warm-water taxa, suggests that *D. bisectus* and *D. stavensis* had an affinity for warmer conditions. Conversely, the warm-water *Discoaster* spp. increased through the Bartonian cooling (μ = 6.5%; max. = 9.4%) and decreased through the late Eocene warming (μ = 3.4%; min. = 1.6%). This is linked to peak abundance of *D. barbadiensis, D. saipanensis,* and *Discoaster nodifer* (Bramlette and Riedel 1954) Bukry 1973 in the Bartonian (μ = 1.7%, 2.2%, and ~1.0%, respectively), declining by 0.5-1.5% each through the Priabonian. Lower abundance during warm intervals may indicate an oligotrophic response to more mesotrophic to eutrophic conditions through this interval at Site 762. *Cyclicargolithus floridanus* (Hay et al. 1967) Bukry 1971 is associated with high productivity (Aubry 1992; Monechi, Buccianti and Gardin 2000). This species was most abundant through CP15a (μ =7.5%) reaching a peak at the base of the late Eocene warming (11.0%), followed by a significant decline through this period. Peak abundance is not centered about the late Eocene warming and $\delta^{18}O$ excursion, and is not likely controlled directly by temperature, but suggests more mesotrophic to eutrophic conditions.

Cool taxa declined through the late Eocene warming (μ = ~1.0%), as indicated by a reduction in both *R. daviesii* and *Chiasmolithus* spp., but rebounded above the event (μ =2.2%) (text-figure 7). *Cribrocentrum reticulatum* increased significantly above the MECO, with peak abundance during the Bartonian cooling (μ = 5.9%; max. = 10.1%), but decreased rapidly at the start of the late Eocene warming (0.2%) (text-figure 5). The abundance of *Lanternithus minutus* Stradner1962 declined through the late Eocene warming (μ = 0.7%), but rebounded significantly just above this event (μ = 4.8%; max. = 8.65%) and through the remainder of CP15b (text-figure 5). This pattern of abundance suggests a cool temperature affinity for this species.

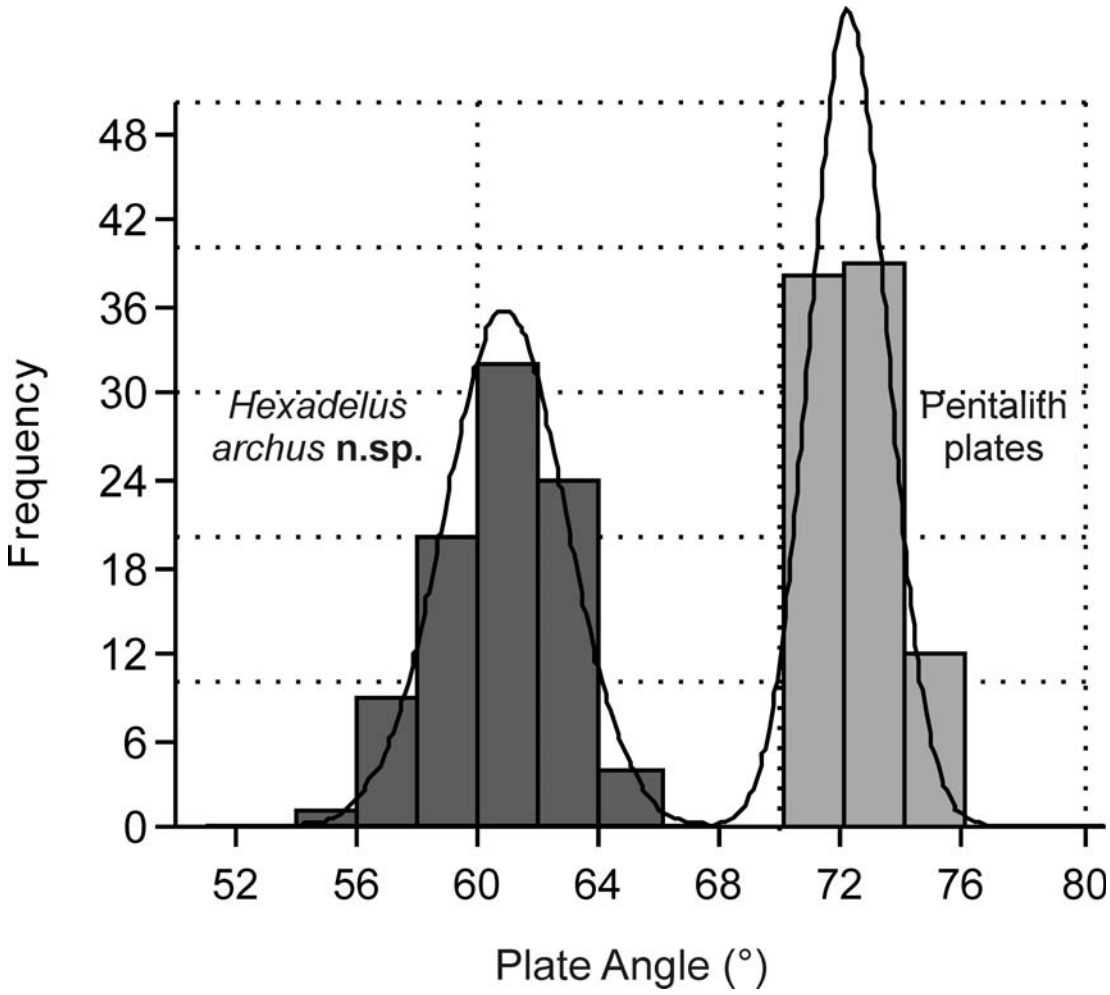

TEXT-FIGURE 11
Histogram demonstrating the non-overlapping relationship between specimens of Braarudosphaeraceae and the type species *Hexalithus archus* **n.sp.**, with respect to the interior angle. Normal distribution curves superimposed. Univariate t-tests show distinct separation between plate geometry of pentaliths and *H. archus* **n. sp**.: At the 95% confidence level, pentalith angle = 71.98-72.52°; *Hexadelus archus* = 60.38-61.23°, p = 9.93 E , N = 90 each species/group.

"terminal Eocene event"

Despite the brief late Eocene warming in the Priabonian, climate deterioration continued into the Oligocene, most notably with Oi-1 and the onset of significant ice sheet growth in Antarctica. The Oi-1 event is not readily identified at Site 762, as isotopic and biostratigraphic data end near this interval. Nevertheless, some of the preceding isotopic shifts and bioevents can be identified. The $\delta^{13}C$ shows a sustained increase of ~1.0‰ just above the CP16a boundary (192.75 mbsf), and coincides with a $\delta^{18}O$ increase of ~0.5‰. A significant drop in Shannon diversity occurred near the top of the section (189.47 mbsf), from an average of 2.9 through CP16a to the lowest diversity (2.674) and species richness (44) decreased as well (text-figure 4). This is attributed to the decline in *E. formosa*, *L. minutus, Z. bijugatus, Bramletteius serraculoides* Gartner 1969, and *Calcidiscus protoannulus* (Gartner 1971) Loeblich and Tappan 1978. The sample immediately above this isotopic shift marks the base of the *Clausicoccus* acme observed in Hole 762C (185.01 msbf). Warm water taxa continued to decline through the Priabonian, while cool taxa, particularly *R. daviesii*, show a maximum near this positive $\delta^{18}O$ shift, but quickly decline again above this interval (text-figure 7).

Dunkley Jones et al. (2008) show peak abundance of holococcoliths ~0.6 My below the E-O boundary, followed by a significant decline. At Site 762, *L. minutus* decreased from a maximum of 8.6% near the base of CP16a to an upper Eocene minimum of ~1.0% at the base of the *Clausicoccus* spp. acme (text-figure 5). Similarly, *Z. bijugatus* declined from an average of 11.2% through CP16a to 5.4% at the base of the *Clausicoccus* spp. acme (text-figure 5). This decline in holococcolith taxa (text-figure 7) and in Shannon diversity (text-figure 4) closely correlate to positive shifts in both $\delta^{18}O$ and $\delta^{13}C$, and may indicate proximity to the E-O boundary at Site 762. Dunkley Jones et al. (2008) also define a group of taxa that are abundant below the Oligocene boundary but decline rapidly through the E-O transition, including *C. protoannulus, L. minutus, Z. bijugatus,* and *Reticulofenestra dictyoda* (Deflandre in Deflandre and Fert 1954) Stradner *in* Stradner and Edwards 1968. At Site 762, this

group exhibited peak abundance at the base of CP16a (~42%) but declined to 21.2% by the top of the section. This trend also suggests proximity to the E-O boundary at Site 762.

Helicosphaera spp. were quite rare during the late Eocene warming (μ = <0.5%), but began to increase above this event, particularly *Helicosphaera compacta* Bramlette and Wilcoxon 1967 (μ = 2.2%). This species showed peak abundance at the excursion (4.0%), with a pattern of abundance similar to *L. minutus* and *Z. bijugatus* (text-figure 5). We also observe an interesting pulse of thinly-calcified, indeterminate nannoliths in Hole 762C (Plate 9-6 to 9-13), with maximum abundance in CP16a (μ = 4.2 %, max. = 5.6%) and a rapid decline (μ = 1.2%) coincident with the base of the *Clausicoccus* spp. acme.

Several lines of evidence suggest that the top of the interval examined in Hole 762C is very near the Oi-1 event, but it cannot be confidently placed. Magnetostratigraphic data for Site 762 terminates in Core 5, with ~14m of Chron C13r, but does not identify the C13n reversal. Our nannofossil biostratigraphy terminates in Core 3, above the CP16a boundary, but we do not identify the CP16b boundary. It is possible to distinguish the base of the *Clausicoccus* acme, where *Clausicoccus* spp. increases from ~1.0% (190.24 msbf) to 6.1% (184.49 msbf), but our data does not identify the acme top. Isotopic stratigraphy continues through Core 2, showing a positive $\delta^{18}O$ shift of 1.02‰ (189.72-171.28 msbf). In addition, a positive shift in $\delta^{13}C$ of 0.95‰ (194.24-179.73 msbf) precedes a decrease of 0.42‰ (171.28 msbf; top of available data). All available datasets terminate near the Oi-1 event, but it cannot be identified fully.

Problem taxa

There is some debate as to the environmental affinities of *Zygrhablithus bijugatus* and *Cribrocentrum reticulatum* as summarized by Villa et al. (2008, table 3), with respect to temperature, nutrient levels, and water depth. Trends observed at Site 762 are discussed below.

Zygrhablithus bijugatus

Data from Hole 762C suggests a possible warm-water affinity for *Z. bijugatus*: Abundance curves mirror $\delta^{18}O$, increasing during the warm Ypresian, peaking through the EECO and declining during the Lutetian cooling; however, above this level, the response does not appear to be primarily linked to temperature, with abundance increasing through the Bartonian cooling and decreasing during the late Eocene warming (text-figure 5). The abundance pattern of *Z. bijugatus* is similar to *Discoaster* spp. (text-figure 6) and inverse to *C. floridanus* (text-figure 5), suggesting a greater affinity for oligotrophic conditions. The environmental factors that drive changes in abundance of *Z. bijugatus* may be complex, accounting for the significant disagreement between various nannofossil workers (Villa et al. 2008) and likely requires a detailed, species-specific study.

Cribrocentrum reticulatum

The paleoecological summary of *Cr. reticulatum* from Villa et al. (2008, table 3) shows warm to 'not warm' temperature preferences and mesotrophic to oligotrophic nutrient affinities. *Cribrocentrum reticulatum* increases through the MECO, with peak abundance through the Bartonian and lower Priabonian (μ = 5.9%; max. = 10.1%), dropping rapidly at the base of the Late Eocene warming (0.2%) (text-figure 5). This suggests a preference for temperate conditions. The pattern of abundance of this species is also similar to *Discoaster* spp. (text-figure 6), with potential for oligotrophic affinities.

Summary

Several notable changes are observed in the nannofossil assemblage that correlate closely to short isotopic excursions or long term trends in $\delta^{13}C$ and $\delta^{18}O$ (text-figures 3-7). Patterns of nannofossil diversity and evenness broadly mirror the $\delta^{18}O$ curve, and are primarily attributed to changes in paleotemperatures, but also to fluctuations in nutrient levels associated with circulation and thermal stratification of the water column. Warm water taxa dominate through much of the Eocene, showing the most significant decline through the Lutetian. Cool taxa show only a modest increase in the Bartonian and Priabonian, supporting an overall temperate to warm water interpretation of the site.

Increased rates of speciation and extinction are associated with the PETM and the end of the EECO. These periods of increased turnover are highlighted by events such as the *Fasciculithus*/*Zygrhablithus* crossover at the PETM and by the *Toweius*/*Discoaster* and *Discoaster*/*Reticulofenestra* assemblage turnovers near the base and top of the EECO, respectively. A significant number of bioevents have been identified across the PETM in high-resolution studies, and data from Site 762 and Jiang and Wise (2009) suggest that many of these key changes can be identified in even coarsely sampled or poorly recovered intervals. Though the dominance reversal of *Toweius* and *Reticulofenestra* is well known, the *Discoaster* acme that links these dominant assemblages, identified at Site 762 and Possango (Agnini et al. 2006), indicates two potentially global and synchronous nannofossil assemblage turnovers associated with the EECO. While several isotopic events correlate to significant changes in the nannofossil assemblage, relatively modest changes were observed across the ETM2, ETM3 or MECO events. This may be a true representation of the nannofossil response, but is likely muted by the moderate sample spacing, requiring a higher-resolution sample interval to identify the changes across these short events.

Patterns of abundance of several taxa suggest that changes in the nannofossil assemblage in the early Eocene were influenced primarily by changes in temperature. Above the MECO abundance patterns of some key taxa, such as *Discoaster* spp. and *C. floridanus*, suggest that the assemblage was also affected by more meso- to eutrophic nutrient levels. Peaks in cool water taxa, holococcoliths, and thinly-calcified indeterminant nannoliths are observed in the Priabonian. Further investigation may reveal significant paleoecological relationships or information on paleoenvironment and nannofossil calcification.

SYSTEMATIC PALEONTOLOGY

Several new taxa were identified during this study including one genus (*Hexadelus*) and nine species or species variants (*Calcidiscus ellipticus*, *Cruciplacolithus nebulosus*, *C. opacus*, *Cyclicargolithus parvus*, *Hayella situliformis* var. *ovata*, *Hexadelus archus, Markalius latus*, *Pedinocyclus annulus*, *P. larvalis* var. *minimus*). It is still unclear whether these variants represent 'normal' phenotypic variation, a preservational artifact, or are unique and distinct species.

Holotype and paratype materials and photographs are located within the collections of the ODP Micropaleontological Refer-

ence Center at the University of Nebraska State Museum (UNSM). Species description uses terms recommended by Young et al. (1997). We follow the higher taxonomic organization of Young and Bown (1997) and Young et al. (2003). Open nomenclature (*ex*: '?', 'cf.', 'indet.') follows the recommendations of Bengtson (1988). Statistical abbreviations used in systematic descriptions are as follows: μ = mean; CA = central area; s.d. = standard deviation; N = numbers of specimens.

Taxonomic notes and/or biostratigraphic observations are given for all species identified at Site 762C. The taxonomic classification system shown here is after Bown and Young (1997) and nannofossil terminology follows the guidelines provided in Young et al. (1997). Notable abundance trends are given for individual species; however, genus and family level abundance trends are treated above. Range data are intended to show uncertainty when LOs or HOs were observed across a hiatus (discussed above).

Recent research on Eocene cores from Tanzania by Bown (2005), Bown and Dunkley Jones (2006), and Bown, Dunkley Jones and Young (2007) has generated a significant image atlas, and numerous taxonomic points have been addressed in these works that will not be reiterated here. We restrict our main discussion and imaging to species that were not addressed, recently named species, or where opinions on taxonomy diverge. Many species that are recently named are shown in XPL (Cross-polarized light) only, as they are well illustrated in the original descriptions. Where two images are provided for one specimen, XPL is always shown before PL (Plane-polarized light).

Numerous new species were recently identified by Bown (2005), Bown and Dunkley Jones (2006) and Bown, Dunkley Jones and Young (2007). Many of these species were observed in the Exmouth section; however, observed ranges of several species extend above and/or below those provided in the original descriptions. A significant portion of such range extensions are likely due to coring gaps in the Tanzania section (Bown 2005, fig 2; Bown, Dunkley Jones and Young 2007, fig. 1). To limit redundancy, we do not treat each range issue separately, but refer the reader to these publications for independent comparison.

MUROLITHS

Order **EIFFELLITHALES** Rood et al. 1971
Family **CHIASTOZYGACEAE** Rood et al. 1973

Jakubowskia leoniae Varol 1989

Observed range: CP9a-12a; NP10-14a

Order **SYRACOSPHAERALES** Hay 1977, emend. Young et al. 2003
Family **CALCIOSOLENIACEAE** Kamptner 1927

Calciosolenia alternans Bown and Dunkley Jones 2006
Plate 1, figure 1

The LO of this species at Hole 762C is extended from the original description (NP16). *Observed range*: CP12a; NP14a

Calciosolenia aperta (Hay & Mohler 1967) Bown 2005
Plate 1, figure 2

Observed range: CP9a, NP10

Family **RHABDOSPHAERACEAE** Haeckel 1894

Most species of *Blackites and Rhabdosphaera* were extremely rare at the locality.

Blackites gracilentus Bown and Dunkley Jones 2006

Observed range: CP14b; NP17

Blackites morionum (Deflandre in Deflandre and Fert 1954) Varol 1989

Observed range: CP9a; NP10

Blackites perlongus (Deflandre in Grassé 1952) Bramlette and Sullivan 1961

Observed range: CP9b; NP11

Blackites spinosus (Deflandre and Fert 1954) Hay and Towe 1962 / ***Rhabdosphaera tenuis*** Bramlette and Sullivan 1961

The vast majority of specimens are incomplete, lacking their diagnostic base. As a result, *B. spinosus* has been grouped with *R. tenuis*, though this diminishes the biostratigraphic utility. This group is most abundant in CP10. *Observed range*: CP8b/9a?-16a; NP9/10?-21

Blackites tortillis Bown and Dunkley Jones 2006
Plate 1, figure 3

The observed LO occurs in mid-CP14a. The HO of this species at Hole 762C is extended from the original description (NP16). *Observed range*: CP14a-15b; NP16-19/20

Rhabdosphaera inflata Bramlette and Sullivan 1961

Observed range: CP12b; NP14b

Rhabdopshaera sola Perch-Nielsen 1971

Observed range: CP9b-10; NP11-12

Rhabdosphaera tenuis Bramlette and Sullivan 1961

See *B. spinosus/R. tenuis*, above.

Rhabdosphaera truncata Bramlette and Sullivan 1961

Observed range: CP9b-12a; NP11-14a

Family **SYRACOSPHAERACEAE** Hay 1977

Syracosphaera Lohmann 1902

Specimens of this genus were rare and sporadic throughout the section and have been grouped as *Syracosphaera* spp. for statistical analysis. *Observed range*: CP9a-16a; NP10-21

Order **ZYGODISCALES** Young and Bown 1997
Family **HELICOSPHAERACEAE** Black 1971

Most species of the genus *Helicosphaera* were rare and sporadic, though the genus as a whole becomes fairly common and consistent in the late Eocene. Average relative abundance = ~0.5% from the genus LO through CP15b, but increases at the base of CP16a (μ = 1.6%, max. = 4.0%)

Helicosphaera bramlettei (Müller 1970) Jafar and Martini 1975

Observed range: CP14a-16a; NP16-21

Helicosphaera compacta Bramlette and Wilcoxon 1967

The LCO occurs in CP14b at this site, with a notable abundance increase in upper CP15b, also shown in Wei and Wise (1990a). *Observed range*: CP14a?-16a; NP16-21

Helicosphaera dinesenii (Perch-Nielsen 1971) Jafar and Martini 1975

Observed range: CP13a-14a; NP15a-16

Helicosphaera heezenii (Bukry 1971) Jafar and Martini 1975

Observed range: CP13c/14a?-14b; NP15c/16?-17

Helicosphaera lophota (Bramlette and Sullivan 1961) Jafar and Martini 1975

LO occurs at the base of CP11, with HO just above the base of CP15b. *Observed range*: CP10-15b; NP12-19/20

Helicosphaera papillata (Bukry and Bramlette 1969) Jafar and Martini 1975

The HO occurs just above base of CP12b. *Observed range*: CP12a-12b; NP14a-14b

Helicosphaera reticulata Bramlette and Wilcoxon 1967

Observed range: CP15a-16a; NP18-21

Helicosphaera salebrosa Perch-Nielsen 1971

Observed range: CP13b-15b; NP15b-19/20

Helicosphaera seminulum (Bramlette and Sulllivan 1961) Jafar and Martini 1975

Observed range: CP10-15b; NP12-19/20

Helicosphaera wilcoxonii (Gartner 1971) Jafar and Martini 1975

Observed range: CP14b-16a; NP17-21

Family **PONTOSPHAERACEAE** Lemmermann 1908

The genera *Pontosphaera* and *Transversopontis* were observed throughout the section from CP8a-16a. Specimens were generally rare and sporadic at this locality, so were grouped together as *Pontosphaera* spp. for data analysis. Detailed biostratigraphic analysis was not conducted on individual species within these two genera, except *Pontosphaera rimosa*. Species that were identified are listed below.

Pontosphaera formosa (Bukry and Bramlette 1968) Romein 1979

Pontosphaera multipora (Kamptner 1948) Roth 1970, emend. Burns 1973

Pontosphaera pectinata (Bramlette and Sullivan 1961) Sherwood 1974

Pontosphaera plana (Bramlette and Sullivan 1961) Haq 1971

Pontosphaera rimosa (Bramlette and Sullivan 1961) Roth and Thierstein 1972

Observed range: CP8b/9a?-13b; NP9/10?-15b

Pontosphaera versa (Bramlette and Sullivan 1961) Sherwood 1974

Transversopontis duocavus (Bramlette and Sullivan 1961) Locker 1973

Transversopontis exilis (Bramlette and Sullivan 1961) Perch-Nielsen 1971

Transversopontis pulcher (Deflandre in Deflandre and Fert 1954) Perch-Nielsen 1967

Transversopontis pulcheroides (Sullivan 1964) Baldi-Beke 1971

Family **ZYGODISCACEAE** Hay and Mohler 1967

Specimens of *Chiphragmolithus* spp. first occur with the LO of *D. lodoensis*, at the base of CP10. Some specimens could not be differentiated to species level due to overgrowth, and have been identified simply as *Chiphragmolithus* sp.

Chiphragmolithus armatus Perch-Nielsen 1971
Plate 1, figure 4

Observed range: CP10; NP12

Chiphragmalithus barbatus Perch-Nielsen 1967
Plate 1, figure 5

Observed range: CP9b-10; NP11-12

Chiphragmolithus calathus Bramlette and Sullivan 1961

Observed range: CP9b-10; NP11-12

Isthmolithus recurvus Deflandre in Deflandre and Fert 1954
Plate 1-6; The LCO of *I. recurvus* marks the base of CP15b. The LO of *I. recurvus* and HO of *C. reticulatum* are often reported as contemporaneous markers; however, rare specimens of *I. recurvus* are observed well below the HO of *C. reticulatum*. This overlap is also reported in Agnini et al. (2011), Fornaciari et al. (2010), Villa et al. (2008), Aubry (1992), and Wei and Wise (1990a, 1989a). *Observed range*: CP15a-16a; NP17-21

Isthmolithus rhenanus Martini 1973
Plate 1, figure 7

Only one specimen of this rare species was identified and was observed below the range given in Wise et al (2004) (CP16c). *Observed range*: CP16a; NP21

Lophodolithus mochlophorus Deflandre in Deflandre and Fert 1954

Observed range: CP12a-13b; NP14a-15b

Lophodolithus nascens Bramlette and Sullivan 1961
Plate 1, figure 8

Peak abundance occurs in CP9b-10. *Observed range*: CP8b/9a?-11; NP9/10?-12

Lophodolithus reniformis Bramlette and Sullivan 1961

The LO was observed very near the CP9b/10 boundary. *Observed range*: CP9b-10; NP11-12

Lophodolithus rotundus Bukry and Percival 1971

Observed range: CP13a; NP15a

Neochiastozygus concinnus (Martini 1961) Perch-Nielsen 1971

The HO occurs in lower CP9b. *Observed range*: CP8b/9a?-9b; NP9/10?-11

Neochiastozygus distentus (Bramlette and Sullivan, 1961) Perch-Nielsen 1971

Observed range: CP8a-9b; NP9-11

Neochiastozygus junctus (Bramlette and Sullivan 1961) Perch-Nielsen 1971

Observed range: CP9a-10; NP10-12

Neochiastozygus rosenkrantzii (Perch-Nielsen 1971) Varol 1989

This species was observed below the range given by Perch-Nielsen (1985) in both this study and Bown (2005). *Observed range*: CP9a-10; NP10-12

Neochiastozygus substrictus Bown 2005

The HO of this species at Hole 762C is extended from the original description (NP10). *Observed range*: CP9a-10; NP10-11

Neococcolithes dubius (Deflandre in Deflandre and Fert 1954) Black 1967

The LO is observed just below the base of CP10. Though fairly consistent in its lower range, we observe a significant gap above CP13a, with a sporadic reappearance in CP14b prior to extinction. This species is commonly reported through CP15a (Villa et al. 2008; Wei and Wise 1990a; Perch-Nielsen 1985); however, Wei and Wise (1989b) also show a HO in CP14b, as at 762C. *Observed range*: CP9b-14b; NP11-17

Neococcolithes minutus (Perch-Nielsen 1967) Perch-Nielsen 1971
Plate 1, figure 9

Observed range: CP12a-14b; NP14a-17

Neococcolithes protenus (Bramlette and Sullivan 1961) Black 1967
Plate 1, figure 10

Observed range: CP8b/9a?-10; NP9/10?-12

Neococcolithes* cf. *protenus (Bramlette and Sullivan 1961) Black 1967
Plate 1, figure 11

Specimens with strikingly similar morphology to *N. protenus* were observed above its commonly recorded HO of CP10. These specimens did not show the narrowly elliptical outline of *N. minutus,* the 'H'-shaped cross of *N. dubius,* or the vertical relief of *Chiphragmolithus* spp., and are here identified as *Neococcolithes* cf. *protenus*. This distinction is given as several members of the Zygodiscaceae family are susceptible to overgrowth, which may affect identification at Hole 762C. *Observed range*: CP11-12b; NP13-14b

Zygodiscus adamas Bramlette and Sullivan 1961

Observed range: CP8b/9a?-9b; NP9/10?-11

Zygodiscus plectopons Bramlette and Sullivan 1961

This species was observed above the range given by Perch-Nielsen (1985) in both this study and Bown (2005). *Observed range*: CP9b; NP11

PLACOLITHS

Order **COCCOSPHAERALES** Haeckel 1894, emend. Young and Bown 1997

Family **CALCIDISCACEAE** Young and Bown 1997

Several new species of *Calcidiscus* have recently been identified by Bown (2005), Bown and Dunkley Jones (2006) and Bown, Dunkley Jones and Young (2007). All these species have since been identified at Exmouth Plateau, though with variances in some ranges. Some disagreement is quite likely due to the stratigraphic gap in the Tanzania sections between Cores 2 and 3 (mid-NP11 to lower NP14b) (Bown Dunkley Jones and Young 2007, fig. 1). This gap can account particularly for the difference in the LO of *C. bicircus* and the LO of *C. parvicrucis.* Variance in the ranges of other species (*C. henrikseniae*, *C. gerrardii)* may represent true stratigraphic differences between sites or in species concepts. Ranges observed at Hole 762C are compared to the most recent work on this genus (Bown Dunkley Jones and Young 2007). The true range of these species will be further refined as additional data is collected.

Calcidiscus? bicircus Bown 2005
Plate 1, figure 12

Only elliptical to broadly subcircular forms were identified as *C. bicircus*, as shown in the holotype and paratype (Bown, 2005, pl. 9 figs. 11, 12, 14, and 15). Circular forms (Bown, 2005, pl. 9 fig. 13) were identified as *Markalius inversus* as the authors believe the description of Bown (2005) may overlap in part with the original description of *Markalius inversus*. The LO of this species was observed below that of the original description (NP15a) and the revision of Bown Dunkley Jones and Young (2007) (NP14b). *Observed range*: CP11-14b; NP12-17

Calcidiscus? ellipticus Shamrock and Watkins, **n. sp.**
Holotype: Plate 1, figure 13; *paratype:* Plate 1, figure 14; *see also:* Plate 2, figure 1

Etymology: For the elliptical outline of this species

Diagnosis: Small to medium sized, elliptical placolith with an open central-area and bright inner collar

Description: Small to medium sized, broadly to normally elliptical placolith with non-birefringent shields and bright, narrow collar. The relatively narrow, non-birefringent shields are composed of ~ 35-50 slightly imbricated elements and give a smooth margin. The central-area is moderately wide and vacant, encircled by a narrow, bright inner collar. The collar shows four thin, slightly oblique isogyres, and both the inner and outer perimeters are well-defined by extinction lines in cross-polarized light.

Dimensions: **Length:** 4.8-7.0μm, μ = 5.8, s.d. = 0.6; **Width:** 3.7-6.0μm, μ = 4.8, s.d. = 0.6; **Eccentricity:** 1.11-1.38, μ = 1.22, s.d. = 0.1; **CA** (% of size): 40-59%, μ = 49.3%, s.d. = 0.3; N = 30 for all data.

Remarks: This species is tentatively placed into the genus *Calcidiscus* due to its resemblance to *C. protoannulus*, but is readily differentiated from the round *C. protoannulus* by its elliptical outline. The LO of *C. ellipticus* n. sp. occurs at the base of CP11 and is most abundant prior to, and for a short time after, the LO of *C. protoannulus* (within CP12a). This stratigraphic relationship, in addition to the morphological similarities, makes *C. ellipticus* n. sp. a likely precursor of *C. protoannulus*.

Calcidiscus ellipticus n. sp. was rare but consistent above CP12a.

*Observed range***:** CP11-16a; NP14a-21

Type Section: ODP Leg 122 Site 762C, Exmouth Plateau

Type Level: 17-5-(49.5-50.5cm), 319.00 mbsf

Calcidiscus*? *gerrardii Bown and Dunkley Jones 2006
Plate 2, figure 2-3

The HO of this species at Hole 762C is extended from the original description (NP16) and of Bown Dunkley Jones and Young (2007) (NP16). *Observed range***:** CP14a?-14b; NP16-17

Calcidiscus*? *henrikseniae Bown 2005
Plate 2, figures 4-5

The HO occurs just above the base of CP14b. This species was observed above the range of the original description (NP15b-c) and that of Bown Dunkley Jones and Young (2007) (NP15c-16). *Observed range***:** CP14a?-14b; NP16-NP17

Calcidiscus*? *pacificanus (Bukry 1971) Varol 1989
Plate 2, figure 6

Peak abundance occurs in CP10-11. *Observed range***:** CP9a-14b; NP10-17

Calcidiscus*? *parvicrucis Bown 2005
Plate 2, figure 7

The HO of this species was observed above that of the original description (NP11), but is in agreement with the revised range of Bown Dunkley Jones and Young (2007). *Observed range***:** CP9a-10; NP10-12s

Calcidiscus protoannulus (Gartner 1971) Loeblich and Tappan 1978
Plate 2, figure 8

Peak abundance occurs in CP14b-15b, also noted in Wei and Wise (1989b). *Observed range***:** CP12b-16a; NP12-21

Coronocyclus nitescens (Kamptner 1963) Bramlette and Wilcoxon 1967
Plate 2, figure 9

The LCO occurs in CP14b. *Observed range***:** CP14a?-16a; NP16-21

Coronocyclus prionion (Deflandre and Fert 1954) Stradner and Edwards 1968
Plate 2, figure 10

This species is considered valid by some authors (e.g. Wise et al. 2004), while others considered it a synonym of *C. nitescens* (Bown, 2005). Although *C. nitescens* is derived from *C. prionion*, and some intermediate forms can be identified, *C. nitescens* and *C. prionion* do show unique characteristics and should be differentiated. *Coronocyclus nitescens* is characterized by a serrate or toothed margin with little to no differentiation between the inner and outer cycles, while *C. prionion* is distinctly bicyclic with a bright, gyred, inner cycle and non-birefringent outer shield. If further analysis shows these two species are indeed synonyms then the earlier named *C. prionion* (Deflandre and Fert, 1954) would take precedence over *C. nitescens* (Kamptner, 1963).

Coronocyclus prionion is also notably similar to *Umbilicosphaera*? *bramlettei* and is differentiated here by size. Descriptions by Bown (2005) and Bown, Dunkley Jones and Young (2007) describe *U.*? *bramlettei* as 3.5-7.5µm. This designation has been followed, and specimens >7.5µm have been identified as *C. prionion*. Maximum abundance (2-3%) occurs early in its range (CP10-12a), becoming rare above CP12a. *Observed range***:** CP10-14b; NP12-17.

Coronocyclus serratus Hay et al. 1966
Plate 2, figure 11

Though *C. serratus* may be a preservational variant of *C. nitescens,* the observed range is notably consistent with other published data. *Coronocyclus nitescens* has a smooth outer margin, in contrast to the serrate or toothed margin of *C. serratus*. Specimens of *Coronocyclus serratus* were smaller than *C. nitescens* at Site 762, but statistical analysis in needed to verify this relationship. In addition, ranges of these species are significantly different, suggesting a valid species. *Observed range***:** CP15b-16a; NP19/20-21

Hayaster* cf. *perplexus (Bramlette and Riedel 1954) Bukry, 1973
Plate 2, figure 12

Perch-Nielsen (1985) identifies the FO of *H. perplexus* in the Oligocene; however, both this study and Bown, Dunkley Jones and Young (2007) show evidence for a considerably earlier first appearance, though extremely rare. The imaged specimen is identified as *Hayaster* cf. *perplexus*, based on the vague central structure visible in Plate 2-12, though this may be a preservational artifact. Observed *range***:** CP13b; NP15b

***Oolithotus* sp.?**
Plate 3, figure 1

Several specimens of uncertain origin have been tentatively assigned to the genus *Oolithotus,* due to the slightly asymmetrical central depression, characteristic of the type species *O. fragilis (*Lohmann, 1912) Martini and Müller 1972. *Observed range***:** CP15a-15b; NP18-19/20

Umbilicosphaera*? *bramlettei (Hay and Towe 1962) Bown, Dunkley Jones and Young 2007
Plate 3, figures 2-3

This species shows peak abundance in CP9b-10, becoming rare in CP12a, and sporadic from CP14a. This species has been limited to specimens < 7.5µm. *Observed range***:** CP9b-14a; NP11-16

Umbilicosphaera jordanii Bown 2005
Plate 3, figure 4

Observed range: CP9a-16a; NP10-21

Family **COCCOLITHACEAE** Poche 1913, emend. Young and Bown 1997

Birkelundia biparteoperculata Varol 1991(a)
Plate 3, figures 5-6

This medium to large species was rare but relatively consistent at Hole 762C. *Birkelundia biparteoperculata* has three weakly birefringent shields (Plate 3-5b), except for two small areas near the long axis, and a characteristic plate covering the center area which becomes bright when the specimen is rotated (Plate 3-6a). *Observed range*: CP15a-16a; NP18-21

Bramletteius serraculoides Gartner 1969
Plate 3, figure 7

The LO is observed near the top of CP13b, with LCO within CP14a, also noted in Wei and Wise (1990a). Peak abundance occurs in CP15a-b (μ = 2.0, max. = 5.4%). *Observed range*: CP13b-16a; NP15b-21

Campylosphaera dela (Bramlette and Sullivan 1961) Hay and Mohler 1967
Plate 3, figure 8

Though the HO of *C. dela* is reported by Perch-Nielsen (1985) as CP14a, Bown (2005), Bralower and Mütterlose (1995), and this study identified *C. dela* in CP14b/NP17. Peak abundance occurs through CP10-11 (μ = 2.1%), with maximum abundance (3.6%) near the ETM3/"X"-event, also shown in Agnini et al. (2007a). *Observed range*: CP9a-14b; NP10-17

Campylosphaera eodela Bukry and Percival 1971
Plate 3, figure 9

This species can be differentiated from *C. dela* by its robust cross inside a more narrow and elliptical CA, in contrast to *C. dela,* which bears a more delicate cross within a larger CA that is 'sub-rectangular' in outline. Intermediate forms may be difficult to differentiate, as *C. eodela* and *C. dela* co-occur for a time at Exmouth Plateau. *Observed range*: CP8b/9a?-9b; NP9/10?-11

Campylosphaera eroskayi (Varol 1989) Bown 2005
Observed range: CP9a-9b; NP10-11

***Campylosphaera* sp. 2** Bown 2005
Plate 3, figures 10-11

Tzhis form shows consistent morphology throughout its observed range and should be given a unique species name; however, this should be done in conjunction with a more thorough quantitative study of *C. dela* and *C. eodela. Observed range*: CP9a-10; NP10-12

Chiasmolithus bidens (Bramlette and Sullivan 1961) Hay and Mohler 1967
HO observed just above the CP10 boundary. *Observed range*: CP8a-10; NP9-12

Chiasmolithus californicus (Sullivan 1964) Hay and Mohler 1967
Plate 3, figure 12

HO observed just above the base of CP12a. *Observed range*: CP 8a-12a; NP9-12/13?

Chiasmolithus consuetus (Bramlette and Sullivan) Hay and Mohler 1967

This species was consistent through CP12b, but rare and/or sporadic above CP14a. The HCO is observed in CP14b, with HO at the top of CP15b. *Observed range*: CP8a-15b; NP18

Chiasmolithus eograndis Perch-Nielsen 1971

The HO of this species was observed just above the base of CP12a in Hole 762c. *Observed range*: CP9a-12a; NP10-14a

Chiasmolithus eoaltus Persico and Villa 2008

The LO occurs near the top of CP14b, before the LO of *Ch. oamaruensis,* as shown in the original description. Persico and Villa (2008) show a stratigraphic gap between the HO of *Ch. eoaltus* in CP15a and the LO of *Ch. altus* in CP16; however, *Ch. eoaltus* was observed throughout this interval at Site 762C. *Observed range*: CP14b-16a; NP17-21

Chiasmolithus expansus (Bramlette and Sullivan 1961) Gartner 1970

The HCO occurs within CP14a with HO at the base of CP14b. *Observed range*: CP10-14b; NP12-17

Chiasmolithus gigas (Bramlette and Sullivan 1961) Radomski 1968

Observed range: CP13b/13c?; NP15b/15c?

Chiasmolithus grandis (Bramlette and Riedel 1954) Radomski 1968

As noted in Marino and Flores (2002), this species is very rare at the top of its range, though the HO used to mark the base of CP15a is consistent with published data. *Observed range*: CP10-14b; NP12-17

Chiasmolithus minimus Perch-Nielsen 1971

Observed range: CP14a; NP16

Chiasmolithus modestus Perch-Nielsen 1971
Plate 3, figure 13

Observed range: CP14a; NP16

Chiasmolithus nitidus Perch-Nielsen 1971
Plate 3, figure 14

Observed range: CP13a-14b; NP15a-17

Chiasmolithus oamaruensis (Deflandre 1954) Hay et al. 1966
Plate 3, figure 15

This species is rare and sporadic at Site 762C. *Observed range*: CP15a-16a; NP18-21

Chiasmolithus solitus (Bramlette and Sullivan 1961) Locker 1968

The HO marks the base of CP14b/NP17, but this species is very rare at this locality. *Observed range*: CP9a-14a; NP9-16

Chiasmolithus titus Gartner 1970
Plate 4, figure 1

Peak abundance occurs in CP14a (max. = 2.6%), becoming rare and sporadic above CP14b. *Observed range*: CP13a-15b; NP15a-19/20

Clausicoccus fenestratus (Deflandre and Fert 1954) Prins 1979
Plate 4, figure 2

Several issues have been encountered concerning the relationships, both taxonomic and stratigraphic, between *C. fenestratus* and *Cruciplacolithus cribellum.* Though Perch-Nielsen (1985) shows the HO of *C. cribellum* within CP9b and the LO of *C. fenestratus* in CP12, similar forms were observed throughout this intermediate interval. The morphological character of these species is quite similar, and the absence of a stratigraphic gap raises questions about the true relationship between them. Bown (2005) has suggested that *C. cribellum* is, in fact, a synonym of *C. fenestratus.* That recommendation has been followed here only for specimens <10μm in length: *Clausicoccus fenestratus* was originally described as a notably small species (4.3 x 3.1μm), whereas *C. cribellum* was first described with greater size variation (6-14μm). Later work by Romein (1979, fig. 29) shows a distinct offset between the appearance of small and large forms of *C. cribellum*, in the *Discoaster multiradiatus* zone (CP8) and *Tribrachiatus orthostylus* zone (CP10), respec-

tively. Such large specimens (>10µm) also appear consistently in CP10 at Exmouth Plateau. Though no specific size division was noted, the authors in this study have informally divided small and large version of "*C. cribellum"* at 10µm. As a result, those specimens <10µm are considered synonymous with *C. fenestratus*, while those >10µm are identified as *C. cribellum* until a more detailed study can be conducted. *Observed range*: CP8b/9a?-16a; NP9/10?-21

Clausicoccus subdistichus (Roth and Hay, in Hay et al. 1967) Prins 1979
Plate 4, figure 3

Peak abundance occurs at the top of the section, from ~1.0% in CP15b and lower CP16a to ~4.0% in the upper two samples, and likely indicates the base of the *Clausicoccus* acme. *Observed range*: CP11-16a; NP12-21

Clausicoccus vanheckiae (Perch-Nielsen 1986) DeKaenel and Villa 1996
Plate 4, figure 4

This species is observed above and below the range given in Perch-Nielsen (1985). The LO occurs very near the CP12a/b boundary, with HO at the top of CP14b. *Observed range*: CP12a-14b; NP14a-17

Coccolithus cachaoi Bown 2005
Plate 4, figure 5

The HO of this species at Hole 762C is extended from the original description (NP14b/15a-15b). *Observed range*: CP12a-14b; NP14a-17

Coccolithus crassus Bramlette and Sullivan 1961

The HO occurs just above the CP11/12a boundary, with a significant acme (max. = 8.6%) and rapid decline over its short range. *Observed range*: CP11-12a; NP12-14a

Coccolithus crucis Bown 2005

Observed range: CP13b-14b; NP15b-17

Coccolithus eopelagicus (Bramlette and Riedel 1954) Bramlette and Sullivan 1961

Observed range: CP12a-16a; NP14a-21

Coccolithus foraminis Bown 2005

The HO of *C. foraminis* occurs significantly above that given in the original description (NP10; CP9a), though rare above CP9b. *Observed range*: CP8b/9a?-12a; NP9/10?-14a

***Coccolithus latus*?** Bown 2005

The observed range of this species at Hole 762C is extended from the original description (NP10/11-11). *Observed range*: CP9a-10; NP10-12

Coccolithus minimus Bown 2005
Plate 4, figure 6

Most abundant in CP9a - lower CP10, *C. minimus* is rare but consistent through CP14a. *Observed range*: CP8b/8a?-14a; NP9/10?-16/17

Coccolithus mutatus (Perch-Nielsen 1971) Bown, 2005
Plate 4, figure 7

Observed range: CP13a-14b; NP15a-17

Coccolithus pelagicus (Wallich 1877) Schiller 1930

Observed range: CP8a-16a; NP9-21

Coccolithus staurion Bramlette and Sullivan 1961

Observed range: CP14a?-14a; NP16

Cruciplacolithus cassus Bown 2005
Plate 4, figure 8

Though similar to *Calcidiscus ellipticus* n. sp., that species has a lower tube cycle and the extinction lines between the tube cycle and the shield is more distinct than in *C. cassus*. *Observed range*: CP8b/9a?-12a; NP9/10?-14a

Cruciplacolithus cribellum (Bramlette and Sullivan 1961) Romein 1979
Plate 4, figures 9-10

Only specimens =10µm were identified as *C. cribellum,* due to the morphological issues discussed in *Clausicoccus fenestratus* (above). Often reported through CP9, work by Sullivan (1965) shows consistent co-occurrence with D. sublodoensis in CP12a. This large form was present, though rare, through CP14b at 762C, and Bralower and Mütterlose (1995) provide a similar range (CP10-CP13b). This robust form may have been previously grouped with the large *Clausicoccus vanheckiae,* but is easily distinguished by its wide shield and broadly elliptical outline. *Clausicoccus vanheckiae* is normally to narrowly elliptical (1.24-1.51, $\mu = 1.34$, N =20) and the CA accounts for a significantly greater proportion of the coccolith (% CA: $\mu_{C.\ cribellum} = 45.9\%$; $\mu_{C.\ vanheckiae} = 61.6\%$; $p_{same} = 1.01E^{-64}$), so that the shield is significantly more narrow. Dimensions are as observed at Site 762C (N = 20): Length: 10.0-13.7 µm, $\mu = 11.8$ µm, s.d. = 1.3; Width: 7.9-12.6 µm, $\mu = 9.9$ µm, s.d. = 1.3; Eccentricity: 1.09-1.27, $\mu = 1.19$, s.d. = 0.1; CA Ratio (% total size): 38.6-55.5%; $\mu = 47.1\%$, s.d. = 3.6. Observed range: CP9b-14b; NP11-17

Cruciplacolithus cruciformis (Hay and Towe 1962) Roth 1970
Plate 4, figures 11-12

This species was consistent from CP9a through the HCO in CP12a. Several short pulses were observed above this level in CP12a, CP13a, and CP14a. This late appearance is also recorded by Bown (2005) from CP13a-14b (NP15a-17). Single specimens are also observed in several samples from CP15a and CP15b. It is difficult to discern if these specimens are reworked, as they are well-preserved, with delicate structures intact. The angle of the cross-bars relative to the axes varied throughout the section, and additional research would establish if these phenotypic variations occur in any systematic fashion.

Observed range: CP8b/9a?-15b?; NP9/10?-19/20?

Cruciplacolithus latipons Romein 1979

Observed range: CP8a/8b?; NP9/10?

Cruciplacolithus nebulosus Shamrock and Watkins. **n. sp.**
Holotype: Plate 4, figure 13; *Paratype*: Plate 4, figure 14; *see also*: Plate 4, figure 14

Cruciplacolithus cf. *primus* BOWN 2005, pl. 5, figs. 20, 22-23

Etymology: (L.) hazy, obscure, cloudy, for the characteristic appearance of the shield.

Calciosolenia., Rhabdosphaera., Zygodisca., Calcidisca

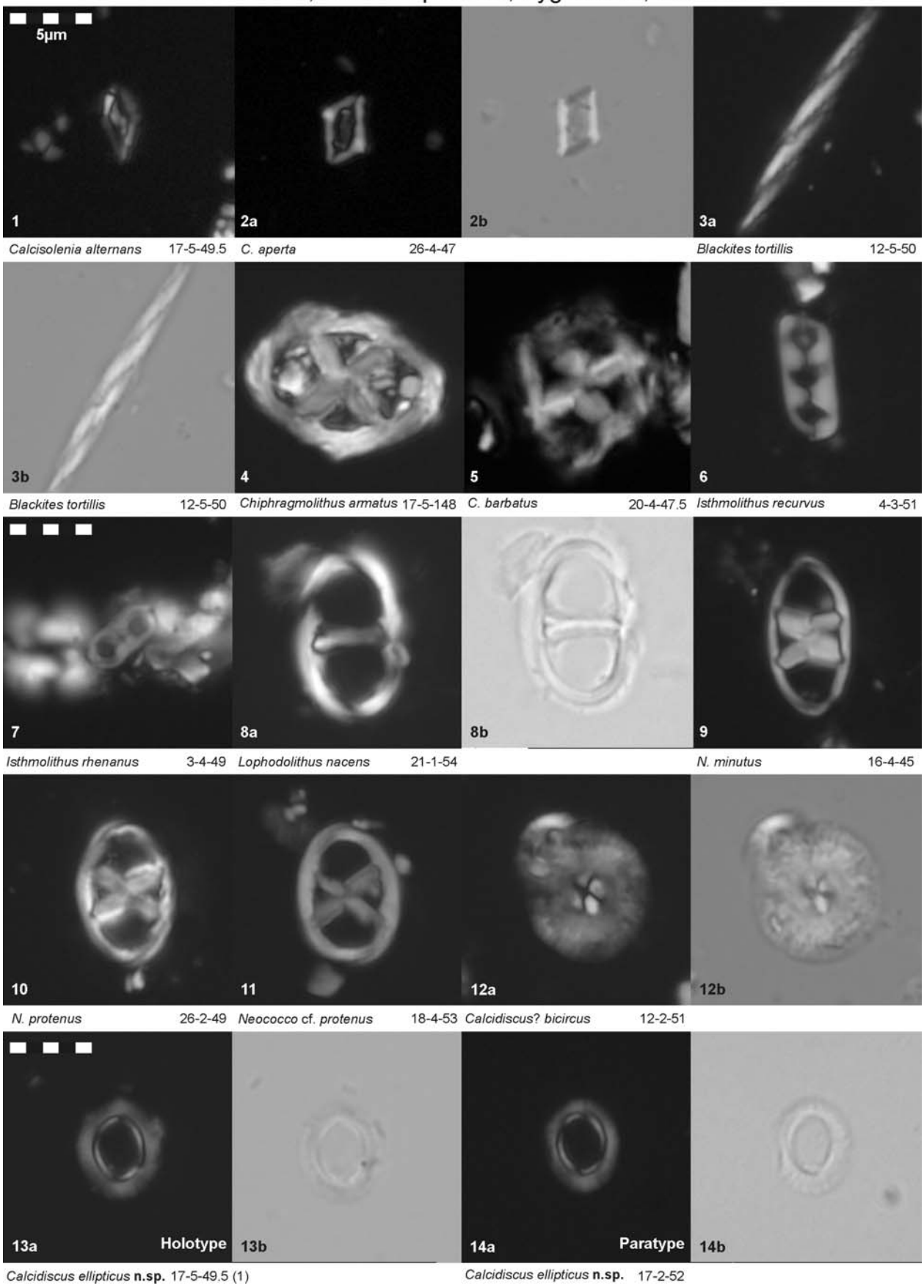

Calcisolenia alternans 17-5-49.5 *C. aperta* 26-4-47 *Blackites tortillis* 12-5-50

Blackites tortillis 12-5-50 *Chiphragmolithus armatus* 17-5-148 *C. barbatus* 20-4-47.5 *Isthmolithus recurvus* 4-3-51

Isthmolithus rhenanus 3-4-49 *Lophodolithus nacens* 21-1-54 *N. minutus* 16-4-45

N. protenus 26-2-49 *Neococco* cf. *protenus* 18-4-53 *Calcidiscus? bicircus* 12-2-51

Calcidiscus ellipticus **n.sp.** 17-5-49.5 (1) *Calcidiscus ellipticus* **n.sp.** 17-2-52

Diagnosis: Small to medium, elliptical placolith with a thin axial-cross spanning the CA.

Description: Small to medium, broadly to normally elliptical placolith with an open CA spanned by an axial cross. The distal shield is comprised of 30-45 weakly birefringent elements that are radially oriented, though interference figures and extinction lines show weak obliquity. Although the elements are discrete in plane light, the shield has a distinctly 'fuzzy' appearance under cross polarizers, for which the species is named. The CA is surrounded by a highly birefringent collar crossed by thin, gyred, off-axis extinction lines. When rotated, the extinction lines within the inner cycle converge toward the longitudinal axis, highlighting a bright element at either end. The open CA comprises 35-50% (μ = 42%) of the long axis and 25-40% (μ = 32%) of the transverse axis of the ellipse. The CA is spanned by a thin, delicate, axial cross which may be slightly asymmetrical. This central cross is birefringent when aligned to the polarizers but extinct at 45°.

Dimensions: Length: 4.4-6.9μm, μ = 6.0, s.d. = 0.7; Width: 3.4-5.5μm, μ = 4.7μm, s.d. = 0.6; CA Length: 2.0-3.0μm, μ = 2.5ìm, s.d. = 0.2; CA Width: 1.2-1.8μm, μ = 1.5, s.d. = 0.2; Eccentricity: 1.23-1.39, μ = 1.29, s.d. = 0.05; N = 30 for all data

*Remarks***:** *Cruciplacolithus nebulosus* **n sp.** is extremely rare from the LO near the CP12b boundary, but shows a minor increase in abundance toward the end of its observed range, in upper CP15b. The central cross is extremely delicate and may be absent even in relatively well-preserved material, but can be indicated by the four, birefringent points of attachment that remain along the collar. *Cruciplacolithus nebulosus* n. sp. can be readily differentiated from other species of *Cruciplacolithus* by size and stratigraphic range, as well as the distinct, 'fuzzy' appearance of the shield. *Cruciplacolithus nebulosus* can be differentiated from *Bramletteius serraculoides,* which also bears a delicate axial cross, by the notably wider shield of the former.

*Observed range***:** CP12a-16a; NP14a-21

Type Locality: ODP Leg 122 Site 762C, Exmouth Plateau

*Type Level***:** 5-1-(50-51cm), 199.00 mbsf

Cruciplacolithus opacus Shamrock and Watkins, **n. sp.**
Holotype: Plate 5-2; *Paratype*: Plate 5-3; *see also*: Plate 5-4

Etymology: (L.) shady, dark, opaque, for the predominantly non-birefringent character of the entire coccolith

Diagnosis: Medium to large, elliptical placolith with a non-birefringent central cross

Description: Medium to large placolith that is broadly to narrowly elliptical, though most specimens show normal eccentricity (μ = 1.28, s.d. = 0.07). The broad shields are composed of 30-40, non-birefringent, radial elements. Weak sutures across the shield bend near the inner margin, giving a weakly birefringent, beaded appearance, particularly at 45° to the polarizers. The CA is narrowly elliptical (μ = 2.06) and encircled by a thin, birefringent inner cycle, crossed by four, curved extinction lines. The center of the coccolith is spanned by a small, non-birefringent, axial cross that appears to fill the small central opening, with sharp, low-angle, diagonal extinction lines at 0°.

Dimensions: Length: 6.7-10.3μm, μ = 8.9μm, s.d. = 1.0; Width: 4.8-8.5μm, μ = 6.9μm, s.d. = 0.9; Eccentricity: 1.19-1.58, μ = 1.28, s.d. = 0.07; CA Length: 2.3-4.5μm, μ = 3.6μm, s.d. = 0.6; CA Width: 1.1-2.9μm, μ = 1.8μm, s.d. = 0.4; CA Eccentricity: 1.51-2.87, μ = 2.06, s.d. = 0.35; N = 30 for all data

*Remarks***:** This species is quite rare from its FO just below the CP13b boundary, but becomes more consistent within CP15b. *Cruciplacolithus opacus* n. sp. can be differentiated form *C. latipons* and *C. cribellum*, which also have axial crosses that appears to fill the CA, by its narrow CA and dark, non-birefringent appearance.

*Observed range***:** CP13a-16a; NP15a-21

*Type Locality***:** ODP Leg 122 Site 762C, Exmouth Plateau

*Type Level***:** 5-1-(50-51cm), 199.00 mbsf

Cruciplacolithus* cf. *tenuis Perch-Nielsen 1977

Though the HO is typically shown within the Paleocene, several specimens of *Cruciplacolithus* cf. *tenuis* are observed in the lowermost Eocene. Bybell and Self-Trail also note occurrence of this form in NP9, and potentially NP10. Though consistently present through this interval, these specimens still may be reworked, and a multi-site study may reveal the true HO of this species. *Observed range***:** CP9a-9b; NP10-11

Cruciplacolithus tarquinius Hay et al.1967

This species is exceedingly rare in this section. *Observed range***:** CP13b; NP15b

Ericsonia cava (Hay and Mohler 1967) Perch-Nielsen 1969

This species is most abundant in the early Eocene, but becomes increasingly rare through its range. *Observed range***:** CP8a-16a; NP9-21

Ericsonia robusta (Bramlette and Sullivan 1961) Perch-Nielsen 1977

*Observed range***:** CP8a; NP9

Ericsonia formosa (Kamptner 1963) Haq 1971

Abundance of this species fluctuates throughout its observed range (min = 0.4%; max = 6.6%; μ. = 3.2%). *Observed range***:** CP9a-16a; NP10-21

Order **ISOCHRYSIDALES** Pascher 1910
Family **NOELAERHABDACEAE** Jerković 1970, emend. Young and Bown 1997

Bicolumnatus ovatus Wei and Wise 1990
Plate 5, figure 5

Some authors consider this species to be a preservational variant of *D. bisectus* (Young and Bown, 1997), while others [Monechi, Buccianti and Gardin (2000); DeKeanel and Villa (1996)] consider it a unique species. The LCO of *B. ovatus* does not occur until the uppermost portion of CP14b, significantly above the LCO of *D. bisectus.* In addition, the relative abundance of this species does not mimic the changes seen in *D. bisectus*, suggesting *B. ovatus* is a unique species. *Observed range***:** CP14b-16a; NP17-21

Calcidiscaceae

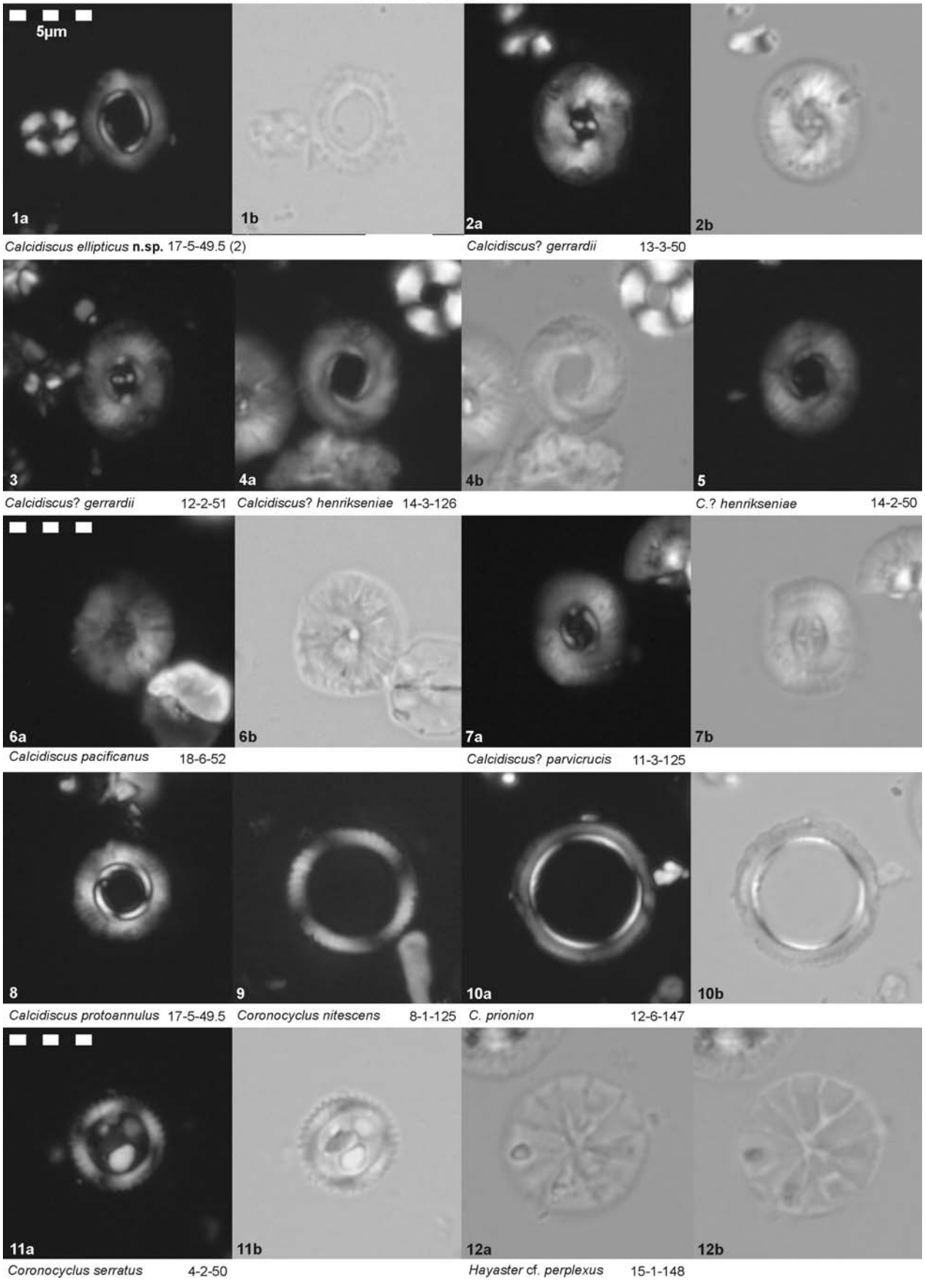

Calcidiscus ellipticus **n.sp.** 17-5-49.5 (2)

Calcidiscus? gerrardii 13-3-50

Calcidiscus? gerrardii 12-2-51

Calcidiscus? henrikseniae 14-3-126

C.? henrikseniae 14-2-50

Calcidiscus pacificanus 18-6-52

Calcidiscus? parvicrucis 11-3-125

Calcidiscus protoannulus 17-5-49.5

Coronocyclus nitescens 8-1-125

C. prionion 12-6-147

Coronocyclus serratus 4-2-50

Hayaster cf. *perplexus* 15-1-148

Cribrocentrum reticulatum (Gartner and Smith 1967) Perch-Nielsen 1971
Plate 5, figure 6

This species consists of a significant proportion of the assemblage from LO into CP15a (5-10%). Sporadic but well-preserved specimens were observed through early CP16a. It is difficult to determine if such specimens are reworked or represent a true HO, as Bralower and Mütterlose (1995) also identify this species within CP16. *Observed range*: CP14a-16a; NP16-21

Cribrocentrum* cf. *reticulatum (Gartner and Smith 1967) Perch-Nielsen 1971

Frequent specimens are observed similar to *C. reticulatum* in size, shape, and rim structure, but lacking the diagnostic central grill. Trends in abundance mimic those of *C. reticulatum* and stratigraphic ranges are nearly identical, therefore, this form is considered a preservational variant. *Observed range*: CP14a?-15b; NP16-19/20

Cyclicargolithus floridanus (Hay et al. 1967) Bukry 1971

This species shows an abundance increase within CP14a and an abundance acme (5-10%) within CP15a. *Observed range*: CP14a?-16a; NP16-21

Cyclicargolithus luminis (Sullivan 1965) Bukry 1971
Plate 5, figures 7-8

Sporadic specimens were identified in the middle Eocene. See also Sullivan (1965, plate 3, #9a-b), Perch-Nielsen (1985, fig. 59: 26-27) and Bybell (1975, pl 5: #6). *Observed range*: CP11-13b; NP12-15b

***Cyclicargolithus parvus* n. sp.**
Holotype: Plate 5, figure 9; *Paratype:* Plate 5, figure 10

Cyclicargolithus luminis BOWN 2005; pl. 2, figs. 1-2

Etymology: (L.) For the small size (μ = 4.2μm) of this form

Diagnosis: Small, circular placolith with a quadrate interference figure.

Description: Small circular placolith with a small central opening and a bicyclic shield. The central opening is square to sub-circular in shape and is surrounded by a bright inner cycle. The shields are composed of 25-40 thin, slightly imbricated elements with clear sutures at the periphery that become less distinct inward. The larger proximal shield is 40-60% larger than the distal shield, and both are weakly birefringent. The quadrate interference figure is thin and sharp as it curves across the bright inner cycle and broadens outward across the shields.

Dimensions: Proximal shield: 3.2-5.0μm, μ = 4.2μm, s.d. = 0.5; Distal shield: 1.6-2.8μm, μ = 2.2μm, s.d. = 0.3; N = 30 for all data

Remarks: Cyclicargolithus parvus differs from *C. luminis* in both stratigraphic range and morphology: *C. parvus* is restricted to CP8a-CP10, while *C. luminis* is generally reported from the middle to late Eocene, though it was observed low in this section (CP11). *Cyclicargolithus luminis* was originally described as 6-8μm in diameter and measured specimens all fall within this range (6.15-7.89μm), while *C. parvus* n. sp. is = 5.0μm. Sutures between shield elements are very distinct in *C. parvus* but are not readily visible in *C. luminis*. In addition, *C. parvus* shows low order grey interference colors while *C. luminis* shows higher order birefringence, primarily pale yellow with a faint orange ring. *Cyclicargolithus parvus* was consistently present through its observed range and is most abundant within CP9b (μ = 2-3%). *Cyclicargolithus parvus* can be differentiated from *Cyclagelosphaera prima* Bybell and Self-Trail 1995 by the straight axial extinction figure of the shield and the relatively low relief of the inner cycle.

Type Locality: ODP Leg 122 Site 762C, Exmouth Plateau

Type Level: 25-1-(50.5-51.5cm), 389.01mbsf

Observed range: CP8a-10; NP9-12

Dictyococcites bisectus (Hay et al. 1966), Bukry and Percival 1971

As noted by Villa et al. (2008), this species rapidly becomes a significant proportion of the assemblage, with values > 10% early in its range, but shows a relative decline (~3-4%) by the top of the Eocene. *Dictyococcites bisectus* shows two notable abundance peaks, also recorded in Wei and Wise (1990a), in CP14b (μ = 8%) and CP15b (μ = 10%), with a maximum abundance of 14.6%. *Observed range*: CP14b-16a; NP17-21

Dictyococcites filewiczii Wise and Wiegand in Wise 1983

Observed range: CP15a-16a; NP18-21

Dictyococcites scrippsae Bukry and Percival 1971
Plate 5, figure 11, plate 6, figure 1

This species shows a notable acme from CP12a-14a (max 15%), decreases steadily through CP14, becoming rare within CP15b. Though considered a synonym of *D. stavensis* by Bown (2005), these species are distinct in several ways: Stratigraphically, *D. scrippsae* appears before both *D. bisectus* and *D. stavensis* and morphologically, the vast majority of *D. scrippsae* specimens were significantly smaller (=7.5μm) than the holotype (~ 9.5μm), while *D. stavensis* must be >10μm. *Dictyococcites scrippsae* shows continuous, sharp extinction figures within the CA that bend sharply before broadening across the shield, while the CA of *D. stavensis* shows a prominent plug with notable relief, showing bright, 2nd order interference colors. *Observed range*: CP11-16a; NP13-21

Dictyococcites stavensis (Levin and Joerger 1967) Varol 1989

Morphologically similar to *D. bisectus* but >10μm in length. The LO occurs slightly above *D. bisectus*, which can be sporadic at the base of its range; however both forms are common and show similar patterns of abundance above this level. The authors agree with Agnini et al. (2010) that the rapid appearance of this larger species may be useful as a biostratigraphic marker. *Observed range*: CP14b-16a; NP17-21

Reticulofenestra daviesii (Haq 1968) Perch-Nielsen 1971 (d)
Plate 6, figures 2-3

This species is included in this genus rather than *Dictyococcites,* since the CA is not filled by a solid plug of radially oriented elements. *Observed range*: CP14a?-16a; NP15b-21

Reticulofenestra dictyoda (Deflandre in Deflandre and Fert 1954) Stradner in Stradner and Edwards 1968

The FO of *R. dictyoda* occurs within CP10, earlier than commonly reported, also noted in Bown (2005) and Bralower and

Calcidiscaceae, Coccolithaceae

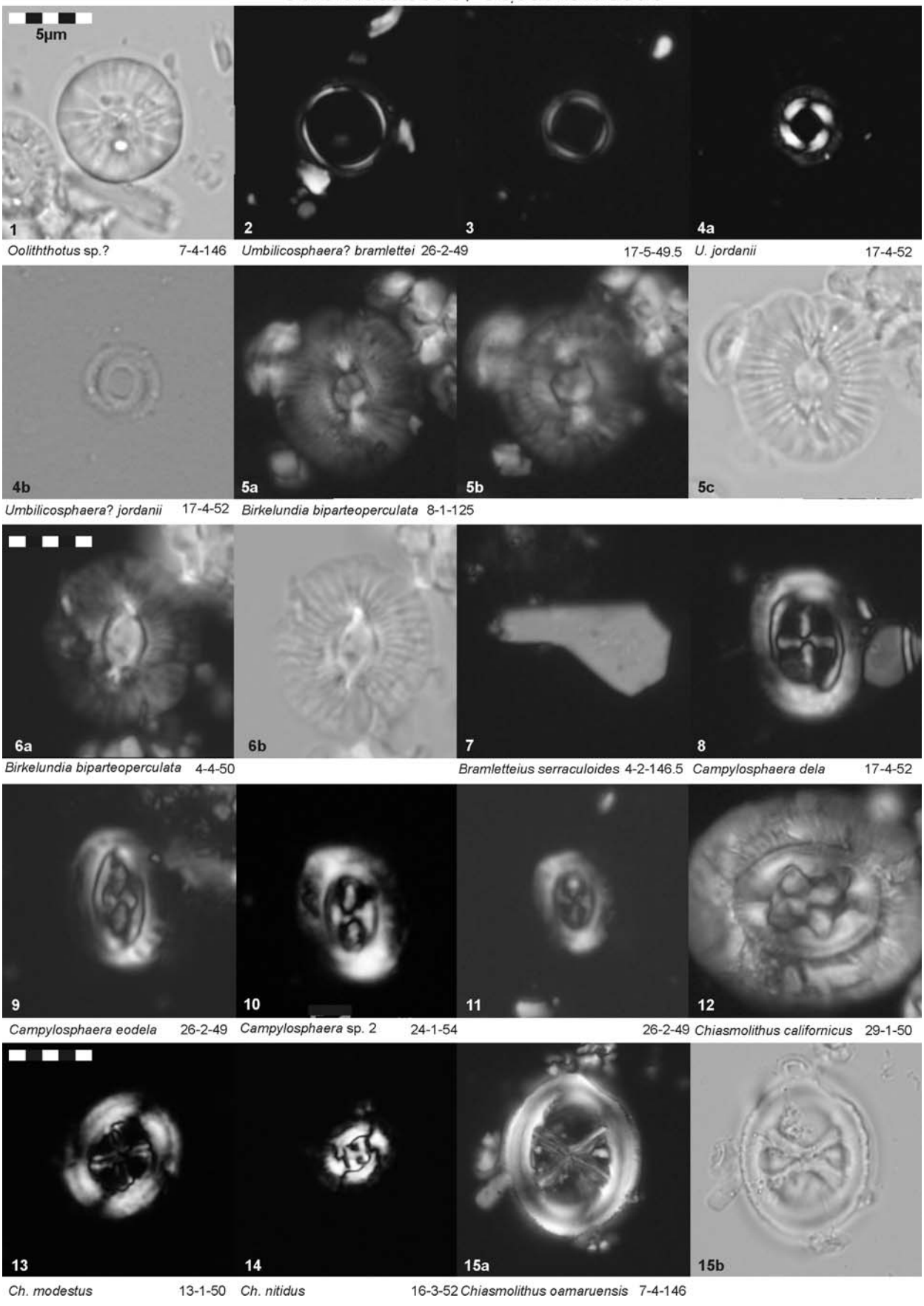

Ooliththotus sp.? 7-4-146 *Umbilicosphaera? bramlettei* 26-2-49 17-5-49.5 *U. jordanii* 17-4-52

Umbilicosphaera? jordanii 17-4-52 *Birkelundia biparteoperculata* 8-1-125

Birkelundia biparteoperculata 4-4-50 *Bramletteius serraculoides* 4-2-146.5 *Campylosphaera dela* 17-4-52

Campylosphaera eodela 26-2-49 *Campylosphaera* sp. 2 24-1-54 26-2-49 *Chiasmolithus californicus* 29-1-50

Ch. modestus 13-1-50 *Ch. nitidus* 16-3-52 *Chiasmolithus oamaruensis* 7-4-146

Mütterlose (1995). Both small (3-5µm) and large (6-14µm) forms appear in the same sample interval, and patterns of abundance suggest that these size variants are likely the same species. This species shows a significant increase in abundance in CP12a and comprises =15% of the assemblage through CP14a. A second increase is observed near the top of CP15 to >20% relative abundance in CP16a. *Observed range*: CP10-16a; NP12-21

Reticulofenestra hillae Bukry and Percival 1971

Smaller specimens with similar morphology to *Reticulofenestra hillae* were identified and informally grouped relative to size into *R. hillae A* (5-10µm), *R. hillae B* (>10-14µ), and *R. hillae C* (s.s.) (>14µm). Unlike *R. dictyoda,* these size groups show a distinct sequence of appearance, and this group could benefit significantly from a systematic, statistical revision.

Reticulofenestra hillae* var. *A
Plate 6, figure 4

Though extremely rare, specimens 5-10µm are first seen in upper CP10, increasing significantly in CP12a up to 15-20% of the total assemblage in CP13b-14a. Though slightly less abundant above these subzones, this form remains dominant through the top of the section (>10%) and is significantly more abundant than larger forms. *Reticulofenestra hillae* var. *A* is distinguished from *R. dictyoda* by the relatively wider central area and thinner collar of the former. *Observed range*: CP10-16a; NP12-21

Reticulofenestra hillae* var. *B
Plate 6, figure 5

This size range is significantly less abundant than those 5-10µm in size, generally < 2%. *Observed range*: CP12a-16a; NP14a-21

***Reticulofenestra hillae* s.s.**
Plate 6, figure 6

Extremely rare specimens were observed in CP14a, becoming rare but consistent just below the CP14b boundary. This is interpreted to be the LCO of this species. *Reticulofenestra hillae* s.s. is distinguished from *R. umbilica* by the thicker, higher, more birefringent collar and relatively more narrow shield to CA ratio of *R. hillae* s.s. The morphological relationship between these two species should be statistically examined to verify and quantify these differences. *Observed range*: CP12b-16a; NP15b-21

Reticulofenestra lockeri Müller 1970

While only one specimen was observed in CP14a, this species has its LCO in CP14b, and a notable abundance increase within CP15a. *Observed range*: CP14a-16a; NP16-21

Reticulofenestra minuta Roth 1970

Though present from the middle Eocene, specimens of *Reticulofenestra* = 3µm in length show a notable increase in abundance within CP15 (max.: = 5.2%; µ = 2.8%) *Observed range*: CP12a-16a; NP14a-21

Reticulofenestra oamaruensis (Deflandre in Deflandre and Fert 1954) Stradner in Haq 1968

The LO is observed above the LO of *I. recurvus* but below the LO of *C. reticulatum. Observed range*: CP15b-16a; NP19/20-21

Reticulofenestra umbilica (Levin 1965) Martini and Ritzkowski 1968

Rare and sporadic early in its range, this species becomes relatively common and consistent above ~280 mbsf. *Reticulofenestra umbilica* is distinguished from *R. hillae* s.s. by the thinner collar and relatively wider shield to CA ratio of *R. umbilica*. *Observed range*: CP14a-16a; NP16-21

Reticulofenestra wadeae Bown 2005

This species was observed both below and above the range provided in the original description (NP15b-c; CP13b-c). This may be in part to difficulty in distinguishing this species from other *Reticulofenestra* spp. morphological end-members. The genus *Reticulofenestra* experienced significant diversification after its appearance (late Ypresian), though much of this diversity was not explored until after well-known, broadly described morphologies encouraged biostratigraphers to habitually 'lump' distinct taxa. This genus is in great need of a thorough revision that explores the morphological and stratigraphic relationships between all species, clearly distinguishes similar taxa, and organizes taxonomic synonyms. *Observed range*: CP12b-15a; NP14b-18

Family **PRINSIACEAE** Hay and Mohler 1967 emend. Young and Bown 1997

Girgisia gammation (Bramlette and Sullivan 1961) Varol 1989
Plate 6, figure 7

The LO is observed just below the LO of *D. lodoensis* at Site 762C, and approximates this biomarker (Agnini et al. 2007a, 2006; Bralower and Mütterlose 1995). The HO of *G. gammation* is observed well below the commonly reported CP14a, though a HO in CP12b is also noted in Bralower and Mütterlose (1995). This species is most abundant from upper CP10-CP11 (max. = 5.0%; µ = 3.5%), also shown in Agnini et al. (2007a). *Observed range*: CP9b-12b; NP11-14b

Girgisia* cf. *gammation
Plate 6, figure 8

The LO of a *Girgisia* spp. is noted as *Girgisia* cf. *gammation*, as it exhibits diagnostic characteristics of this species, but bears a square-shaped opening in the CA. This variation is concurrent with *G. gammation* through much of its range, and may be a preservational variant. *Girgisia* cf. *gammation* is distinguished here from *G. gammation* s.s. based on the comments of Perch-Nielsen (1985) who states that *G. gammation* bears "no central opening". In addition, *Girgisia* cf. *gammation* appears to be smaller than *G. gammation* s.s. This form shows peak abundance in CP10-11, with HCO at the base of CP12a, and may be an indication of reduced preservation. *Observed range*: CP9b-12a; NP11-13

Prinsius bisulcus (Stradner 1963) Hay and Mohler 1967

Observed range: CP8a/8b?; NP9/10?

Coccolithaceae

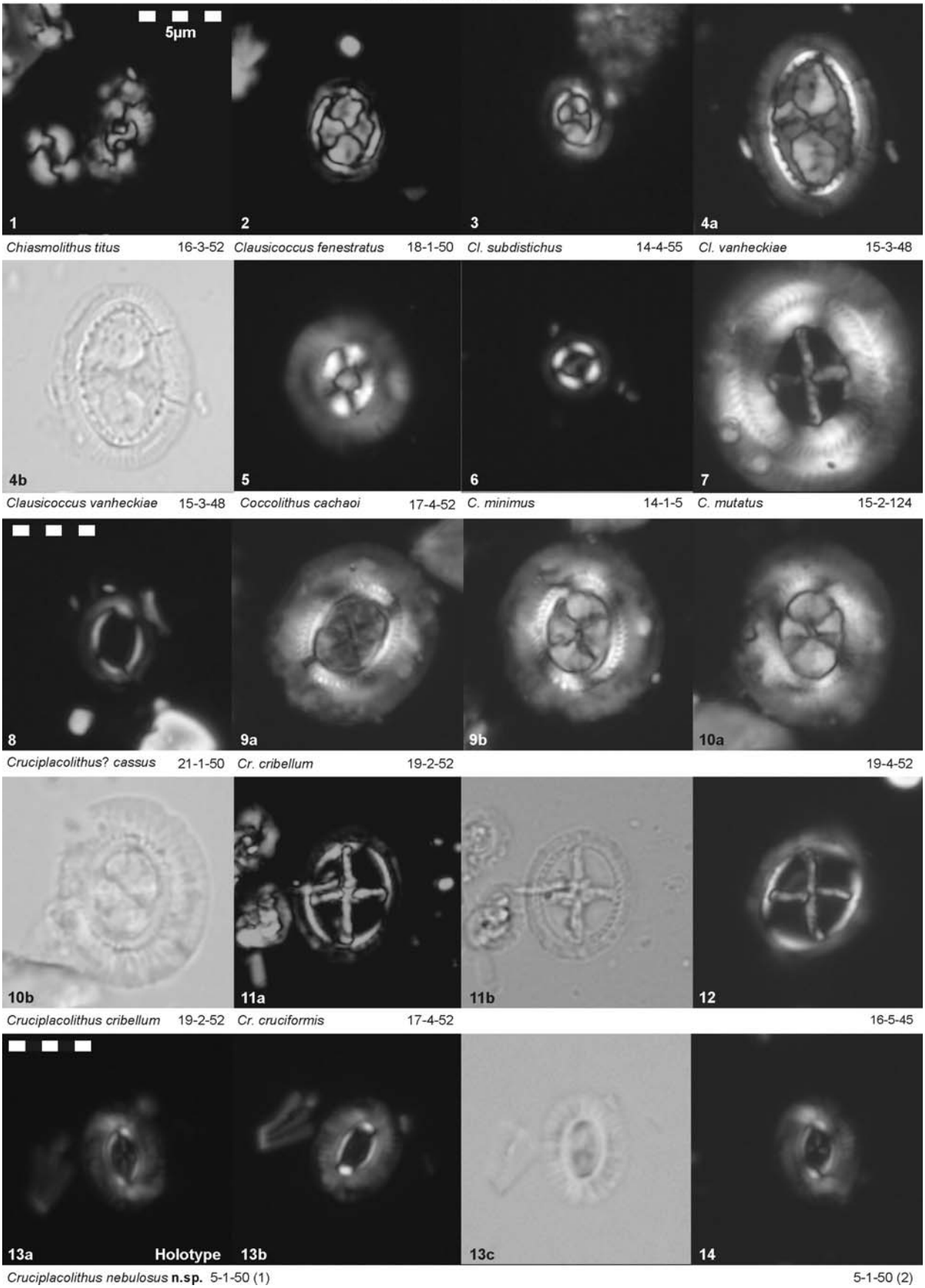

Toweius callosus Perch-Nielsen 1971

The observed LO in CP8a is well below that commonly reported (CP10). Wei and Wise (1990a; 1989b) and Bybell and Self-Trail (1995) show similar trends, with LO in lower CP8a. In addition, images of this species in Bown (2005) are derived from cores spanning CP8a-9b. These observations give robust evidence for a significantly earlier LO than has been commonly reported. This species shows a considerable acme in CP9a-10 (min.: 7.4%; max.: 11.8%; μ: 9.3%) followed by a rapid decline within CP10. *Observed range***:** CP8a-12b; NP9-14b

Toweius eminens (Bramlette and Sullivan 1961) Perch-Nielsen 1971

The HCO of this species occurs at the base of CP9b, with HO within this subzone. *Toweius eminens* is extremely abundant in CP8a (max.: > 17%); however, this interval may be affected by the PETM and indicates a skewed assemblage toward more dissolution resistant species. Though notably robust at the base of the section, the overall size of *T. eminens* appears to decrease through its observed range. This large morphotype may be associated with the Paleocene-Eocene boundary interval, and should be analyzed quantitatively. *Observed range***:** CP8a-9b; NP9-11

Toweius*? *magnicrassus (Bukry 1971) Romein 1979

*Observed range***:** CP9b-12b; NP11-14b

Toweius occultatus (Locker 1967) Perch Nielsen 1971

*Observed range***:** CP9b-11; NP11-12

Toweius pertusus (Sullivan 1965) Romein 1979

This species is most abundant in CP9a-b, with μ= ~6.6% through CP9a. The HCO of *T. pertusus* occurs near the top of CP10, but continues sporadically above this range to the base of CP12a. *Observed range***:** CP8a-12a; NP9-14a

Toweius rotundus Perch-Nielsen in Perch-Nielsen et al. 1978
Plate 6, figures 9-10

The LO is observed in upper CP9a with peak abundance in CP9b - lower CP10. Though Bown (2005) documented this species in CP9 (NP11), Bown and Pearson (2009) show *T. rotundus* as an extinction taxa across the PETM. This is in contrast to our observations and the original description by Perch-Nielsen, which gives an early Eocene type level (CP9b/NP11) and shows a consistent to common abundance through this interval. It is possible that this species experienced a significant contraction in its range and/or abundance during the PETM, but recovered sometime after the excursion. *Observed range***:** CP9a-10; NP10-12

Toweius serotinus Bybell and Self-Trail 1995

This species is notably abundant during CP8a-9a (μ: ~3.0%; max.: 4.4%). *Observed range***:** CP8a-9b; NP9-10

Toweius tovae Perch-Nielsen 1971

*Observed range***:** CP8a; NP9

***Toweius* sp. 1** Bown 2005
Plate 6, figure 11

This species was observed consistently throughout its range with reliable morphological characteristics, including the diagnostic finely-perforate central plate showing a diagonal cross extinction figure. The HO of this species at Hole 762C is extended from the original description (NP10).Published data for his form to date is limited to the Indian Ocean. The global distribution should be examined and the form should be statistically analyzed and systematically described. *Observed range***:** CP8b/9a?-10; NP9/10?-12

***Toweius* sp. 2** Bown 2005
Plate 6, figure 12

This species was observed consistently throughout its range. Key morphological characteristics include an elliptical-subcircular outline, and a diagnostic central plate showing two "V" extinction figures aligned to the long axis that point inward toward the central area. The HO of this species at Hole 762C is extended from the original description (NP11).Published data for his form to date is limited to the Indian Ocean. The global distribution should be examined and the form should be statistically analyzed and systematically described. *Observed range***:** CP8b/9a?-10; NP9/10?-12

Placolith Genera *incertae sedis*

Ellipsolithus distichus (Bramlette and Sullivan 1961) Sullivan 1964

*Observed range***:** CP8a-10; NP9-12

Ellipsolithus lajollaensis Bukry and Percival 1971

*Observed range***:** CP12b-13b; NP14a-15b

Ellipsolithus macellus (Bramlette and Sullivan 1961) Sullivan 1964

This species varies considerably in size, with several specimens <7μm, notably smaller than the size range provided in the original description (9-15μm). The LO is observed at the base of CP9a, and HO near the top of CP12a. *Observed range***:** CP8b/9a?-12a; NP9/10?-14a

Hayella*? *gauliformis Troelsen and Quadros 1971

This species is rare and sporadic throughout its range. *Observed range***:** CP9b-14a?; NP11-16

Hayella? simplex Bown and Dunkley Jones 2006
Plate 6, figures 15-16; plate 7, figure 1

This species is most abundant in CP10-11, becoming rare from CP12a, with HO at the base of CP15a. The LO was observed well below the ranges provided in Bown and Dunkley Jones (2006) or Bown, Dunkley Jones and Young (2007, fig. 1). Plates 6-16 and 7-1 illustrate a preservational variant of this species. These two forms do not differ significantly with respect to the size of the shield or CA, and both show similar degrees of vertical relief and taper. The only morphological variable in which these two forms show statistically significant variation is with respect to the number of shield elements ($\mu_{H.\ simplex} = 30.5$; $\mu_{H.\ simplex\ petalus} = 15.6$; $p_{same} = 1.3E^{-31}$). The full stratigraphic range of this preservational form is contained within a notable abundance peak of *H.*? *simplex*, during an interval of reduced preservation relative to the entire section. This form is likely the result of either loss of the distal shield of *H.*? *simplex* or coarsening of shield elements via dissolution and re-precipitation. It may be shown that this form is indeed independent of *H.*? *simplex,* but will require identification in a section with better preservation. *Hayella* is still considered a provisional genus for this species. Though both of these forms show some constriction

Coccolithaceae, Noelaerhabdaceae

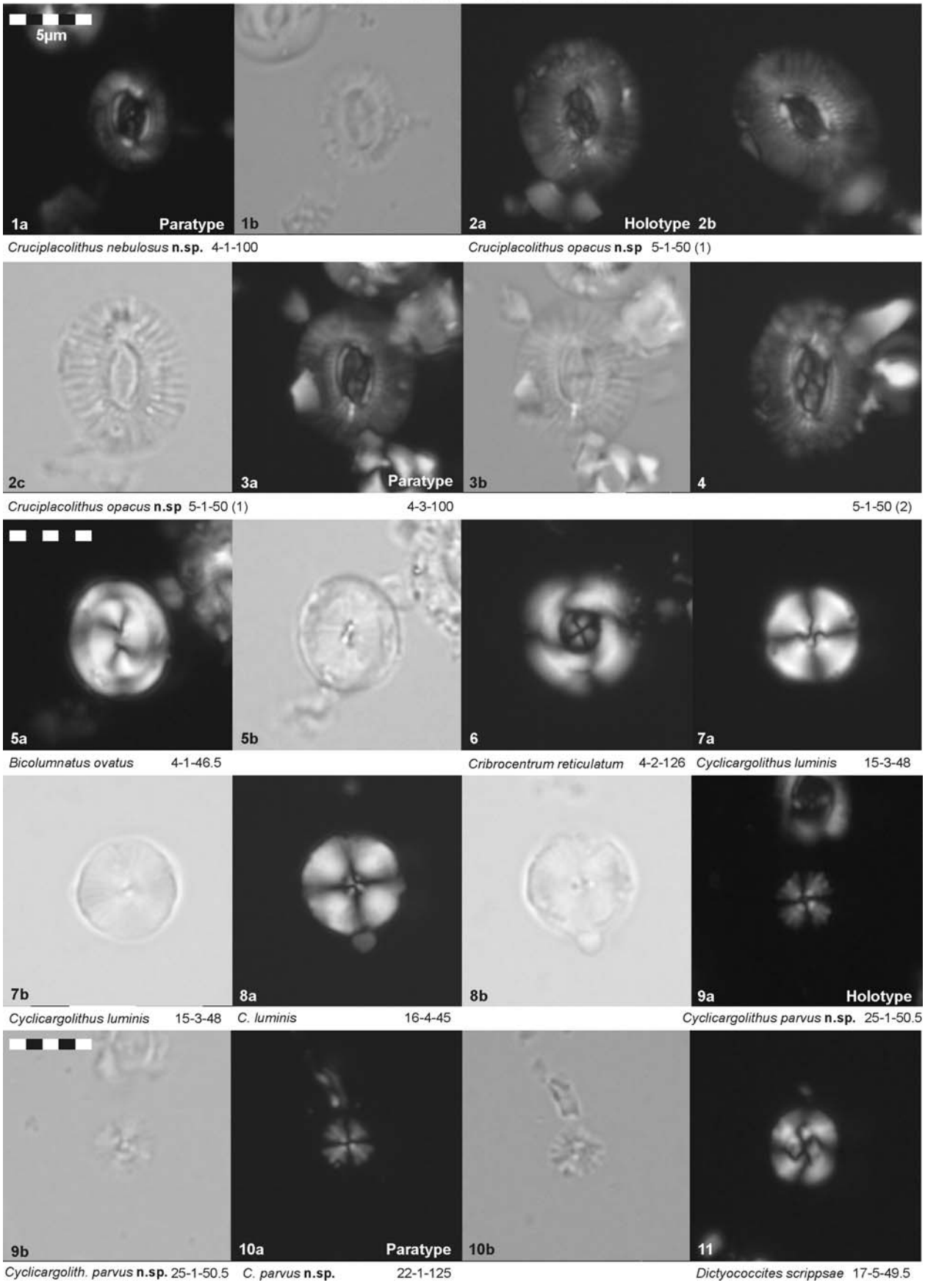

when focusing upwards, they lack the vertical relief and strong conical taper that characterizes the type species *H. situliformis*. *Observed range*: CP10-15a; NP12-17

Hayella situliformis Gartner 1969
Plate 7, figure 2

The LCO was observed within CP15a. *Observed range***:** CP14a-16a; NP16-21

Hayella situliformis* var. *ovata (Gartner 1969) Shamrock and Watkins, **n. var.**
Plate 6, figures 13-14

Hayella situliformis BOWN 2005, pl. 10, fig. 9

Etymology: For the elliptical outline of both shield and collar

Diagnosis: Elliptical placolith with a birefringent shield and high, constricted collar.

Description: Medium to large, broadly to normally elliptical placolith with a wide, open central-area. The birefringent shield is constructed of 25-40 elements that show a quadrate interference figure ~45° to the axes of the ellipse. Elements of the proximal shield appear sinistrally oblique when the distal side (collar) is oriented upward. The form shows high relief, tapering upward like a truncated cone, with the constricted end bearing a distinctly elliptical beaded collar.

Dimensions: Length: 6.9-9.1µm; µ = 8.1µm, s.d. = 0.7; Width: 5.6-7.8µm, µ = 6.6µm, s.d. = 0.7; Collar Length: 2.3-3.4µm, µ = 3.0µm, s.d. = 0.4; Collar Width: 1.7-2.9µm, µ = 2.0µm, s.d. = 0.3; Collar Eccentricity: 1.12-1.95, µ = 1.5µm, s.d. = 0.23; N =17 for all data

Remarks: This species is similar to *H. situliformis* with respect to shield type and high conical taper, but shows a distinctly elliptical outline of both shield and collar. This form was rare at this locality, and biometric data is available for only 17 specimens. More data must be collected on the stratigraphic range of this variant, to determine if the range is identical to *H. situliformis* or more restricted.

*Observed range***:** CP14b-16b; NP16-21

Type Locality: ODP Leg 122 Site 762C, Exmouth Plateau

Type Level: 4-4-(50-51cm), 194.00 mbsf

Markalius inversus (Deflandre *in* Deflandre and Fert 1954) Bramlette and Martini 1964
Plate 7, figure 3

Although the description of Bramlette and Martini (1964) states that the central area of this species can vary in size, the original images of Deflandre (Deflandre and Fert, pl. 9, figs. 4-7) show only specimens with a relatively constricted central area. Measurements of the holotype of Deflandre (Deflandre and Fert, 1954, pl. 9, fig. 4-5) give a CA of ~33%. In addition, measurements provided in the original description of *M. astroporus* (Stradner 1963, considered a synonym by Bramlette and Martini, 1964) also indicate a maximum CA diameter of ~30% (both the original micrograph and sketch in this publication show a CA that is ≤ 33 % of the CA). These accounts suggest that the earliest species concepts of *M. inversus* pertain to specimens with a relatively constricted CA, as opposed to those forms with a more expanded CA, discussed below. As a result, specimens with a central-area ≤ 33% the total diameter of the coccolith have been identified as *M. inversus*. CA: 22.4-33.2 %, µ = 27.8 %, s.d. = 2.5, N = 28. *Observed range***:** CP8b/9a?-16a?; NP9/10?-21

Markalius latus Shamrock and Watkins, **n. sp.**
Holotype: Plate 7, figure 4; *Paratype*: Plate 7, figure 5

Markalius inversus BRAMLETTE and MARTINI 1964, plate 2, figures 7-8. – BYBELL and SELF-TRAIL 1994, plate 36, figures 26, 31

Etymology: (L.) broad or wide, for the expanded central-area that occupies approximately > 33% of the coccolith diameter.

Diagnosis: Medium to large, circular placolith with broad, birefringent CA

Description: Medium to large, bicyclic, circular placolith with a wide CA occupying > 33 % of the coccolith diameter. The distal shield is narrower than the proximalshield, and each is composed of 30-50 oblique elements that are weakly birefringent. The broad CA is depressed and filled with blocky element that are highly birefringent and show a thin, quadrate extinction figure that is slightly off-axis.

Dimensions: Shield diameter: 5.5-9.1µm; µ = 7.2µm, s.d. = 1.13; CA diameter: 2.3-3.8µm, µ = 3.1µm, s.d. = 0.44; CA/Shield ratio: 36.9-48.7 %; µ = 43.8 %; s.d. = 2.9; N = 23 for all data

Remarks: The relative size of the CA was measured in 50 specimens of *Markalius*. This data shows a distinctly non-normal distribution (Figure 9a), with specimens clustering into two dominant populations (Fig 8b), those with a relatively constricted CA (< 33%) and those with a more expanded CA (> 33%). When separated, both groups approach normal distribution (Figure 9c, d), and comparison of these two populations indicate that they are morphologically unique ($\mu_{M.\ inversus\ s.s.}$ = 27.8%,$\mu m_{.\ inversus\ var.\ latus}$ = 43.9%, $p_{same} = 3.24\ E^{-26}$). In addition, *M. inversus* and *M. latus* have discrete stratigraphic ranges.

Type Locality: ODP Leg 122 Site762C, Exmouth Plateau

Type Level: 23-3-(51-52cm), 373.01 msbf

*Observed range***:** CP8b/9a?-12b; NP 9/10-14b

Pedinocyclus Bukry and Bramlette 1971 emend.

Description: Circular to elliptical coccolith constructed of a single thin, nearly flat, weakly birefringent shield. This shield is constructed of slightly inclined to radial elements that are not clearly imbricate. The central opening is relatively small.

Pedinocyclus annulus Shamrock and Watkins **n. sp.**
Holotype: Plate 7, figure 6; *Paratype:* Plate 7, figure 7; *see also*: Plate 7, figure 8s

Etymology: (L.) from ring, for the open CA

Diagnosis: Medium to large elliptical placolith with a bright inner cycle and open CA

Description: Medium to large, broadly to normally elliptical placolith with a wide, weakly birefringent shield, showing a range of first-order grays. The shield is composed of 35-50 slightly imbricated elements that are radially oriented along most of the shield, but show slight curvature near the longitudi-

Noelaerhabdaceae, Prinsiaceae, Placolith genera *incertae sedis*

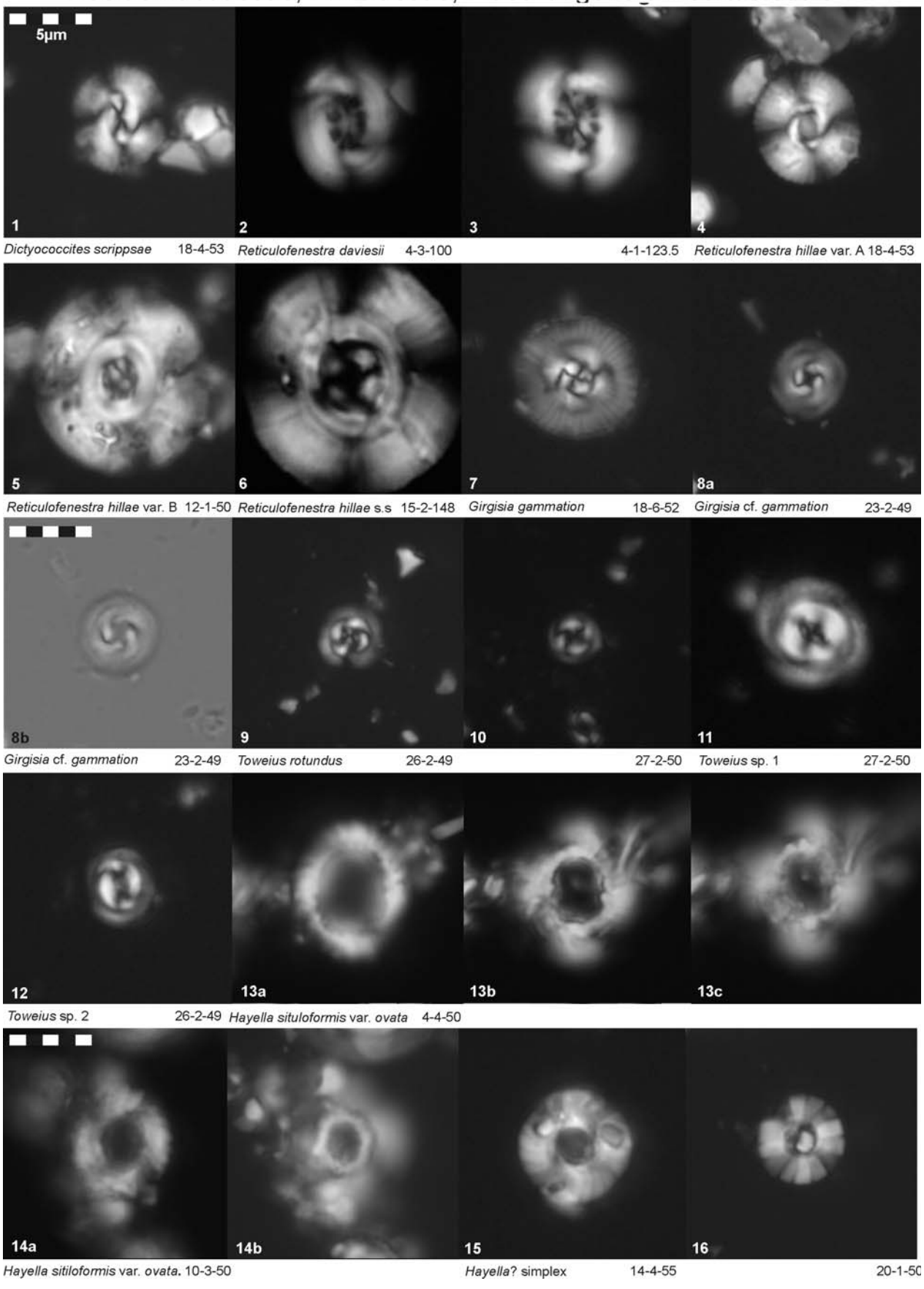

nal axis of the ellipse. The open CA occupies ~40% of the longitudinal axis and is surrounded by a thin, birefringent inner cycle. The gyred extinction lines within the inner cycle are off-axis at 0° but approach the long axis when rotated to 45°.

Dimensions: Length: 6.7-10.3µm, µ = 8.1µm, s.d. = 0.9.; Width: 5.3-8.1µm, µ = 6.7µm, s.d. = 0.8; Eccentricity: 1.11-1.30, µ = 1.20, s.d. = 0.05; CA Length: 2.6-5.4µm, µ = 3.3µm, s.d. = 0.6; CA Length Ratio (% of size): 33.0-52.5%, µ = 40.3%, s.d. = 4.9; CA Width: 1.7-3.1µm, µ = 2.3µm, s.d. = 0.3; CA Width Ratio (% of size): 27.3-41.7%, µ = 33.9%, s.d. = 4.2; N = 30 for all data

Remarks: The LO is observed near the base of CP13a, and this species is very rare and sporadic throughout its range. This species is tentatively placed into the genus *Pedinocyclus* due to similarities with *P. larvalis* with respect to shape, orientation, and birefringence of the shield elements. *Pedinocyclus annulus* n. sp. can be differentiated from *Calcidiscus ellipticus* n. sp. by the wider shield of the former, and from *C.? henrikseniae* which shows strong, gyred extinction from the CA outward across the shield.

Type Locality: ODP Leg 122 Site 762C, Exmouth Plateau

Type Level: 14-4-(55-56cm), 289.05 mbsf

Observed range: CP12b-CP16a; NP14b-21

Pedinocyclus larvalis (Bukry and Bramlette 1969) Loeblich and Tappan 1973
Plate 7, figure 9

The oldest specimens of *P. larvalis* were identified only as fragments; however, the distinct shield structure and low order birefringence allows confidence in identification. The first whole specimens are observed in CP11, accompanied by a modest increase in abundance. *Observed range*: CP10-16a; NP12-21

Pedinocyclus larvalis* var.? *minimus (Bukry and Bramlette 1969) Loeblich and Tappan 1973
Plate 7, figures 10-11

Whole specimens of *P. larvalis* were generally > 10µm as indicated in the original description; however, beginning in CP13 very rare specimens < 10µm are observed, with several as small as 7.0µm, becoming more common upward. Due to the rarity of this genus in this section, it is difficult to determine if this form is either a morphological variant or an independent species that can be reliably differentiated from *P. larvalis* s.s. This taxonomic issue may be resolved with sufficient statistical data via study from multiple sections. Observed measurements are provided, although it is important to note that this is not a statistically significant population: Shield Diameter: 7.0-9.5µm, µ = 8.4µm, s.d = 0.8; CA Diameter: 1.3-2.8µm, µ = 2.3µm, s.d. = 0.4; N = 10 for all data. *Observed range*: CP13a?-16a?; NP15a?-21?

Tetralithoides symeonidesii Theodoridis 1984
Plate 7, figure 12; plate 8, figure 1

As indicated in Bown (2005), this species is not typically known prior to the Miocene. Observations of Bown (2005) from CP13b-c (NP15b-c), coupled with identification in this section indicate this species does occur in the Eocene, though extremely rarely. *Observed range*: CP12a-15b; NP14a-19/20

HOLOCOCCOLITHS

Family **CALYPTROSPHAERACEAE** Boudreaux and Hay 1969

Corannulus germanicus Stradner 1962
Plate 8, figure 2

This species is extremely rare at 762C. *Observed range*: CP15b-16a; NP19/20-21

Corannulus horridulus Bown 2005

Observed range: CP9a; NP10

Daktylethra* cf. *punctulata Gartner and Bukry 1969
Plate 8, figure 3

Only one specimen of this species was observed. *Observed range*: CP12a; NP14a

Lanternithus arcanus Bown 2005

Observed range: CP12b-13b/13c?; NP14b-15b/15c?

Lanternithus simplex Bown 2005

Observed range: CP8b/9a?-12b; NP9/10?-14b

Lanternithus minutus Stradner 1962

The LO is observed at the base of CP12a, below the CP12b LO of Bown (2005) and Wise et al. (2004). A significant increase in abundance is observed through CP15b (max: 8.6%). A notable proportion of specimens were somewhat overgrown, obscuring the central opening. *Observed range*: CP12a-16a; NP14a-21

Several unique specimens of *Lanternithus* were observed through the section, with two examples provided below.

***Lanternithus* sp. 1**
Plate 8, figure 4-5

This form bears two robust blocks of calcite that fill the CA. *Observed range*: CP13b; NP15b

Multipartis* cf. *ponticus Varol 1991(b)

This species was observed sporadically at Exmouth Plateau, above the range provided in the original description. *Observed range*: CP8b, 12b; NP9, 14b

Peritrachelina joidesa Bukry and Bramlette 1968

Observed range: CP16a; NP21

Youngilithus oblongatus Bown 2005

This very rare species is observed below the range given in the original description (NP15b-c). *Observed range*: CP13a-13c.14a?; NP15a-15c/16?

Zygrhablithus bijugatus (Deflandre Deflandre and Fert 1954) Deflandre 1959

Noted in numerous publications and above, this species shows a significant rise in abundance above the HO of *Fasciculithus* spp., slightly above the PETM (>12-20%). Though fairly abundant below and within the PETM interval (~5-8%), most observed specimens were reduced in length and notably dissolved. *Observed range*: CP8a-16a; NP9-21

Placolith genera *incertae sedis*

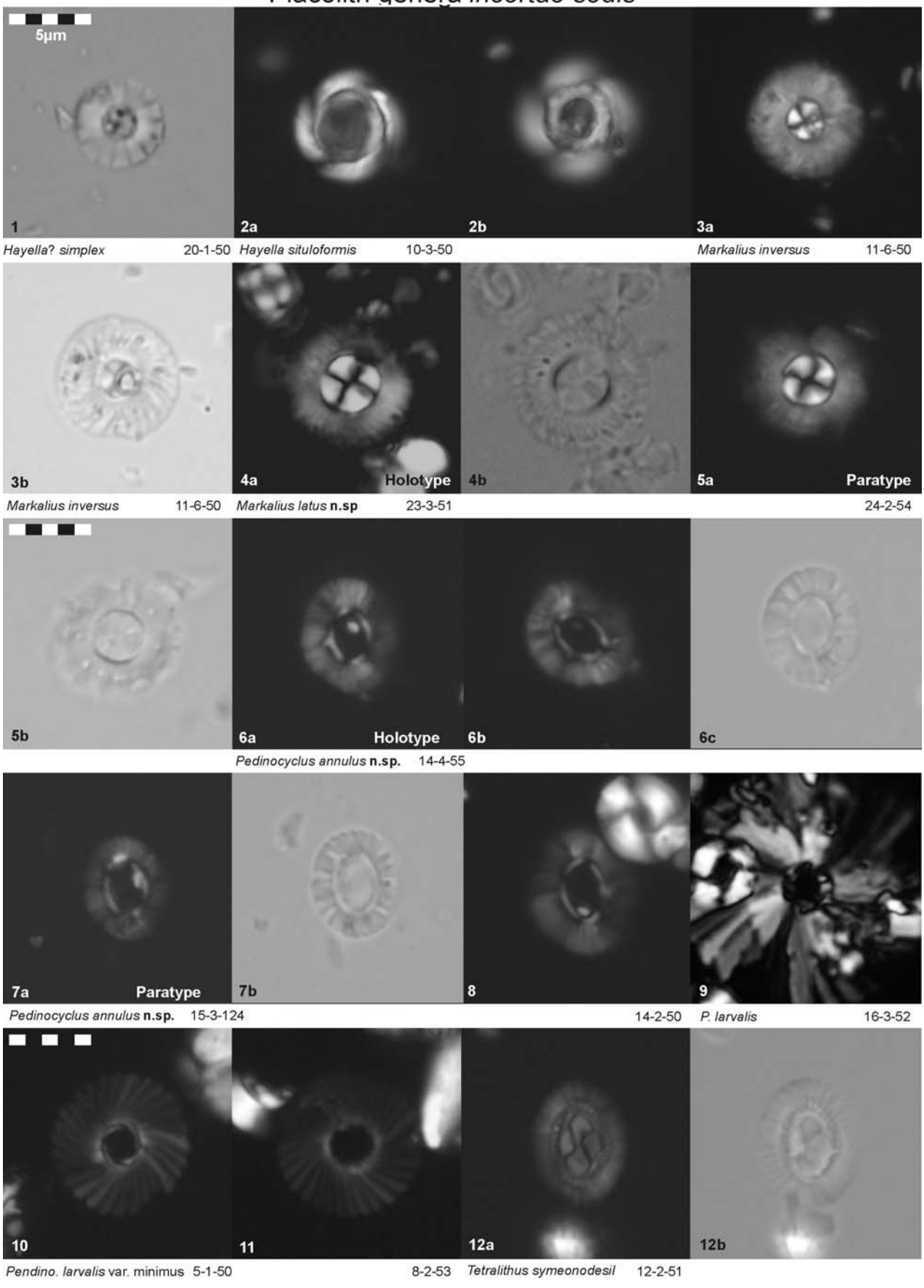

Holococcolith sp. 1
Plate 8, figures 7-8

Small, elliptical holococcolith composed of 10-12 radially oriented elements that are weakly to moderately birefringent and show a quadrate extinction figure. *Observed range*: CP15b; NP19/20

NANNOLITHS

Family **BRAARUDOSPHAERACEAE** Deflandre (1947)

This family was extremely rare at 762C, with no observed *Micrantholithus* spp. and only an occasional *Braarudosphaera* or rare *Pemma* fragment.

Braarudosphaera bigelowii (Gran and Braarud, 1935) Deflandre 1947

This species is rare and sporadic throughout the section, though most consistent in CP10. *Observed range*: CP9a-15b; NP10-21

Pemma papillatum Martini 1959

Only extremely rare, disarticulated plates of this species were observed. *Observed range*: CP15b; NP19/20

Family **LAPIDEACASSACEAE** Bown and Young 1997

Lapideacassis* cf. *blackii Perch-Nielsen *in* Perch Nielsen and Franz, 1977
Plate 8, figure 9

A short but notable abundance peak was observed at the top of CP15a. *Observed range*: CP15a-15b; NP18

Order **DISCOASTERALES** Hay 1977
Family **DISCOASTERACEAE** Tan 1927

Relative abundance varied considerably among species within this genus. Please see (location of data) for more detailed abundance data.

Discoaster acutus Bown 2005

Observed range: CP9a-9b; NP10-11

Discoaster cf. ***backmanii*** Agnini et al. 2008

Similar to *D. backmanii*, but observed above the range provided in the original description. This may extend the true range of this species or this may be a unique form. *Observed range:* CP10-12b; NP12-14b

Discoaster barbadiensis Tan 1927, emend. Bramlette and Riedel 1954

This species shows two abundance peaks, first in upper CP11-12b, and again within CP14b. This species and *D. saipanensis* become very rare near the end of their range, which has caused difficulty in placement of the CP15b/16a boundary, typically marked by the concurrent HO of these species. The boundary is placed at the HCO of both species, though both occur sporadically in CP16a. Though some specimens in CP16a are poorly preserved and likely reworked, others are quite well preserved. *Observed range*: CP8b/9a?-15b; NP9/10?-19/20

Discoaster bifax Bukry 1971

This species was very rare in this assemblage so that range and abundance could not be adequately tracked. *Observed range*: CP14

Discoaster binodosus Martini 1958

The HO is observed at the base of CP12a. *Observed range*: CP8b/9a?-12a; NP9/10?-12/13?

Discoaster cruciformis Martini 1958

Observed range: CP10-12a; NP12-14a

Discoaster decoratus Dang Dik Nga and Shumenko 1975

Observed range: CP16a; NP21

Discoaster deflandrei Bramlette and Riedel 1954
Plate 8, figure 10

Observed range: CP9b-16a; NP11-21

Discoaster diastypus Bramlette and Sullivan 1961

Observed range: CP8b/9a?-10; NP9/10?-12

Discoaster distinctus Martini 1958

Observed range: CP10; NP12

Discoaster elegans Bramlette and Sullivan 1961

Observed range: CP9a-9b; NP10-11

Discoaster falcatus Bramlette and Sullivan 1961

Observed range: CP9a; NP10

Discoaster gemmeus Stradner 1959

Observed range: CP13a-14b; NP15a-17

Discoaster gemmifer Stradner 1961

The LO occurs just below the CP10 boundary. *Observed range*: CP9b-12b; NP11-14b

Discoaster germanicus Martini 1958

The HO of *D. germanicus* is considerably lower than commonly reported (near the CP14a-b boundary). *Observed range*: CP10-12a; NP12-12/13

Discoaster kuepperi Stradner 1959
Numerous specimens are observed early in CP10 that are smaller in size (4.5-6.0µm) than previously described (7.1-15.3µm, N = 30). *Discoaster kuepperi* shows a notable acme (max. = 6.6%; µ. = 5.9%) from upper CP10-lower CP12, which coincides with the *Discoaster* spp. acme observed at 762C. *Observed range*: CP10-12b; NP12-14b

Discoaster lenticularis Bramlette and Sullivan 1961

Observed range: CP8a-9b; NP9-10

Discoaster lodoensis Bramlette and Riedel 1954

Though rare early in its range, *D. lodoensis* shows a notable acme in upper CP10 - basal CP12a (max. =7.2%; µ = 5.7%) followed by rapid decrease prior to extinction. *Observed range*: CP10-12a; NP12-14a

Placolith genera *incerte sedis*; Calyptrosphaera., Lapideacassa., Discoaster

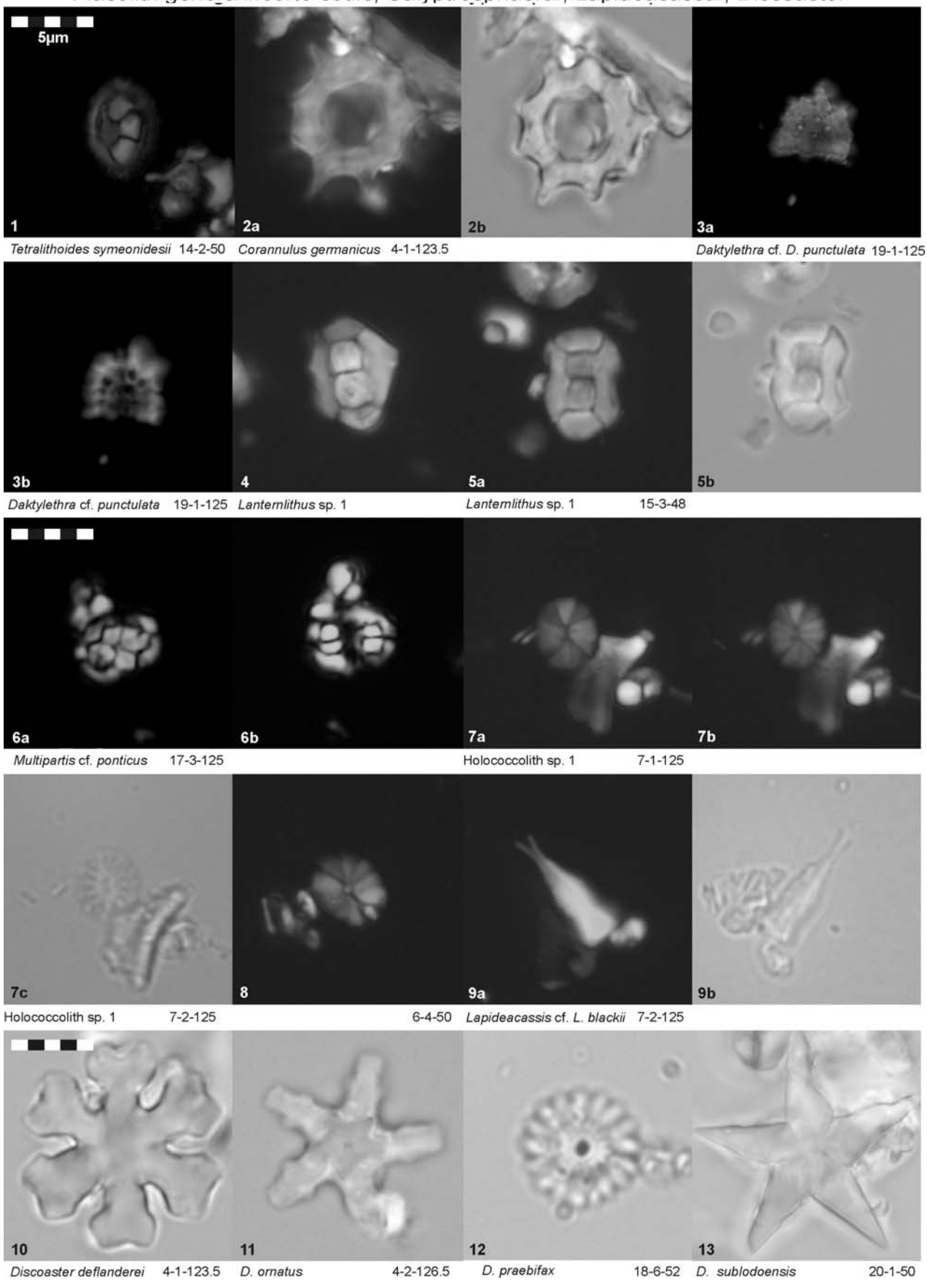

Discoaster mediosus Bramlette and Sullivan 1961

Observed range: CP9a; NP10

Discoaster minimus Sullivan 1964

Observed range: CP10; NP12

Discoaster mohleri Bukry and Percival 1971

Observed range: CP8a/8b?; NP9/10?

Discoaster multiradiatus Bramlette and Riedel 1954

Abundance and range data of this species is similar to that recorded by Agnini et al. (2007a), with peak abundance through the PETM. *Observed range*: CP8a-9b; NP9-11

Discoaster nobilis Martini 1961

Observed range CP8a/8b?; NP9/10?

Discoaster nodifer
Observed range: CP14a-16a; NP16-21

Discoaster nonaradiatus Klumpp 1953

Observed range: CP11-12a; NP12-14a

Discoaster ornatus (Bramlette and Wilcoxon 1967) Bown 2005
Plate 8, figure 11

Specimens of *D. ornatus* were identified when diagnostic nodes were present, but were grouped with *D. tanii* when overgrowth prohibited such differentiation. *Observed range*: CP14b-16a; NP17-21

Discoaster pacificus Haq 1969
Observed range: CP9b-11; NP11-12

Discoaster perpolitus Martini 1961
Observed range: CP9a; NP10

Discoaster praebifax Wei and Wise 1989
Plate 8, figure 12

The authors agree with Wei and Wise (1989a) in that *D. bifax* may be an unreliable marker for the base of CP14a, as *D. praebifax* transitions into *D. bifax*, creating issues with intermediate forms and synchroniety. This species is most abundant from LO through CP12a. *Observed range*: CP11-13b: NP13-15b

Discoaster robustus Haq 1970
Observed range: CP9b-11; NP10-13

Discoaster saipanensis Bramlette and Riedel 1954
Though rare in its lower range, this species shows a significant abundance increase in CP14b, becoming rare again within CP15b. See *D. barbadiensis* above. *Observed range*: CP13a-15b; NP15a-19/20

Discoaster salisburgensis Stradner 1961
The HO is observed at the base of CP11. *Observed range*: CP8b/9a?-11; NP9/10?-12

Discoaster septemradiatus (Klumpp 1953) Martini 1958
Observed range: CP10-12a; NP12-14a

Discoaster strictus Stradner 1961
The LO was observed earlier than commonly reported (CP12b), in the upper portion of CP12a. The HCO corresponds to Perch-Nielsen (1985, CP14b), but it is seen sporadically above this range at Site 762C. *Observed range*: CP12a-15a; NP14a-17

Discoaster sublodoensis Bramlette and Sullivan 1961
Plate 8, figure 13

This species is consistently present in the range provided below, though a pulse of specimens seemingly identical to *D. sublodoensis* are observed in upper CP10 and CP11. These specimens (8.1-21.6µm, µ = 13.4, s.d. = 3.0) do not differ in size or morphology from specimens observed higher in the section (7.8-19.8µm, µ = 14.6µm, s.d. = 3.3). Specimens of *D. sublodoensis* are also observed by Agnini et al. (2006) and Wei and Wise (1990a) in CP10 and CP11, prior to the LCO and base of CP12a. It is possible that *D. sublodoensis* shows an early LO at Site 762C. *Observed range*: CP12a-13b; NP14a-15b

Discoaster tanii Bramlette and Riedel 1954
Plate 9, figure 1

The LO occurs in upper CP14a. *Observed range*: CP14a-16a; NP17-21

Discoaster cf. ***tanii*** Bramlette and Riedel 1954
Plate 9, figure 2

Very rare but fairly consistent specimens of *Discoaster* cf. *tanii* were observed well below the commonly reported LO of CP14b/NP17. Specimens show typical characteristics of *D. tanii,* and biometric analysis shows early specimens are marginally smaller; however, they do not vary significantly enough from specimens higher in the section to be differentiated ($\mu_{D.\ tanii}$ = 10.9µm, $\mu_{D.\ cf.\ tanii}$ = 9.5µm, $p_{same} = 3.2E^{-2}$). It should be noted that the maximum size of *D. tanii* (17.6µm) is much greater than those identified as *D.* cf. *tanii* (13.8µm). Specimens are identified as *D.* cf. *tanii* until the base of CP14b, though these specimens may represent an early occurrence of *D. tanii* at this locality. *Observed range*: 12a-14a; NP14a-16

Discoaster wemmelensis Achuthan and Stradner 1969

Observed range: CP12a-14a?; NP14b–16

Family **FASCICULITHACEAE** Hay and Mohler 1967

Fasciculithus alanii Perch-Nielsen 1971

Observed range: CP8a/8b?; NP9/10?

Fasciculithus clinatus Bukry 1971

Observed range: CP8a/8b?; NP9/10?

Fasciculithus hayii Haq 1971

Observed range: CP8a/8b?; NP9/10?

Fasciculithus lillianae Perch-Nielsen 1971

Observed range: CP8a/8b?; NP9/10?

Fasciculithus tonii Perch-Nielsen 1971

Observed range: CP8a/8b?; NP9/10?

Fasciculithus tympaniformis Hay and Mohler 1967

Observed range: CP8a/8b?; NP9/10?

Discoasteraceae, Sphenolithaceae

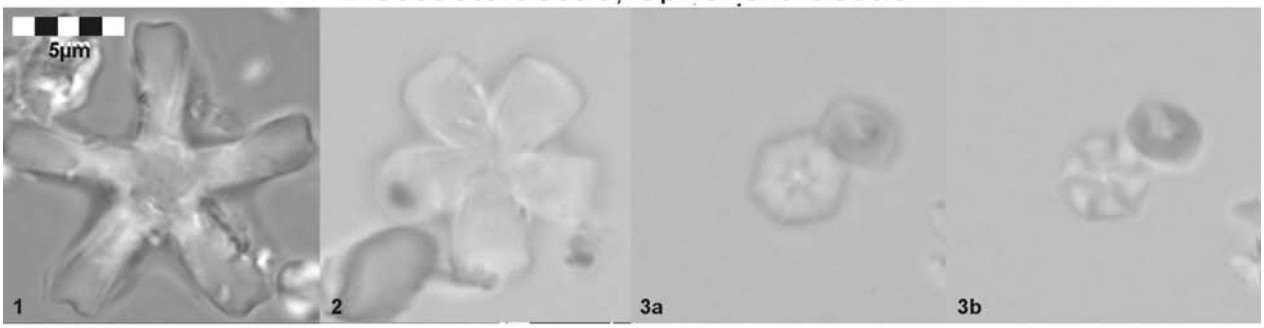

Discoaster tani 7-3-119 *Discoaster* cf. *tani* 15-1-148 *Discoaster* sp. 1 19-2-52

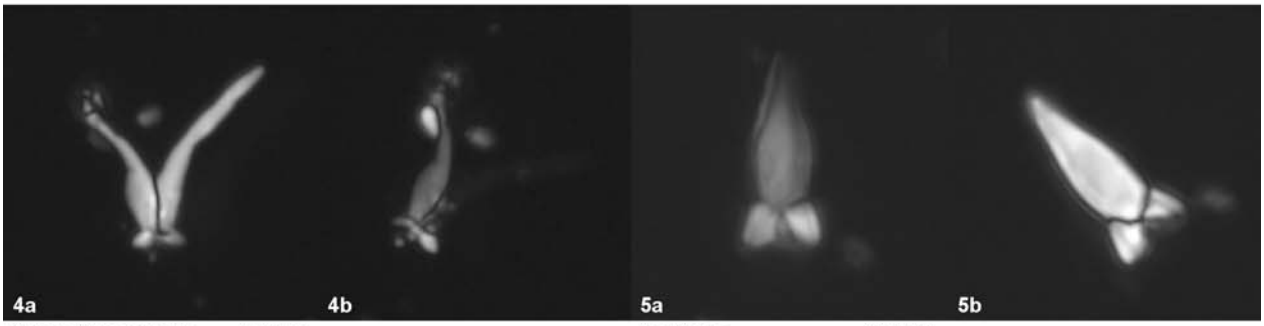

Sphenolithus cuniculus 14-4-55 *S. obtusus* 11-1-50

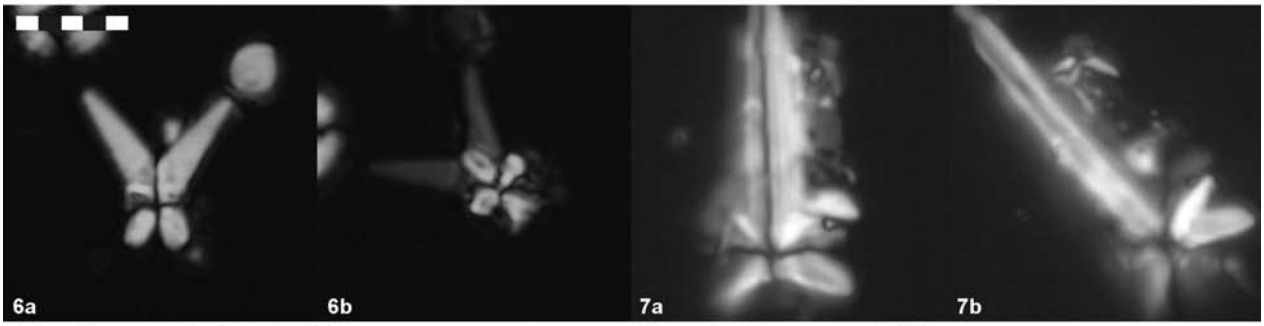

Sphenolithus perpendicularis 16-2-125 *S. pseudoradians* 4-3-51

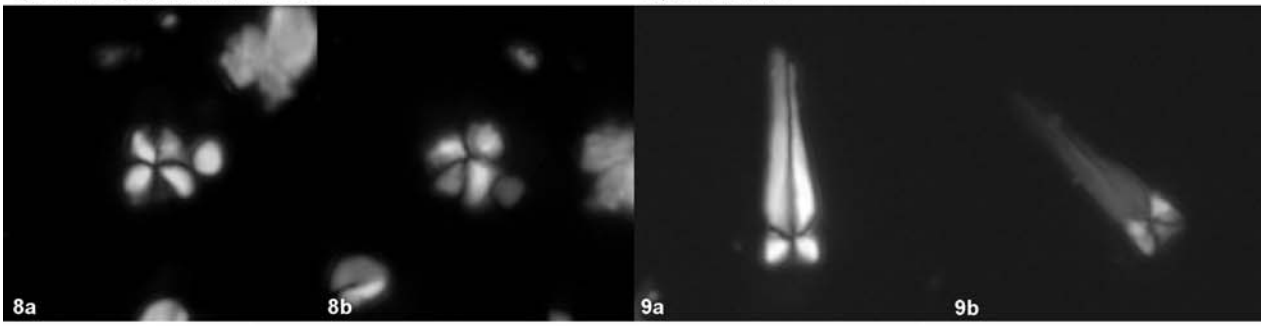

Sphenolithus spiniger 15-2-124 *Sphenolithus strigosus* 14-1-5

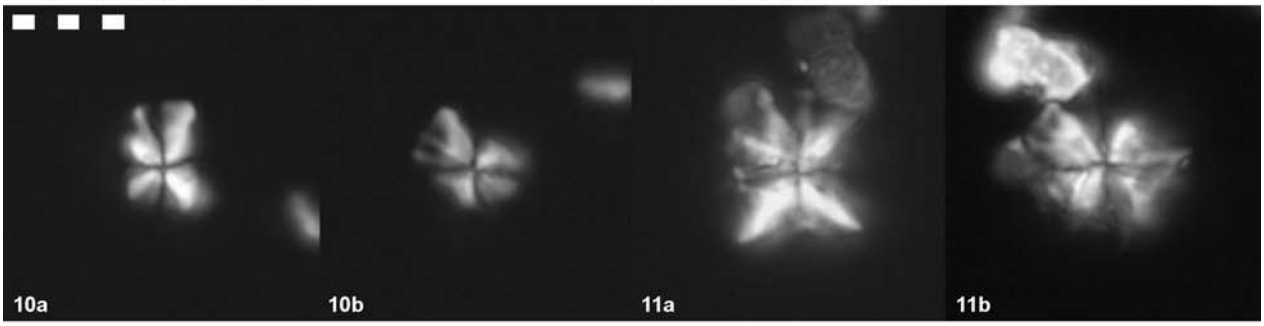

Sphenolithus cf. *S. dissimilis* 4-2-50 4-2-146.5

***Fasciculithus* spp.** base

Observed range: CP8a/8b?; NP9/10?

Family **HELIOLITHACEAE** Hay and Mohler 1967

Bomolithus elegans Roth 1973

Observed range: CP8a; NP9

Heliolithus kleinpellii Sullivan 1964

Observed range: CP8a; NP9

Family **RHOMBOASTERACEAE** Bown 2005

All observed genera within Rhomboasteraceae were rare at Exmouth Plateau.

***Nannotetrina* sp.** Achuthan and Stradner 1969
Some specimens of this genus could not be identified to species level due to preservation or specimen orientation and have been identified simply as *Nannotetrina* sp. *Observed range*: CP13a-14b; NP15a-16

Nannotetrina cristata (Martini 1958) Perch-Nielsen 1971

Observed range: CP13a-14a?; NP15a-16

Nannotetrina fulgens (Stradner in Martini and Stradner 1960) Achuthan and Stradner 1969

This species was grouped with *N. quadrata,* as overgrowth inhibited differentiation. *Observed range*: CP13a-13c/14a?; NP15a-15c/16?

Nannotetrina nitida (Martini 1961) Aubry 1983

Observed range: CP12b; NP14b

Nannotetrina quadrata (Bramlette and Sullivan 1961) Bukry 1973

Observed range: See *N. fulgens*

Rhomboaster cuspis Bramlette and Sullivan 1961

Observed range: CP8b/9a?; NP9/10?

Tribrachiatus* (*Rhomboaster*) *bramlettei (Brönnimann and Stradner 1960) Bybell and Self-Trail 1995

Observed range: CP8b/9a?; NP9/10?

Tribrachiatus contortus (Stradner 1958) Bukry 1972

Observed range: CP8b/9a?; NP9/10?

Tribrachiatus digitalis Aubry 1996

The range of *T. digitalis* occurs within the lower range of *T. contortus* at Site 762C. This is in agreement of findings of Raffi, Backman and Pälike (2005) and Agnini et al. (2007a), creating a crossover of the NP10a-d subzones of Aubry (1995). Results from these three studies include sites from the Indian, equatorial Pacific and North Atlantic Oceans, and likely indicate a global signal. *Observed range*: CP9a; NP10

Tribrachiatus orthostylus (Bramlette and Riedel 1954) Shamrai 1963

This species was consistently present to the HO at the base of CP12a, the LCO of *D. sublodoensis. Observed range*: CP9b-12a; NP11-13

Family **SPHENOLITHACEAE** Deflandre 1952

Sphenolithus acervus Bown 2005

Specimens of *S. acervus* (>8.0µm) are rare in the early Eocene. Similar large forms are also seen in the middle Eocene, as noted in Bown (2005). *Observed range*: CP9a and CP13b-c; NP10 and NP15b-16.

Sphenolithus anarrhopus Bukry and Bramlette 1969

Observed range: CP8a-9b; NP9-11

Sphenolithus celsus Haq 1971

Observed range: CP16a; NP21

Sphenolithus conspicuus Martini 1976

The LO is just below the CP10 boundary, with HO at the base of CP11. *Observed range*: CP9b-11; NP11-12

Sphenolithus cuniculus Bown 2005
Plate 9, figure 4

This species shows an abundance increase near the CP14a/b boundary (max. = 3%). *Observed range*: CP13b-14b; NP15b-17

Sphenolithus editus Perch-Nielsen in Perch Nielsen et al. 1978
The LO occurs just below the CP9a/b boundary, with HO at the base of CP12a. *Observed range*: CP9a-12a; NP10-13/14a?

Sphenolithus elongatus Perch-Nielsen 1980

This species is extremely rare and sporadic at this locality. *Observed range*: CP13b-13c/14a?; NP15b-15c/16?

Sphenolithus furcatolithoides Locker 1967

This species is most common in CP13b. A HO in CP14a is also observed by Agnini et al. (2011). *Observed range*: CP13b-14a?; NP15b-16

Sphenolithus intercalaris Martini 1976

Observed range: CP14a-15a; NP16-17

Sphenolithus moriformis (Brönnimann and Stradner 1960) Bramlette and Wilcoxon 1967
Peak abundance (4.4%; 276.71 m) is observed during an abundance increase (µ: 3.1%) that may be associated with the MECO (276 m). *Observed range*: CP8a-16a; NP9-21

Sphenolithus obtusus Bukry 1971
Plate 9, figure 5

The LCO (CP14b) agrees with Perch-Nielsen (1985); however, very rare specimens are observed in two samples within CP14a. *Observed range*: CP14a-14b; NP16-17

Sphenolithus orphanknollensis Perch-Nielsen 1971

This species was rare through its range. *Observed range*: CP11-14a?; NP13-16

Sphenolithaceae, nannoliths *incertae sedis,* indeterminant nannoliths

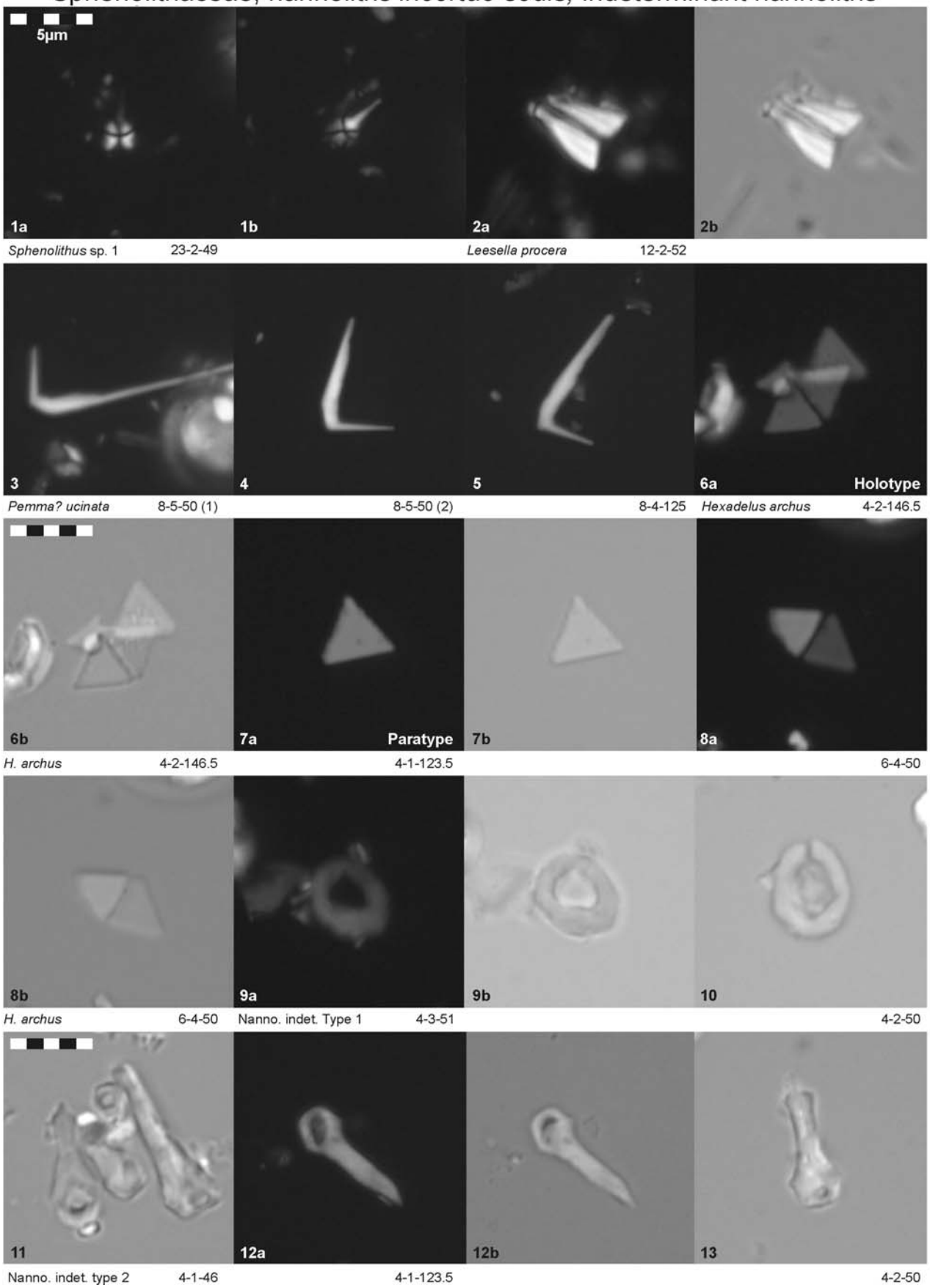

Sphenolithus perpendicularis Shamrock 2010
Plate 9, figure 6

Observed range: CP13a; NP15a

Sphenolithus predistentus Bramlette and Wilcoxon 1967

Though consistently present in CP14b and 15b, no specimens were observed in CP15a. This curious absence was also noted by Fornaciari et al (2010) and Wei and Wise (1990a; 1989b). *Observed range*: CP14b-16a; NP16-21

Sphenolithus primus Perch-Nielsen 1971

Observed range: CP8b/9a?-9b; NP9/10?-11

Sphenolithus pseudoradians Bramlette and Wilcoxon 1967
Plate 9, figure 7

Observed range: CP14a-16a; NP16-21

Sphenolithus radians Deflandre in Grasse 1952

This species is fairly abundant and consistent from the LO, but rare above CP10 and sporadic above CP13b. *Observed range*: CP9b-16a; NP11-21

Sphenolithus runus Bown and Dunkley Jones 2006
Observed range: CP14a?-14b; NP16-NP17

Sphenolithus spiniger Bukry 1971
Plate 9, figure 8

This species is consistently observed above the commonly reported range of CP13/NP15. Fornaciari et al. (2010) also observe the HCO of *S. spiniger* within CP14a (NP17). *Observed range*: CP12a-14b; NP14a-17

Sphenolithus stellatus Gartner 1971

This species is very rare and sporadic. *Observed range*: CP12b-13b/13c?; NP14b-15b/15c?

Sphenolithus strigosus Bown and Dunkley Jones 2006
Plate 8, figure 9

This species is seen consistently through lower CP14b. The HO of this species at Hole 762C is extended from the original description (NP16). *Observed range*: CP14a?-14b; NP16-17

Sphenolithus villae Bown 2005

Only one specimen of this species was observed. *Observed range*: CP10; NP11

Sphenolithus* cf. *dissimilis Bukry and Percival 1971
Plate 8, figures 10-11

Specimens similar to *S. dissimilis*, bearing a tripartite apical spine, are observed from middle and upper Eocene sediments at Site 762C. Specimens with four apical terminations are also observed. Similar specimens are also reported from Bown (2005, pl. 45:21-25), but are identified as *S. conicus*. *Observed range*: CP14b-16a; NP17-21

***Sphenolithus* sp. 1**
Plate 10, figure 1

Several, notably small (3-5 μ) specimens of *Sphenolithus* were identified in the Ypresian at Site 762C. These forms show a bright proximal and lateral cycle when aligned to the polarizers (0°), and a small apical spine birefringent at 45° to the polarizers. Observed range: CP9a-CP11; NP10-12/13?

Nannoliths ***incertae sedis***

Biantholithus flosculus Bown 2005

The HO is occurs near the CP9b boundary. *Observed range*: CP8a-9a; NP9-10

Leesella procera Bown and Dunkley Jones 2006
Plate 10, figure 2

The HO of this species at Hole 762C is extended from the original description (NP16). *Observed range*: CP14b; NP17

Pemma*? *uncinata Bown and Dunkley Jones 2006
Plate 10, figures 3-5

Numerous specimens are observed that resemble this form, but lack the thin connective structures shown in the type specimens. This form was tentatively assigned to the genus *Pemma* by Bown and Dunkley Jones (2005) as it closely resembles disarticulated pentaliths, Although that assignment is followed here, the form is still considered *incertae sedis,* as all specimens were observed as individual segments. Measurement of the interior and exterior angles are highly variable, both in our specimens and those provided in the original description (Holotype (pl. 9, fig. 17): Interior angle: 62.8°, Exterior angle: 57.8°; Paratype (pl. 9, fig. 13): Interior angle: 103.76°, Exterior angle: 89.3°; All specimens (N = 50): Interior angle: 68.0-104.9, μ = 87.5, s.d. = 7.0; Exterior angle: 57.5-82.7, μ = 71.7°, s.d. = 4.8). Despite the high angular variability, the mean external angle approximates that need to form a pentalith, and may suggest this is the correct affiliation for this strange form. Specimens should continue to be tentatively assigned to the genus *Pemma* until more is understood. The range of this species at Hole 762C is extended from the original description (NP19/20-21). *Observed range*: CP14b-15a; NP17-18

Pseudotriquetrorhabdulus inversus (Bukry and Bramlette 1969) Wise *in* Wise and Constans 1976

This species occurs consistently below its commonly reported range of CP12b. *Observed range*: CP12a-14b; NP14a-17

INDETERMINATE NANNOLITHS

There is a notable increase in indeterminant nannoliths in the uppermost Eocene, particularly within CP15b-16a, many of which are extremely thin and non-birefringent. This increase may be due to increased preservation or may be environmentally driven by Late Eocene cooling.

Genus *Hexadelus* new genus

Etymology: (Gr.) From *hexa*, referring to the six-fold arrangement of plates, and *adelus* (unseen, unknown, secret), for the delicate and enigmatic nature of the specimens.

Description: Hexagonal form composed of six flat, triangular plates. Each plate has three sides of equal length with three 60° angles, forming an equilateral triangle. This genus is extremely delicate, occurring primarily as disarticulated plates, though several partially articulated specimens suggests the relative relationships between these individual segments. Although similar plates belong to members of the pentalith family Braarudosphaeraceae, the consistent angular measurements indicate that these plates belong to a separate group: The interior

angle of a pentalith must average ~72° (69.9°-75.1°, μ = 72.3°, s.d. = 1.28, N = 90), while plates that are 60° require six segments in order to complete the cycle (Figure 10). Univariate t-tests show distinct separation between plate geometry of pentaliths and the type specimen *Hexadelus archus* n. sp.: At the 95% confidence level pentalith angle = 72.0-72.5°, while *Hexadelus archus* = 60.4-61.2°; $p_{(same\ \mu)} = 9.93\ E^{-100}$ (Figure 11).

Type species: *Hexadelus archus* n. sp.

Hexadelus archus Shamrock and Watkins **n. sp.**
Holotype: Plate 10, figure 6; *Paratype*: Plate 10, figure 7; *see also*: Plate 10, figure 8

Etymology: (Gr.) from *arche*, meaning beginning, or chief

Description: Small to medium hexagonal form composed of six, flat plates, each a near equilateral triangle. The plates are very thin and show relatively low birefringence. The form is extremely fragile, and is observed primarily as disarticulated plates. Articulated specimens show weak alternating birefringence between plates.

Measurements: Length (of individual plates): 1.9-4.0μm, μ = 3.1, s.d. = 0.6, N = 30; Diameter (whole specimen, as shown in Figure 10): 3.3-7.0μm, μ = 5.3μm, s.d. = 1.0, N = 30; Plate angle: 55.6-64.5°, μ = 60.8°. s.d. = 2.0, N = 90

Remarks: Extremely fragile, this species will likely be found only in well preserved samples. This species can be differentiated from the disarticulated plates of pentaliths such as *Braarudosphaera* spp. and *Micrantholithus* spp. by the more narrow angles of the plates. Pentaliths must have at least one angle that is ~72°, while plates from this species show all three angles at ~60° (Figure 10). *Hexadelus archus* n. sp. shows a HO just below the CP16a boundary.

Observed Range: CP15b-16a; NP19/20-21

Type Locality: ODP Leg 122 Site 762C, Exmouth Plateau

Type Level: 4-2-(146.5-147.5cm), 191.77 mbsf

Hexadelus triquetra Bown and Dunkley Jones 2006
Pemma? *triquetra* BOWN and DUNKLEY JONES 2006, pl. 9, fig. 1-4, 6-8

This species was tentatively placed into the genus *Pemma*, as it is quite similar to the disarticulated plates of known pentaliths. Measurements of specimens from the original description, as well as that identified at Site 762C, indicate that this species also shows interior angles of ~60°, indicating that plates would also create a hexagonal form if articulated by their edges. Only one specimen from these original images (pl 9: 5) illustrates interior angles (52.4°, 52.0°, 86.0°) or side lengths (6.5μm, 5.6μm, 5.4μm) that do not fit the necessary geometric relationships, and may in fact be a different species. Measurements are given for the holotype and paratype, as well as additional specimens provided in Bown and Dunkley Jones (2006, pl. 9: 4-5): Holotype(pl 9: 6-8): *Angle*: θ1 = 62.7°, θ2 = 62.5°, θ3 = 57.6°; *Length*: L1 = 4.9μm, L2 = 5.2μm, L3 = 5.3μm; Paratype (pl 9: 1-3): *Angle*: θ1 = 62.6°, θ2 = 58.4°, θ3 = 61.8°; *Length*: L1 = 5.8μm, L2 = 5.9μm, L3 = 5.8μm; All specimens: *Angle*: 57.6-63.5°, μ = 60.8, s.d. = 1.8, N = 30; *Length*: 4.57-6.0μm, μ = 5.3μm, s.d. 0.5, N = 10; *Diameter*: 7.9-10.4, μ = 9.2, s.d. = 0.9, N = 10. *Observed Range:* CP15a-15b; NP18-19/20

Indeterminate nannolith- Type 1 Bown and Dunkley Jones 2006
Plate 10, figures 9-10

There is a notable increase in abundance of this species at the base of CP16a (max. = 2.6%). Two variations are observed: complete rings as shown in Bown and Dunkley Jones (2006, pl. 9: 21-25) and those that appear as a recumbent horseshoe, where the tips remain unattached. These variations were not separated in this study due to the generally enigmatic nature of this form. *Observed range***:** CP15b-16a; NP19/20-21

Indeterminate nannolith - Type 2
Plate 10, figures 11-13

An unidentifiable nannolith was recorded just below the CP16a boundary and was consistently observed through the remaining section examined. There is some indication that these nannoliths may be highly dissolved or weakly calcified remnants of *Zygrhablithus bijugatus*, where the form is broken along the central suture, so that half of the base and stem remain. *Observed range***:** CP15b-16a; NP19/20-21

CONCLUSIONS

Numerous recent advances in our knowledge of Eocene calcareous nannofossil biostratigraphy, taxonomy, abundance trends, and paleoecology provide an opportunity to reevaluate the Eocene biostratigraphic succession and its relationship to long-term assemblage changes at Site 762. This research was conducted to fulfill a need for a continuous Eocene calcareous nannofossil reference section, containing range and abundance data for a vast number of Eocene species, relative to the preexisting CP and NP biostratigraphic zonation schemes.

Cross-correlation between the CP and NP standard nannofossil zonation schemes identified three stratigraphic hiatuses at Site 762: Hiatus A (CP8b) occurs across the Paleocene-Eocene boundary. The highly skewed assemblage in CP8a suggests dissolution in association with the PETM. Hiatus B (NP13) indicates a stratigraphic break in the upper Ypresian, closely correlated to the EECO. Hiatus C is identified by the absence of CP13c/NP15c and the convergence of the LOs of *Reticulofenestra umbilica* and *Nannotetrina fulgens* with the HO of *Chiasmolithus gigas*. A paleogeographic and stratigraphic summary of the northwestern Australian margin (Gradstein 1992; Haq et al. 1992) suggests an erosional disconformity on portions of the central Exmouth Plateau in the middle Eocene, though Site 762 was thought to show continuous deposition. Results from this study suggest that at least part of the stratigraphic record is affected by erosion or non-deposition on the central Exmouth plateau.

Most taxa in the CP and NP zonation schemes represent highly useful and reliable bioevents; however, comparison of our data to both the Site 762 nannofossil biostratigraphy of Siesser and Bralower (1992) and to other research highlights several problem taxa where rarity or potential diachroniety inhibits (or prohibits?) their application at many sites. The rarity of some taxa, such as *Chiasmolithus grandis* and *Ch. gigas*, was overcome by increasing the number of FOVs; however some marker taxa were too sporadic (*Discoaster bifax)* or absent entirely (*Blackites gladius*) at Site 762 and could not be applied biostratigraphically. Comparison of the range of *Discoaster sublodoensis* (CP12a/NP14a) from several sites suggests this bioevent is inconsistent and should be applied tentatively.

Well-calibrated alternative bioevents are needed to act as proxies for rare and or/diachronous marker taxa. Some species already show great potential as proxy events, such as the LO of *S. radians*, while others, such as the LOs of *D. bisecta* and *S. spiniger*, will require additional investigation and calibration. These secondary markers need not be synchronous with the primary marker, as long as the relative offset between events is understood across both paleolatitude and paleodepth. The notably diverse and robust Eocene assemblages shown at Site 762 and by Bown and others (2007, 2006, 2005) suggests a wealth of potential bioevents. The potential to increase the biostratigraphic resolution of the Eocene will be further influenced by the development of high-precision orbital biochronology.

Advancements in global isotope stratigraphy since the original expedition allows the calcareous nannofossil data from Exmouth Plateau to be correlated to $\delta^{13}C$ and $\delta^{18}O$ data from Site 762. These data were compared to the isotope records generated by previous workers, in order to examine the relationships between nannofossil turnovers and assemblage shifts with known climate variability throughout the Eocene. Several changes are observed in the nannofossil assemblages that closely correlate to both short isotopic excursions and long term trends in $\delta^{13}C$ and $\delta^{18}O$ (text-figures 3-7), including the PETM, ETM2, ETM3, EECO, MECO, a period of late Eocene warming, and the Oi-1 isotopic events. Increased rates of nannofossil turnover were observed primarily at the PETM and during the EECO, but were also associated with the ETM3 event. Arguably the most significant turnovers occur near the base and top of the EECO, among the *Toweius, Discoaster and Reticulofenestra* groups, also documented at Possango (Italy) (Agnini et al. 2006). Patterns of nannofossil diversity, evenness, and species richness broadly mirror changes in $\delta^{18}O$, with highest diversity during warmer periods. This reflects the affinity of calcareous nannoplankton for stable, stratified surface water, allowing niche partitioning within this generally oligotrophic group.

Though nannofossil abundance patterns appear to be primarily temperature driven through the Ypresian and Lutetian, abundance trends of *Discoaster* spp. and *Cyclicargolithus floridanus* suggests the influence of meso- to eutrophic nutrient levels in the Bartonian and Priabonian. Despite the general cooling and climate deterioration associated with the late Eocene, nannofossil diversity and species richness remains relatively high throughout the late Eocene at Site 762. The relationship between temperature and trophic affinity can be difficult to unravel within a nannofossil assemblage; however, there is significant evidence to suggest that these communities were greatly affected by both shorter term environmental perturbations and long term climate change, with originations, extinctions, and dominance shifts that permanently alter the structure of the nannoplankton community. Significant advancements continue to be made in calcareous nannofossil biostratigraphy, taxonomy, and community structure, even within relatively well-understood geologic time periods. Such studies contribute significantly to our knowledge, but also highlight the need for continuing research in both paleoecology and well-calibrated nannofossil biochronology.

ACKNOWLEDGMENTS

This research used samples and data provided by the Ocean Drilling Program (ODP). The ODP is sponsored by the National Science Foundation (NSF) and participating countries under the management of Joint Oceanographic Institutions (JOI) Inc. The authors would like to thank Mary Anne Holmes, Tracy Frank (University of Nebraska-Lincoln, Geosciences), Paul Hanson (UN-L, School of Natural Resources) and Kurt Johnston (ExxonMobil), as well as one anonymous reviewer for their suggestions and revisions, which greatly improved this manuscript.

REFERENCES

Due to the large number of taxonomic references, particularly within the appendix, the authors refer the reader to Perch–Nielsen (1985), which contains all taxonomic references prior to that reference's publication date. Taxonomic references not included in Perch–Nielsen (1985) are included below.

AGNINI, C., FORNACIARI, E., RAFFI, I., RIO, D., RÖHL, U. and WESTERHOLD, T., 2007a. High–resolution nannofossil biochronology of middle Paleocene to early Eocene at ODP Site 1262: Implications for calcareous nannoplankton evolution. *Marine Micropaleontolgoy*, 64: 215–248.

AGNINI, C., FORNACIARI, E., RIO, D., TATEO, F., BACKMAN, J. and GIUSBERTI, L., 2007b. Responses of calcareous nannofossil assemblages, mineralogy and geochemistry to the environmental perturbations across the Paleocene/Eocene boundary in the Venetian Pre–Alps. *Marine Micropaleontology*, 63: 19–38.

AGNINI, C., FORNACIARI, E., GIUSBERTI, L., GRANDESSO, P., LANCI, L., LUCIANI, V., MUTTONI, G., PALIKE, H., RIO, D., SPOFFORTH, D. J. A., and STEFANI, C., 2011. Integrated biomagnetostratigraphy of the Alano section (NE Italy): A proposal for defining the middle–late Eocene boundary. *Geological Society of Amemerica Bulletin,* 123 (5-6): 841-872. Online 21 January 2011. doi:10.1130/B30158.1

AGNINI, C., MUTTONI, G., KENT, D. V. and RIO, D., 2006. Eocene biostratigraphy and magnetic stratigraphy from Possagno, Italy: the calcareous nannofossil response to climate variability. *Earth and Planetary Science Letters*, 241: 815–830.

AUBRY, M.–P., 1991. Sequence stratigraphy: Eustacy or tectonic imprint? *Journal of Geophysical Research*, 96: 6641–6679.

———, 1992. Late Paleogene calcareous nannoplankton evolution: a tale of climatic deterioration. In: Prothero, D. R. and Berggren, W. A. (Eds). *Eocene–Oligocene climatic and biotic evolution,* 272–309. Princeton: Princeton University Press.

———, 1995. Toward an upper Paleocene–lower Eocene high resolution stratigraphy based on calcareous nannofossil stratigraphy. *Israel Journal of Earth Sciences*, 44: 239–253.

BENGTSON, P., 1988. Open nomenclature. *Palaeontology*, 31: 223–227.

BERGGREN, W. A., KENT, D. V., SWISHER, C. C. and AUBRY, M.–P., 1995. A revised Cenozoic geochronology and chronostratigraphy. In: Berggren, W. A., Kent, D. V. and Hardenbol, J. (Eds), *Geochronology, time scales and global stratigraphic correlations,* 129–212. Tulsa, OK: Society for Stratigraophic Geology (SEPM). Special Publication 54.

BOHATY, S. M. and ZACHOS, J. C., 2003. Significant Southern Ocean warming event in the late middle Eocene. *Geology*, 31: 1017–1020.

BOHATY, S. M., ZACHOS, J. C., FLORINDO, F. and DELANEY, M. L., 2009. Coupled greenhouse warming and deep–sea acidification in the Middle Eocene. *Paleoceanography*, 24: 16pp. doi:10.1029/2008PA001676.

BOWN, P. R., 2005. Paleogene calcareous nannofossils from the Kilwa and Lindi areas of coastal Tanzania (Tanzania Drilling Project 2003–4). *Journal of Nannoplankton Research*, 27: 21–95.

BOWN, P. R. and DUNKLEY JONES, T., 2006. New Paleogene calcareous nannofossils taxa from coastal Tanzania: Tanzania Drilling Project Sites 11 to 14. *Journal of Nannoplankton Research*, 28: 17–34.

BOWN, P. R. and PEARSON, P., 2009. Calcareous plankton evolution and the Paleocene/Eocene Thermal Maximum event: new evidence from Tanzania. *Marine Micropaleontolgoy*, 71: 60–70

BOWN, P. R. and YOUNG, J. R., 1997. Proposals for a revised classification system for calcareous nannoplankton. *Journal of Nannoplankton Research*, 19: 15–47.

———, 1998. Techniques. In: Bown, P. E., Ed., *Calcareous nannofossil biostratigraphy,* 16–28. London: Kluwer Academic.

BOWN, P. R., DUNKLEY JONES, T. and YOUNG, J. R., 2007. *Umbilicosphaera jordanii* Bown, 2005 from the Paleogene of Tanzania: confirmation of generic assignment and Paleocene origination for the Family Calcidiscaceae. *Journal of Nannoplankton Research*, 29: 25–30.

BRALOWER, T. J., 2002. Evidence of surface water oligotrophy during the Paleocene–Eocene thermal maximum: Nannofossil assemblage data from Ocean Drilling Program Site 690, Maud Rise, Weddell Sea. *Paleoceanography,* 17: 1–12. doi:10.1029/2001PA000662.

BRALOWER, T. J. and MUTTERLOSE, J., 1995. Calcareous nannofossil biostratigraphy of Site 865, Allison Guyot, Central Pacific Ocean: a tropical Paleogene reference section. In: Winterer, E. L. et al. (Eds), *Proceedings of the Ocean Drilling Program: Scientific Results, 143*, 31–74. College Station, TX: Ocean Drilling Program.

BRAMLETTE, M. N. and MARTINI, E., 1964. The great change in calcareous nannoplankton between the Maestrichtian and the Danian. *Micropaleontology*, 10: 291–322.

BYBELL, L. M., 1975. Middle Eocene calcareous nannofossils at Little Stave Creek. *Tulane Studies in Geology and Paleontology*, 11: 177–247.

BYBELL, L. M. and GARTNER, S., 1972. Provincialism among mid–Eocene calcareous nannofossils. *Micropaleontology*, 18: 319–336.

BYBELL, L. M. and SELF–TRAIL, J. M., 1994. *Evolutionary, biostratigraphic, and taxonomic study of calcareous nannofossils from the continuous Paleocene–Eocene boundary section in New Jersey.* Washington, DC: US Geological Survey. Professional Paper 1554, 36pp.

CAMPBELL, R. J., HOWE, R. W. and REXILIUS, J. P., 2004. Middle Campanian–lowermost Maastrichtian nannofossil and foraminiferal biostratigraphy of the northwestern Australian margin. *Cretaceous Research*, 25: 827–864.

CASCELLA, A. and DINARÉS–TURELL, J., 2009. Integrated calcareous nannofossil biostratigraphy and magnetostratigraphy from the uppermost marine Eocene deposits of the southeastern Pyrenean foreland basin: evidences for marine Priabonian deposition. *Geologica Acta*, 7: 281–296.

CHANG, Y.–M., 1967. Accuracy of fossil percentage estimation. *Journal of Paleontology*, 41: 500–502.

CRAMER, B. S., WRIGHT, J. D., KENT, D. V. and AUBRY, M.–P., 2003. Orbital climate forcing of δC excursions in the late Paleocene–early Eocene (chrons C24n –C25n). *Paleoceanography*, 18: 1097, 25pp. doi:10.1029/2003PA000909.

DANG DIK NGA and SHUMENKO, S. I., 1975. New species of calcareous nannoplankton from the Eocene of the Ukraine. *Akademia Nauk SSSR, Paleontologiski Zhurnal*., 1: 22–26. [In Russian]

DEFLANDRE, G., 1952. Classe des Coccolithophoridés *(Coccolithophoridae* Lohmann, 1902). In: Grassé, P. P., Ed., *Traité de Zoologie. Anatomie, Systématique, Biologie (*Vol. 1, Pt. 1): Phylogénie. Protozoaires: Généralités. Flagelles: Paris (Masson), 439–470. Paris: Masson.

DE KAENEL, E. and VILLA, G., 1996. Oligocene–Miocene calcareous nannofossil biostratigraphy and paleoecology from the Iberia Abyssal Plain. In: Whitmarsh, R. B. et al. (Eds.), *Proceedings of the Ocean Drilling Program: Scientific Results, 149*, 79–145. College Station, TX: Ocean Drilling Program.

DENNISON, J. M. and HAY, W. W., 1967. Estimating the needed sampling area for subaquatic ecologic studies. *Journal of Paleontology*, 41: 706–708.

DUNKLEY JONES, T., BOWN, P. R., PEARSON, P. N., WADE, B. S., COXALL, H. K. and LEAR, C. H., 2008. Major shifts in calcareous phytoplankton assemblages through the Eocene–Oligocene transition of Tanzania and their implications for low–latitude primary production. *Paleoceanography*, 23: PA4204, 14pp. doi:10.1029/2008PA001640.

GAELOTTI, S., KRISHNAN, S., PAGANI, M., LANCI, L., GAUDIO, A., ZACHOS, J. C., MONECHI, S., MORELLI, G., LOURENS, L., 2010. Orbital chronology of Early Eocene hyperthermals from the Contessa Road section, central Italy. *Earth and Planetary Science Letters*, 290: 192–200.

GALBRUN, B., 1992. Magnetostratigraphy of Upper Cretaceous and lower Tertiary sediments, Sites 761 and 762, Exmouth Plateau, northwest Australia. *In*: Rad, U. von, Haq, B. U. et al., *Proceedings of the Ocean Drilling Program: Scientific Results, 122*, 699–716: College Station, TX: Ocean Drilling Program.

GIBBS, S. J., BOWN, P. R., SESSA, J. A., BRALOWER, T. J. and WILSON, P. A., 2006b. Nannoplankton extinction and origination across the Paleocene–Eocene Thermal Maximum. *Science*, 314: 1770–1773.

GIBBS, S. J., BRALOWER, T. J., BOWN, P. R., ZACHOS, J. C. and BYBELL, L. M., 2006a. Shelf and open ocean calcareous phytoplankton assemblages across the Paleocene–Eocene thermal Maximum: Implications for global productivity gradients. *Geology*, 34: 233–236.

GRADSTEIN, F. M., 1992. Legs 122 and 123, northwestern Australian margin – a stratigraphic and paleogeographic summary. In: Gradstein, F. M. et al., Eds., *Proceedings of the Ocean Drilling Program, Scientific Results, 123*, 801–816. College Station, TX: Ocean Drilling Program.

HAMMER, Ø., HARPER, D. A. T. and RYAN, P. D. 2001. PAST: Paleontological Statistics Software Package for Education and Data Analysis. *Palaeontologia Electronica* 4: 9pp. http: //palaeo–electronica. org/2001_1/past/issue1_01. htm, 5–27–2009.

HAQ, B. U., 1970. The structure of Eocene coccoliths and discoasters from a Tertiary deep–sea core in the Central Pacific. *Stockholm University Contributions to Geology*, 21: 1–19.

HAQ, B. U., and LOHMANN, G. P., 1976. Early Cenozoic calcareous nannoplankton biogeography of the Atlantic Ocean. *Marine*

Micropaleontology, 1: 119–194. doi:10.1016/0377–8398(76)90008–6.

HAQ, B. U., BOYD, R. L., EXON, N. F., and VON Rad, U., 1992. Evolution of the central Exmouth Plateau: a post–drilling perspective. *In* Rad, U. von, Haq, B. U. et al., *Proceedings of the Ocean Drilling Program: Scientific Results, 122*, 801–818/ College Station, TX: Ocean Drilling Program,

HAQ, B. U., RAD, U. VON, O'CONNELL, S. et al., 1990. *Proceedings of the Ocean Drilling Program: Initial Reports, 122,* 826pp: College Station, TX: Ocean Drilling Program. doi:10.2973/odp.proc.ir.122.1990.

JIANG, S. and WISE, S. W., JR, 2009. Distinguishing the influence of diagenesis on the paleoecological reconstruction of nannoplankton across the Paleocene/Eocene Thermal Maximum: An example from the Kerguelen Plateau, southern Indian Ocean. *Marine Micropaleontolgoy*, 72: 49–59.

JOVANE, L., FLORINDO, F., COCCIONI, R., DINARES–TURELL, J., MARSILI, A., MONECHI, S., ROBERTS, A. P. and SPROVIERI, M., 2007. The middle Eocene climatic optimum event in the Contessa Highway section, Umbrian Apennines, Italy. *Geological Society of America Bulletin*, 119: 413–427. doi:10.130/1325917.1.

KAHN, A. and AUBRY, M.–P., 2004. Provincialism associated with the Paleocene/Eocene thermal maximum: temporal constraint. *Marine Micropaleontology*, 52: 117–131.

LEES, J. A., 2002. Calcareous nannofossil biogeography illustrates paleoclimatechange in the Late Cretaceous Indian Ocean. *Cretaceous Research*, 23: 537–634. doi:10.1006/cres.2003.1021.

LOURENS, L. J., SLUIJS, A., KROON, D., ZACHOS, J. C., THOMAS, E., ROHL, U., BOWLES, J. and RAFFI, I., 2005. Astronomical pacing of late Paleocene to early Eocene global warming events. *Nature*, 435: 1083–1087. doi:10.1038/nature03814.

MARINO, M. and FLORES, J. –A., 2002a. Data report: calcareous nannofossil data from the Eocene to Oligocene, Leg 177, Hole 1090B. In: Gersonde, R., Hodell, D. A., and Blum, P., Eds, *Proceedings of the Ocean Drilling Program: Scientific Results, 177,* 14pp. College Station, TX: Ocean Drilling Program. doi:10.2973/odp.proc.sr.177.115.2002.

———, 2002b. Middle Eocene to early Oligocene calcareous nannofossil stratigraphy at Leg 177 Site 1090. *Marine Micropaleontology*, 45: 383–398.

MARTINI, E., 1971. Standard Tertiary and Quaternary calcareous nannoplankton zonation. In*:* Farinacci, A. (Ed.), *Proceedings of the Second Planktonic Conference, Roma, 1970*, *2,* 739–785. Roma: Edizioni Tecnoscienza.

MITA, I., 2001. Data Report: Early to late Eocene calcareous nannofossil assemblages of Sites 1051 and 1052, Blake Nose, northwestern Atlantic Ocean. In: Kroon, D. et al., Eds., *Proceedings of the Ocean Drilling Program, Scientific Results, 171B,* 1–28. College Station, TX: Ocean Drilling Program. doi:10. 2973/odp. proc. sr. 171B. 122. 2001.

MONECHI, S. and ANGORI, E., 2006. Data report: calcareous nannofossil biostratigraphy of the Paleocene/Eocene boundary, Ocean Drilling Program Leg 208 Hole 1266C. In: Kroon, D. et al., *Proceedings of the Ocean Drilling Program, Scientific Results, 208,* 1–9. College Station, TX: Ocean Drilling Program. doi:10.2973/odp.proc.sr.208.2006.

MONECHI, S. and THIERSTEIN, H. R., 1985. Late Cretaceous–Eocene nannofossil and magnetostratigraphic correlations near Gubbio, Italy. *Marine Micropaleontology*, 9: 419–440.

MONECHI, S., ANGORI, E. and SALIS, K. VON, 2000. Calcareous nannofossil turnover around the Paleocene/Eocene transition at Alamedilla (southern Spain). *Bulletin de la Societe Geologique de France*, 171: 477–489.

MONECHI, S., BUCCIANTI, A. and GARDIN, S., 2000. Biotic signals from nannoflora across the iridium anomaly in the upper Eocene of the Massignano section: evidence from statistical analysis. *Marine Micropaleontology*, 39: 219–237.

NICOLO, M. J., DICKENS, G. R., HOLLIS, C. J. and ZACHOS, J. C., 2007. Multiple early Eocene hyperthermals: Their sedimentary expression on the New Zealand continental margin and in the deep sea. *Geology,* 35: 699–702.

OGG, J. G, OGG, G. and GRADSTEIN, F. M., 2008. *The concise geologic time scale.* Cambridge: Cambridge University Press, 177 pp.

OKADA, H. and BUKRY, D., 1980. Supplementary modification and introduction of code numbers to the low–latitude coccolith biostratigraphic zonation (Bukry, 1973, 1975). *Marine Micropaleontology*, 5: 321–325.

PÄLIKE, H., NORRIS, R. D., HERRLE, J. O., WILSON, P. A., COXALL, H. K., LEAR, C. H., SHACKLETON, N. J., TRIPATI, A. K. and WADE, B. S., 2006. The heartbeat of the Oligocene climate system. *Science,* 314: 1894–1898. doi:10.1126/science.1133822.

PASCHER, A., 1910. Chrysomonaden aus dem Hirschberger Grossteiche. *Monographien und Abhandlungen zur Internationalen Revue der gesamten hydrobiology und Hydrographie*, *1.* Leipzig: Werner Klinkhardt, 66 pp.

PEARSON, P. N., MCMILLAN, I. K., WADE, B. S., DUNKLEY JONES, T., COXALL, H. K., BOWN, P. R. and LEAR, C. H., 2008. Extinction and environmental change across the Eocene–Oligocene boundary in Tanzania. *Geology*, 36: 179–182.

PERCH–NIELSEN, K., 1985. Cenozoic calcareous nannofossils. In: Bolli, H. M., Saunders, J. B. and Perch–Neilsen, K., Eds., *Plankton stratigraphy*, 427–554. Cambridge: Cambridge University Press.

———, 1986. New Mesozoic and Paleogene calcareous nannofossils. *Eclogae Geologicae Helvetiae*, 79: 835–847.

PERSICO, D. and VILLA, G., 2008. A new Eocene *Chiasmolithus* species; hypothetical reconstruction of its phyletic lineage. *Journal of Nannoplankton Research*, 30: 23–33.

PHLEGER, F. B., 1960. *Ecology and distribution of recent Foraminifera*. Baltimore: John Hopkins Press, 297 pp.

RAFFI, I. and DE BERNARDI, B., 2008. Response of calcareous nannofossils to the Paleocene–Eocene Thermal Maximum: Observations on composition, preservation and calcification in sediments from ODP Site 1263 (Walvis Ridge – SW Atlantic). *Marine Micropaleontology*, 69: 119–138.

RAFFI, I., BACKMAN, J. and PÄLIKE, H., 2005. Changes in calcareous nannofossil assemblages across the Paleocene/Eocene transition from the paleo–equitorial Pacific Ocean. *Palaeogeography, Palaeoclimatology, Palaeoecology*, 226: 93–126.

RAFFI, I., BACKMAN, J., FORNACIARI, E., PÄLIKE, H., RIO, D., LOURENS, L. and HILGEN, F., 2006. A Review of calcareous nannofossil astrobiochronology encompassing the past 25 million

years. Quaternary Science Reviews, 25: 3113–3137. doi:10.1016/j.quascirev.2006.07.007.

RAD, U. VON, HAQ, B. U. et al., Eds., 1992. *Proceedings of the Ocean Drilling Program, Scientific Results, 122*, 934pp. College Station, TX: Ocean Drilling Program. doi:10.2973/odp.proc.sr.122.1992.

REVETS, S. A., 2004. On confidence intervals from micropalaeontological counts. *Journal of Micropaleontolgoy*, 23: 61–65.

RÖHL, U, WESTERHOLD, T., MONECHI, S., THOMAS, E., ZACHOS, J. C. and DONNER, B., 2005. The third and final Early Eocene thermal maximum: characteristics, timing, and mechanisms of the "X" event. *Geological Society of America, Abstracts of Programs,* 37: 1 page.

ROMEIN, A. T. J., 1979. Lineages in early Paleogene calcareous nannoplankton. *Utrecht Micropalaeontological Bulletin*, 22: 1–22.

ROTH, P. H. and BERGER, W. H., 1975. Distribution and dissolution of coccoliths in the south and central Pacific. *Cushman Foundation for Foraminiferal Research, Special Publications*, 13: 87–113.

ROTH, P. H. and THIERSTEIN, H. R., 1972. calcareous nannoplankton: Leg 14 of the Deep Sea Drilling Project. In: Hayes, D. E., Pimm, A. C, et al., *Initial Reports of the Deep Sea Drilling Program, 14*: 41–85. Washington, DC: U. S Governmentr Printing Office,

SALAMY, K. A. and ZACHOS, J. C., 1999. Latest Eocene–Early Oligocene climate change and Southern Ocean fertility: inferences from sediments accumulation and stable isotope data. *Palaeogeography, Palaeoclimatology, Palaeoecology*, 145: 61–77.

SHAMROCK, J. L., 2010. A new calcareous nannofossil species of the genus *Sphenolithus* from the Middle Eocene (Lutetian) and its biostratigraphic significance. *Journal of Nannoplankton Research,* 31: 5–10.

SHAMROCK, J. L. and WATKINS, D. K., 2012. World Data Center–A. http: //www.ncdc.noaa.gov/paleo/data.html, Boulder, Colorado.

SHIPBOARD SCIENTIFIC PARTY, 1990. Site 762. *In* Haq, B. U., von Rad, U., O'Connell, S. et al., *Proceedings of the Ocean Drilling Program, Scientific Results, 122*, 213–288. College Station, TX: Ocean Drilling Program,. doi:10.2973/odp.proc.ir.22.108.1990.

SIESSER, W. G., 1998. Calcareous nannofossil genus *Syracosphaera*: structure, taxonomy, biostratigraphy, and phylogeny. *Micropaleontology*, 44: 351–384.

SIESSER, W. G. and BRALOWER, T. J., 1992. Cenozoic calcareous nannofossil biostratigraphy of the Exmouth Plateau, eastern Indian Ocean. *In*: Rad, U. von et al., Eds., *Proceedings of the Ocean Drilling Program, Scientific Results, 122,* 601–631. College Station, TX: Ocean Drilling Program. doi:10.2973/odp.proc.sr.122.162.1992.

SLUIJS, A., BRINKHUIS, H., CROUCH, E. M., et al.,, 2008. Eustatic variations during the Paleocene–Eocene greenhouse world. *Paleoceanography*, 23: 18pp. PA4216. doi:10.1029/2008PA001615.

STENIMEZ, J. C., 1994. Sedimentation of coccolithophores. In: Winter, A. and Seisser, W. G., (Eds.), *Coccolithophores,* 179–197. Cambridge: Cambridge University Press.

SULLIVAN, F. R., 1965. Lower Tertiary Nannoplankton from the California Coast Ranges II. Eocene. *University of California Publications in Geological Science*, 53: 1–74.

THEODORIDIS, S., 1984. Calcareous nannofossil biostratigraphy of the Miocene and revision of Heliolithus and Discoasters. *Utrecht Micropaleontological Bulletin,* 32: 1–271.

THOMAS, E., SHACKLETON, N. J. and HALL, M. A., 1992. Data Report: carbon isotope stratigraphy of Paleogene bulk sediments, Hole 762C (Exmouth Plateau, eastern Indian Ocean). In: Rad, U. von, Eds., *Proceedings of the Ocean Drilling Program, Scientific Results, 122*, 897–901. College Station, TX: Ocean Drilling Program. doi:10.2973/odp.proc.sr.122.195.1992.

TOFFANIN, F., AGNINI, C., FORNACIARI, E., RIO, D., GIUSBERTI, L., LUCIIANI, V., SPOFFORTH, D. J. A., and PÄLIKE, H., 2011. Changes in calcareous nannofossil assemblages during the Middle Eocene Climatic Optimum : Clues from the central–western Tethys (alano section, NE Italy). *Marine Micropaleontology*, 81: 22–31.

TREMOLADA, F. and BRALOWER, T. J., 2004. Nannofossil assemblage fluctuations during the Paleocene–Eocene Thermal Maximum at Sites 213 (Indian Ocean) and 401 (North Atlantic Ocean): paleoceanographic implications. *Marine Micropaleontology*, 52: 107–116.

TRIPATI, A. K., DELANEY, M. L., ZACHOS, J. C., ANDERSON, L. D., KELLY, D. C. and ELDERFIELD, H., 2003. Tropical sea–surface temperature reconstruction for the early Paleogene using Mg/Ca ratios of planktic foraminifera. *Paleoceanography*, 18: 13pp. doi:10.1029/2003PA000937

VAROL, O., 1989. Eocene calcareous nannofossils from Sile, (Northwest Turkey). *Revista Española de Micropaleontología*, 21: 273–320.

———, 1991a. New Cretaceous and Tertiary calcareous nannofossils. *Neues Jahrbuch fur Geologie und Palaontologie. Abhandlungen,* 182: 211–237.

———, 1991b. Paleocene calcareous nannofossil biostratigraphy. In: Crux, J. A. and van Heck, S. E., Eds., *Nannofossils and their applications*, 267–310. Chichester: Ellis Hoewood Limited. British Micropaleontological Society Series.

VILLA, G., FIORONI, C., PEA, L., BOHATY, S. and PERSICO, D., 2008. Middle Eocene–late Oligocene climate variability: calcareous nannofossil repsonse at Kerguelen Plateau, Site 748. *Marine Micropaleontology*, 69: 173–192.

VONHOF, H. B., SMITH, J., BRINKHUIS, H., MONTANARI, A. and NEDERBERG**,** A. J., 2000. Global cooling accelerated by early late Eocene impacts? *Geology*, 28: 687–690.

WEI, W. and WISE, S. W., Jr., 1989a. Discoaster praebifax n. sp. : a possible ancestor of Discoaster bifax Bukry (coccolithophoridae). *Journal of Paleontology*, 63: 10–14.

———, 1989b. Paleogene calcareous nannofossil magnetobiochronology: results from South Atlantic DSDP Site 516. *Marine Micropaleontology*, 14: 119–152.

———, 1990a. Middle Eocene to Pleistocene calcareous nannofossils recovered by Ocean Drilling Program Leg 113 in the Weddell Sea. In: P. F. Breker et al., Eds., *Proceedings of the Ocean Drilling Program, Scientific Results*, *113,* 639–666. College Station, TX: Ocean Drilling Program.

———, 1990b. Biogeographic gradients of middle Eocene–Oligocene calcareous nannoplankton in the South Atlantic Ocean. *Palaeoceanography, Palaeoclimatology, Palaeoecology*, 79: 26–61.

WISE, S. W., Jr., 1983. Mesozoic and Cenozoic calcareous nannofossils recovered by Deep Sea Drilling Project Leg 71 in the Falkland Plateau region, Southwest Atlantic Ocean. *In*: Lugwig, W. J. et al., Eds., *Initial Reports of the Deep Sea Drilling Program, 71*, 481–550. Washington DC: U. S. Governmrent. Printing Office.

WISE, S. W., Jr., BYBELL, L. M, COVINGTON, J. M., et al., 2004. *Cenozoic Nannoware database version 2004. 1. 3*. International Nannoplankton Association CD ROM No. 1

YOUNG, J. R. and BOWN, P. R., 1997. Proposals for a revisited classification system for calcareous nannoplankton. *Journal of Nannoplankton Research*, 19: 15–47.

YOUNG, J. R., BERGEN, J. A., BOWN, P. R., et al., 1997. Guidelines for coccolith and calcareous nannofossil terminology. *Paleontology*, 40: 875–912.

YOUNG, J. R., GEISEN, M., CROS, L., KLEIJNE, A., SPRENGEL, C., PROBERT, I. and OSTERGAARD, J., 2003. *A guide to extant coccolithophore taxonomy*. *Journal of Nannoplankton Research, Special Issue* 1: 125 pp.

ZACHOS, J. C., PAGANI, M., SLOAN, L., THOMAS, E. and BILLUPS, K., 2001. Trends, rhythms, and aberrations in global climate 65 Ma to present. *Science*, 292: 686–693.

Receieved April 18, 2011
Accepted April 5, 2012
Published September, 2012